Understanding Flow-induced Particle Migration for improved Microfiltration

Anna Marie Christine van Dinther

Thesis committee

Thesis supervisor
Prof.dr.ir. R.M. Boom
Professor of Food Process Engineering, Wageningen University

Thesis co-supervisor
Dr.ir. C.G.P.H. Schroën
Associate professor, Food Process Engineering Group, Wageningen University

Other members
Prof.dr. J. P.M. van Duynhoven
Wageningen University/ Unilever Research Vlaardingen
Dr.ir. D.C. Nijmeijer
University of Twente
Prof.dr.ir. H.H.M. Rijnaarts
Wageningen University
Dr.ir. E. Roesink
Pentair X-Flow Enschede

Understanding Flow-induced Particle Migration for improved Microfiltration

Anna Marie Christine van Dinther

Table of Contents

Introduction

Design of Microsieves and Microsieve Processes for Suspension Fractionation

This chapter is based on:

- van Dinther, A. M. C., C. G. P. H. Schroën, R.M. Boom (2009). "Design of Microsieves and Microsieve Processes for Suspension Fractionation." New Membranes and Advanced Materials for Wastewater Treatment, American Chemical Society. 1022: 137-149.
- Schroën, K., A. M.C. van Dinther, S. Bogale, M. Vollebregt, G. Brans, R.M. Boom (2010). "Membrane Processes for Dairy Fractionation." Membrane Technology: Membranes for Food Applications, Volume 3, Wiley-VCH Verlag GmbH & Co. 25-43.

1. Design of Microsieves and Microsieve Processes for Suspension Fractionation

1.1. General aspects of microfiltration

The membrane industry had a total turnover of US$20 to 30 billion per year in 2006 (Rideal 2005; Sutherland 2006), with an estimated annual growth rate of 12-15% (Li, Fane et al. 2008). In the food industry, the market volume of membrane is about 850 millon euros and in here microfiltration has a membrane market share of 33% (Peinemann, Nunes et al. 2010). Microfiltration is now a mature process for separating components between 0.01 and 10 micron and is used in different industries, such as wastewater treatment, food processing, biotechnology and the chemical and pharmaceutical industry (Strathmann 2001). Often, cross-flow microfiltration is used, in which the feed suspension flow is fed parallel to the membrane. The liquid that permeates through the membrane as a result of the trans-membrane pressure is called the permeate and is often the product. An example from the food industry is the removal of yeast from beer.

As long components that need to be separated are sufficiently different in size (e.g. separate bacteria which are in the micrometre range, from proteins that are in the nanometre range), they can be separated efficiently by microfiltration. Fractionation, which we will use to denote separation processes in which components to be separated are not very different in size, is much more difficult. Some examples are described by Brans *et al.* (2004) (Brans, Schroën et al. 2004). The main challenge is the (control of) accumulation of components on the membrane which changes the retention characteristic of the membrane and strongly reduces the flux. Besides, adsorption of these components may take place on the membrane surface and/or inside the membrane pores, and this also leads to changes in retention characteristics. When pores effectively become smaller because of the accumulated components, suspended particles are more easily retained and that can lead to even further accumulation on the membrane. As a result, the flux and retention change in time, which increases the need for cleaning, generally responsible for 5 to 20% of the total operational costs (Fane 1997). Cleaning cycles often take 10 minutes to 3 hours and are required from once every

day, to about 4 to 6 weeks depending on the application (Pilutti 2003). If accumulation would not occur, the process would run much more efficient in terms of product quality, time, reliability and costs.

In this thesis, we investigate whether it is possible to operate at constant flux and retention by taking the dynamics of the suspension itself as a starting point in the design of filtration processes. In the next section, we discuss the mechanisms that are responsible for the accumulation of particles above and on the membrane (concentration polarization, cake formation and adsorption) followed by different routes from literature targeted at controlling the accumulation of particles. We will take a totally different approach in this thesis, by redesigning the process in such a way that fouling is totally prevented. Membrane design and back-transport mechanisms that may be used are discussed in the design of deposition-free filtration processes, and we conclude with an overview of the various elements of the thesis in which we combine particle migration behaviour with process design.

1.1.1. Concentration polarization and cake layer formation

Due to the intrinsic nature of a filtration process, components are carried towards the filter due to the permeate flow that is removed through the membrane from the feed solution. At low trans-membrane pressures, the concentrations close to the membrane are low and strong accumulation of components is not likely. The flux is then still equal to the clean-liquid flux and can be described by equation 1.1.

$$J = \frac{\Delta P}{\eta_0 R_m}$$

(1.1)

In which J is the permeate flux (m/s), ΔP the trans-membrane pressure (Pa), η_0 the viscosity of the permeate (Pa·s) and R_m the membrane resistance (m^{-1}).

At higher trans-membrane pressure, more components are carried towards the membrane where they are retained with greater (friction) force. Due to the higher concentration near the membrane compared to the bulk, some back-diffusion or re-dispersion will take place. The net accumulation resulting from the transport towards the membrane by convective flow and back-diffusion is called concentration polarization. When the pressure is high enough, the suspended and

retained particles are dragged to the membrane with so much force that they deposit on the surface, forming a cake layer which reduces flux and retention considerably. At that moment the steady-state trans-membrane flux is only determined by the back-transport mechanism in the concentration polarization layer above the cake layer, and not by the trans-membrane pressure. A higher trans-membrane pressure simply leads to a thicker cake layer, and a steadying of the flux at the original level. The cake layer can even become more compact upon application of higher pressures, leading to true flux and retention reduction with increasing pressure. Simultaneously with particle accumulation on the membrane, there is often accumulation of particles onto or inside the membrane pores as well. As a result, the effective pore diameter and retention of the membrane change (Figure 1.1).
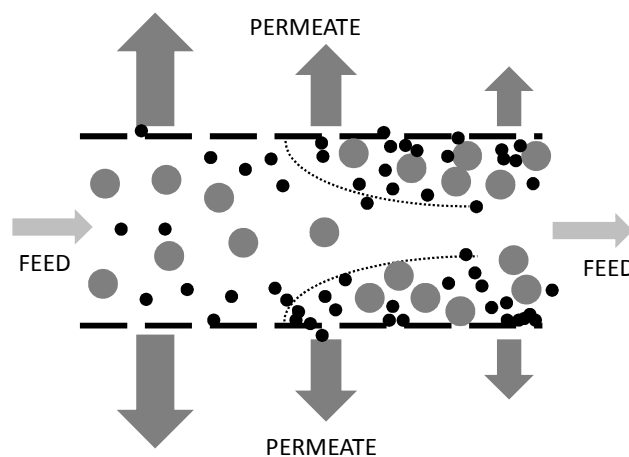
Figure 1.1. Schematic representation of a cross-flow microfiltration process with a decrease in permeate flux over the length of the membrane due to pore blocking and particle adsorption in the pores and on the membrane walls.

To improve membrane microfiltration in terms of constant flux and retention, there is ongoing research for new opportunities, related to specific membrane or module design, but also related to optimization of process conditions. The design of the whole process should be such that preferred flux and retention are obtained by controlling concentration polarization and other deposition layers. It is generally accepted that not the membrane, but (the rate of) accumulation is the limiting factor for membrane filtration (Makardij, Chen et al. 1999), although there

is debate about the different aspects of the accumulated layer as being most relevant (e.g. depth deposition and/or pore blocking) (Bowen, Doneva et al. 2003; James, Jing et al. 2003). In spite of the differences in opinion, a number of concepts have been developed to keep the flux at acceptable levels (as presented in the next section), through mediation of short term flux decrease. Besides that, cleaning is needed to mediate long-term flux decrease.

1.1.2.   Process concepts
a.   Critical flux concept

In the critical flux concept proposed by Field *et al.* (1995) and Howell (1995), and recently reviewed by Pollice (2005) for membrane bioreactors, three regions are distinguished as indicated in Figure 1.2. In region I, the trans-membrane pressure is below a critical pressure and the flux is linearly dependent on the applied pressure. In this regime, the accumulation of particles does not yet lead to the formation of a cake layer or to blockage of pores, and equation 1.1 is valid. Filtration in this region is known as sub-critical flux operation and gives optimal selectivity, since the permanent accumulation of particles on the surface is minimal. However, at these low pressures, fluxes are low and the required membrane area is high; the most optimal conditions for sub-critical flux operation is the point where the flux/pressure curve starts to deviate from linearity (Field, Wu et al. 1995; Howell 1995; Pollice, Brookes et al. 2005).

While the concept of sub-critical operation is derived for systems with only one type of suspended particle, in reality the situation is more complex. The critical pressure depends on the type of particles suspended. Particles that adhere strongly to the membrane surface or that are smaller in size, give a lower critical pressure. This also implies that when a suspension is contaminated with a small amount of particles that adhere more strongly to the membrane, or that are smaller in size and hence have a lower critical flux, the performance of the membrane may deteriorate slowly, while the system seems to be sub-critical relative to the major fraction of suspended particles. In region II, the flux is no longer linearly dependent on the trans-membrane pressure, and the flux is dominated by the maximum rate of back-transport from cake layer on the membrane, towards the flowing bulk of the feed suspension. A higher pressure

only results in a thicker cake layer, not in a higher steady-state flux. The only way to increase the flux, is by increasing the cross-flow velocity, as this enhances the back-transport of particles from cake layer to suspension. The value of the flux can be estimated from the gel filtration model and/or back-transport models (Belfort, Davis et al. 1994). Although the selectivity of the membranes is now co-determined by the properties of the cake layer, this region is often used in practice because volumetric productivity is highest. In region III, the applied pressure is so high, that the particles inside the cake layer are deformed. The porosity of the cake layer is reduced, which leads to flux decrease. Since this compaction is irreversible and becomes worse with time, the cake layer needs to be removed at short intervals, e.g. through frequent back-pulsing.
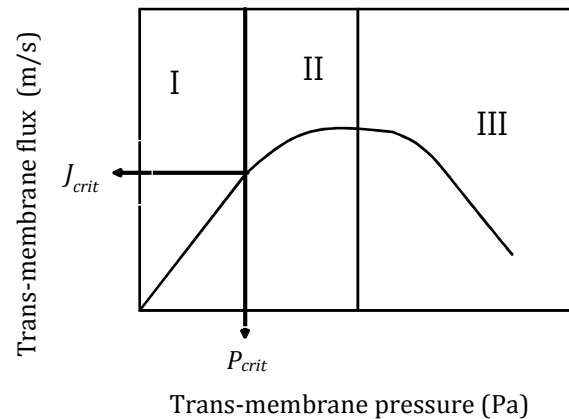
Figure 1.2. Schematic representation of the critical flux concept. In region I, the flux is linearly dependent on pressure until at a critical pressure (P_{crit}), the critical flux (J_{crit}) is reached. The flux levels of as a function of pressure in region II, and even decreases in region III when the pressure is increased further (adapted from reference (Brans, Schroën et al. 2004)).

b. Turbulence promotion

Another approach is to promote particle transport from membrane to bulk through turbulence. Various options have been proposed, such as vibrating modules (Al-Akoum, Ding et al. 2002), rotating disk modules (Belfort, Pimbley et al. 1993; Engler and Wiesner 2000; Ding, Al-Akoum et al. 2002), static mixing inserts (Krstić, Tekić et al. 2002), spacers, turbulence promoters and the use of Dean vortices or micro-turbulence (Winzeler and Belfort 1993). Some methods influence particle deposition through increased shear rate close to the membrane

surface, by either vibration or rotation, and although interesting effects can be realized, the module design is rather complex, especially for larger scale application. Furthermore, it is difficult to clean the module and prevent microbial contamination on large scale. Investment costs are relatively high, although the second generation devices become more competitive (Jaffrin 2008). In a review by Jaffrin (2012), it was shown that creation of flow instabilities, such as Dean and Taylor vortices, is an elegant method to locally increase mass transfer, but poses limitations on the membrane configuration (Jaffrin 2012).

c. Uniform low trans-membrane pressure concept (UTP)

To induce and increase turbulence, the cross-flow velocity and thereby the Reynolds number can be increased, although this also results in a larger pressure drop along the length of the membrane module, leading to a non-uniform trans-membrane pressure. To tackle this, a new concept was proposed, called the uniform low trans-membrane pressure concept (UTP), patented by Sandblom (1978). It allows a constant trans-membrane pressure over the entire length of the membrane module, through application of cross-flows on both the permeate and feed side (Sandblom 1978; Plett 1989). Vadi and Rizvi (2001) obtained significantly better results with UTP compared to without for the concentration of casein from milk, especially for long membrane modules (Vadi and Rizvi 2001). Although extra energy is needed to operate the second cross-flow, UTP is currently a popular strategy against flux decrease during filtration. Instead of a cross-flow on the permeate side, also membranes can be adjusted to generate UTP as is the case in Isoflux and Gradient Porosity membranes (Saboya and Maubois 2000). These membranes have a decreasing membrane resistance over the length of the tube, which has the same effect as UTP, but without the need of an imposed cross-flow on the permeate side. Membrane, module and application should be very well defined, to effectively apply this process (Saboya and Maubois 2000); therefore, the design and operation of these membranes processes is relatively expensive.

d. Back-pulsing and flow reversal

Various terms are in use for the temporary reversal of flow through the membrane, such as back-pulsing, back-washing, back-flushing, and back-shocking (Redkar, Kuberkar et al. 1996; Mores and Davis 2002), and in all these cases permeate is periodically pressed back into the feed stream (also leading to turbulence).

Through this type of reversal of flow, the deposited components are lifted from the membrane and carried away by the cross-flow. The frequency at which flow is reversed can be low (once every few minutes or even hours) or high (0.1-1.0 s^{-1}) as reported by Rodgers and Sparks (1992), and Guerra *et al.* (1997) (Rodgers and Sparks 1992; Guerra, Jonsson et al. 1997). Wenten *et al.* (1994) have even reported much higher frequencies which allowed low cross-flow velocities and cell removal from reverse membranes (Wenten, Koenhen et al. 1994). Cross-flushing can be induced by periodically stopping the permeate (Kuruzovich and Piergiovanni 1996).

Besides permeate flow reversal, the feed flow as such can be used to improve filtration performance, by pulsating flow or even reversal of the feed flow direction. In this case, rapid velocity changes occur in the cross-flow channel (Jaffrin, Gupta et al. 1994; Curcio, Calabrò et al. 2002). It should be mentioned that the pulsating cross-flow is difficult to use at large scale, because the effect of the pulses dampens out over larger distances. In general, high-frequency back-pulsing is the method of choice in industrial applications, possibly in combination with UTP application.

e. Other methods

Other options reported are the introduction of air slugs or scouring particles, to enhance turbulence locally (Cui and Wright 1996; Noordman, de Jonge et al. 2002; Cui, Chang et al. 2003). These methods can be very effective, but air slugs can also induce foaming and may induce denaturation of proteins on the air-water interface, while scouring particles are hard to re-use and cause damage to the membrane and the installation (Noordman, de Jonge et al. 2002). They can therefore only be used with selected systems. Acoustic waves and sonication causes local vibrations and cavitation, which facilitates the transport of suspension particles, but at the same time may also induce denaturation of protein (Wakeman and Tarleton 1991; Villamiel and de Jong 2000; Duriyabunleng, Petmunee et al. 2001) which is not desirable in e.g. beer filtration. Further there is the possibility of using electric fields, either constant or pulsed (Wakeman and Tarleton 1986; Visvanathan and Aim 1989; Wakeman 1998), which also may affect the pH of the liquids in an undesirable way.

Although all these methods are successful to some extent, the results are difficult to interpret because many factors act simultaneously, such as the pore size distribution, which causes local differences in permeate flux. Besides, particle behaviour is not that well understood that it can be used in membrane process design yet. In the next section, we discuss the newest developments in membranes with uniform pores and show examples of results that were obtained.

1.1.3.   Process improvement options

a.   Membrane design

Micro-engineered membranes, such as microsieves are a new type of membrane of which the pore size and geometry can be tailored to an extent that is unprecedented in 'regular' membranes (Kuiper, van Rijn et al. 2002); see also Figure 1.3). Characteristics of the membranes are their extremely thin active top layer, relatively high porosity, and open support structure. As a result their clean-water fluxes can be two or three orders of magnitude higher than fluxes of conventional membranes, even at very low trans-membrane pressures. The top surface is much smoother than for any other membrane, which may have advantages in relation to accumulation and cleaning. Furthermore, there is a great freedom in design of the pores (e.g. size, geometry), as well as positioning of the pores (Figure 1.3b and c). Given the uniform pore size and the possibility to tune the system to the separation issue at hand, engineered membranes are interesting for fractionation purposes (Kuiper, van Rijn et al. 2002; Brans, Kromkamp et al. 2006; Gironès and Girones 2006).

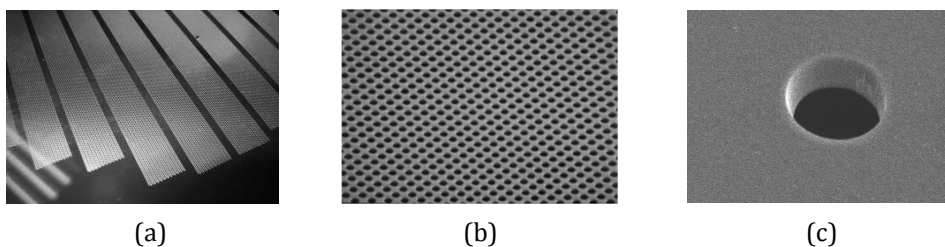| (a) | (b) | (c) |

Figure 1.3. Microsieves from different scale perspective. (a) Part of a wafer with sieve fields and solid lanes, (b) porous field, (c) close-up of one pore. Pictures are courtesy of Aquamarijn Microfiltration BV, The Netherlands.

Because of their extremely high permeability, the critical flux is reached already at very low pressures, which implies that process control needs to be much stricter than for conventional membranes. This was found to be one of the most important limitations of these membranes.

Also other membranes are available with uniform pores, such as the Veconic sieves used in this thesis. We used membranes having pore sizes much larger than the particles in the suspension, since we expected this would have minimal influence on rejection, and lead to constant fluxes if particle accumulation can be controlled. Some examples of results from literature and how we used these insights to formulate our own research are shown in the next section.

b. Process Conditions and Particle Migration

For milk fat globules, it was shown that fractionation could be achieved with a membrane with relatively large pores (Goudédranche, Fauquant et al. 2000; Kromkamp, Faber et al. 2006). When the cross-flow velocity and permeate flux were varied with such a membrane, while all other conditions including wall shear rate were kept constant in the work of Kromkamp *et al.* (2006), the particle size distributions in the permeate were different from the feed. This shows that fractionation takes place, even though one would not expect any separation based on the large membrane pore size. For the highest cross-flow velocity, the particle size and fat content in the permeate were relatively constant as function of the flux, but much lower than in the feed. For lower cross-flow velocities, the particle size and fat content in the permeate increased at higher flux, and eventually almost reached the values of the feed solution (Kromkamp, Faber et al. 2006). These effects were not related to particle accumulation (pore blockage or cake layer formation), since there was a linear relation between permeate flux and trans-membrane pressure, indicating sub-critical operation. Therefore, it was suggested that the flow conditions induced the segregation of the suspension already in the bulk suspension while flowing through the module. These effects were investigated by CSLM, using fluorescent polystyrene particles (1.6, 4.0 and 9.8 µm in size) to visualize their deposition behaviour on the membrane. The pore size of the membrane was in this case so small that none of the particles could pass the membrane. In Figure 1.4, deposition of a bidisperse suspension is shown at three

times during filtration; the feed solution consists of 97.5% (v/v) large particles, while 2.5% is small (Kromkamp, Faber et al. 2006). During filtration, many small and some large particles deposit, but in a completely different ratio as expected from their ratio in the feed: there are far less larger particles present on the membrane surface than expected from their ratio in the feed. We infer from this that segregation of particles occurs already in the fluid above the membrane, which then leads to preferential deposition of smaller particles, even when the overwhelming majority of all particles is large (Kromkamp, Faber et al. 2006). For our own research we also concluded that this could imply that the composition of the permeate may be controlled not through size exclusion from the pores, but through combination of the right cross-flow velocity and the permeate flux. Crucial for this is of course that the particle behaviour is sufficiently understood.
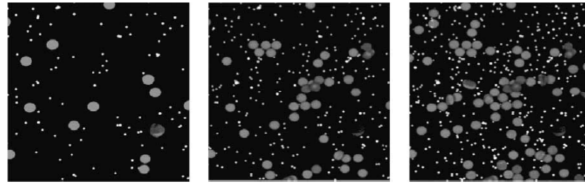
Figure 1.4. Deposition of small (1.6 μm) and large particles (9.8 μm) onto the membrane during microfiltration monitored with CSLM. Time proceeds from left to right. Reproduced with permission (Kromkamp, Faber et al. 2006).

1.2.   Particle behaviour

For typical suspension particles present in microfiltration, three important transport mechanisms can be distinguished: Brownian diffusion, shear-induced diffusion, and inertial lift (Samuelsson, Huisman et al. 1997). Their relative importance depends on the particle size, the concentration and the viscosity of the suspension, and the flow velocities used in the system. Shear-induced diffusion is expected to be the major back-transport mechanism for particles between 0.1 and 10 μm, as used in this thesis. The shear-induced diffusion coefficient is proportional to $\dot{\gamma}a^2$ (Karnis, Goldsmit et al. 1966; Lee and Clark 1998) as described with equation 1.2 (Leighton and Acrivos 1987).

$$D_{shear} = \dot{\gamma}a^2D_{\phi} \qquad\qquad (1.2)$$

Where $\dot{\gamma}$ is the shear rate (s^{-1}), ϕ is the solid volume fraction (-) and a is the particle radius (m). The dimensionless part D_ϕ in this diffusion coefficient is strongly dependent on the composition, and is defined in equation 1.3 for a monodisperse suspension.

$$D_\phi = \frac{1}{3}\phi^2(1+0.5e^{8.8\phi})$$
(1.3)

Obviously, larger particles are much more influenced by shear-induced diffusion given the quadratic relation in equation 1.2. In flow, particles pass other particles in slower-moving fluid streamlines and interact (either by direct collision or by longer-range interaction through disturbance of the surrounding flow field). Depending on their size these effects will be bigger or smaller. When these interactions involve three or more particles at some stage, they are irreversibly displaced from their fluid streamlines (Eckstein, Bailey et al. 1977), leading to a random dispersal of particles. This creates a net migration away from the membrane towards the bulk (Breedveld, van den Ende et al. 2001), since due to the flow towards the membrane, the volume fraction of particles near the membrane is larger than in the bulk. Larger particle migrate faster than small particles, which results in the local segregation of bidisperse suspensions: larger particles tend to accumulate in the regions with the lowest shear rate, while the smaller ones accumulate in the regions with higher shear rates. This effect of shear-induced segregation explains the behaviour seen in the experiments described in the previous section (Kromkamp, Faber et al. 2006).

Phillips *et al.* (1992) proposed that this particle diffusion is not only due to gradients in local concentrations, but also gradients in viscosity and in shear rate induce displacements towards regions with lower viscosity or shear rate (Phillips, Armstrong et al. 1992). Since the flow in a channel necessarily has regions with large shear rate near the membrane, and a region with almost no shear rate in the centre of the channel, this alone will cause displacement of the particles from the membrane towards the centre of the feed channel. These effects are also strongly dependent on the size of the particles, once more this causes segregation; even in the absence of concentration polarization (Figure 1.5).
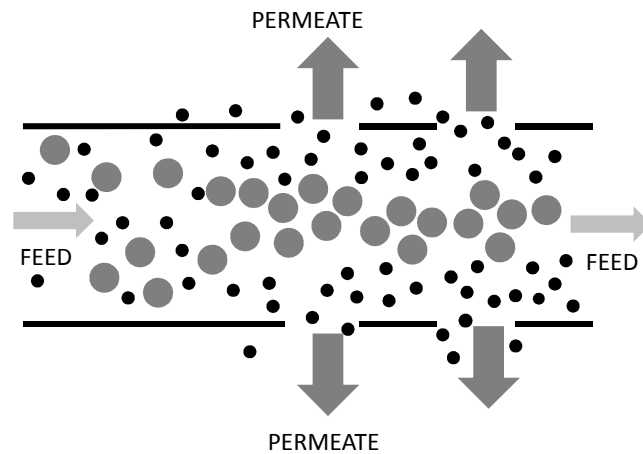
Figure 1.5. Schematic representation of a cross-flow microfiltration process with a constant permeate flux over the length of the membrane due to shear-induced particle migration in combination with the use of a closed entrance length and large pores.

It is clear that when using these effects for separation, a quite robust system against fouling of the membrane, by the suspension particles, would be within reach. At this moment however, these effects are not well understood, especially for multicomponent suspensions. Better insight and better quantification of the effects, as function of flow conditions and composition of the suspensions is paramount.

1.3.   Research aim and thesis outline

It is obvious from the previous section that many aspects are important in membrane separation and more importantly in fractionation, where the components to be fractionated are not very different in size. While many researchers in the past have focused on the design of the membrane itself (pore size and shape, etc); the discussion above indicates that the fluid dynamics have an influence that is as least as large as the design of the membrane itself, not only for optimization of the flux but for retention as well. In fact, depending on the particle composition and flow conditions, the fluid dynamics might even be more important than the membrane. This poses great challenges on the design of a microfiltration process, since it implies that size scales ranging from colloidal (particles and pore; microns) to module size (meters) have to be taken into account. Since optimisation of the mentioned flow effects may well lead to a

process that is much more robust, could work at high dispersed phase volume fractions, and of which the separation properties could be tuned by changing the flow conditions, the perspective of this thesis is to obtain insight in the behaviour of the feed solutions under well-defined flow conditions, and translate this behaviour to the design of suspension separation processes.

The overall aim of the work reported in this thesis therefore was to investigate the possibilities to separate and fractionate emulsions and suspensions with microfiltration at constant permeate flux and retention in time. The influence of process design (involving membrane and module design and process conditions) on particle migration was investigated and the obtained knowledge was applied to the design of microfiltration processes at preferred fluxes and retentions.

The thesis starts with an evaluation of different existing experimental techniques to measure velocity and concentration profiles in microfluidic devices, described in the **second** chapter. These velocity and concentration profiles give information about the influence of process conditions and module design on particle migration, and besides an outlook is given for future development of these techniques. In the **third** chapter the influence of process conditions (i.e., flow) on concentration profiles in concentrated bidisperse suspensions is measured with CSLM in microchannels. The **fourth** chapter shows how the obtained knowledge from the previous chapters can be used in the design of filtration processes, for the fractionation of bidisperse, concentrated emulsions and chapter **five**, further elaborates on that, by also including pore design of membranes. Further it discusses the use of particle migration for the creation of new separation processes for the industrial fractionation of concentrated emulsions and suspensions. In chapter **six**, dilute suspensions are investigated, in relation to particle migration mechanisms, also including fluid skimming. In the **discussion** session, the results are summarized, and an outlook for application of this new technology is given.

Chapter 2

Suspension Flow in Microfluidic Devices – A Review of Experimental Techniques focussing on Concentration and Velocity Gradients

2. Suspension Flow in Microfluidic Devices – A Review of Experimental Techniques focussing on Concentration and Velocity Gradients

Chapter

2

2.1. Abstract

Microfluidic devices are an emerging technology for processing suspensions in e.g. medical applications, pharmaceutics and food. Compared to larger scales, particles will be more influenced by migration in microfluidic devices, and this may even be used to facilitate segregation and separation. In order to get most out of these completely new technologies, methods to experimentally measure (or compute) particle migration are needed to gain sufficient insights for rational design. However, the currently available methods only allow limited access to particle behaviour.

In this review we compare experimental methods to investigate migration phenomena that can occur in microfluidic systems when operated with natural suspensions, having typical particle diameters of 0.1 to 10 μm. The methods are used to monitor concentration and velocity profiles of bidisperse and polydisperse suspensions, which are notoriously difficult to measure due to the small dimensions of channels and particles. Various methods have been proposed in literature: tomography, ultrasound, and optical analysis, and here we review and evaluate them on general dimensionless numbers related to process conditions and channel dimensions. Besides, eleven practical criteria chosen such that they can also be used for various applications are used to evaluate the performance of the methods.

We found that NMR and CSLM, although expensive, are the most promising techniques to investigate flowing suspensions in microfluidic devices, where one may be preferred over the other depending on the size, concentration and nature of the suspension, the dimensions of the channel, and the information that has to be obtained. The chapter concludes with an outlook on future developments of measurement techniques.

Chapter

2

2.2. Introduction

Microfluidic devices are increasingly used in for example (cell) biology, food, pharmaceutics and chemical synthesis (Whitesides 2006). Their advantages are the small volume and large surface area, leading to better mass and heat transfer. Besides, they can be used to manipulate multiphase systems (e.g. for the preparation of droplets or particles) but also to manipulate particle suspensions or emulsions and induce migration phenomena. Particles can migrate to specific regions in a channel as a result of fluid flow phenomena and particle interactions. Migration of particles perpendicular to the flow can be a disadvantage when heat treatment of suspensions is concerned; residence time distribution occurs with different heat treatment as a result. This can lead to rheological and structural changes of the product (Hong, Sheetz et al. 1991; Pal 1994; Lareo, Fryer et al. 1997; McCarthy and Kerr 1998; Barigou, Fairhurst et al. 2003) and for foods even to implications for microbial food safety (Sastry and Zuritz 1987). However, migration of particles to specific regions in the channel, can also be beneficial, for example in (membrane) separation processes (Kromkamp 2005; Kulrattanarak, van der Sman et al. 2008). Especially in the last decade, the interest in the separation and fractionation of food suspensions is increasing; illustrative examples are removal of specific components (e.g. bacteria from milk), concentration (e.g. removal of water from fruit juices) or isolation of specific fractions as new food products or ingredients (e.g. milk fat globules from milk proteins) (Goudédranche, Fauquant et al. 2000; Rausch 2002; Roda, Zattoni et al. 2009; van Dinther, Schroën et al. 2011). Biological cells can be cultivated and investigated individually in microfluidic devices, and in order to control migration, this is often done in microdroplets in microchannels, also known as 'biphasic', 'segmented', or 'plug-based' microfluidics (Teh, Lin et al. 2008; Theberge, Courtois et al. 2010), where liquid segments are used to compartmentalise the device. Mostly this is not an option and migration will take place when flowing a suspension through a microchannel, be it in biological applications, medicine or oceanography, where cell types can be differentiated based on flow behaviour in a fast and accurate manner (Krishnan and David T. Leighton 1995; David, Pignon et al. 2008; Hur, Tse et al. 2010; Zhang and Balcom 2010). The newest developments in the field of separation revolve around microfluidic devices that can be used to sort cells and DNA (Yamada, Nakashima et al. 2004; Aguilera 2005; Toner and

Irimia 2005; Ros, Hellmich et al. 2006; Skurtys and Aguilera 2008; Yoo and Kim 2008; Bhagat, Kuntaegowdanahalli et al. 2009).

In microfluidic devices, it is not easy to trace micron-sized particles in narrow channels and at these small scales, process conditions also influence migration strongly, which makes it difficult to establish concentration and velocity profiles that are needed to effectively use migration phenomena in the design of such devices (Ros, Hellmich et al. 2006; Yoo and Kim 2008). Besides, natural suspensions tend to be concentrated and this makes measurement of particle migration even more complex. To understand particle behaviour in microfluidic devices it is of eminent importance to be able to measure the influence of process conditions on particle migration. Here, we distinguish three common migration phenomena, for particles that are in the range of nanometres to millimetres, being shear-induced diffusion, inertial lift and Brownian diffusion. Particles in the order of nanometres are mainly sensitive to Brownian diffusion; for particles between 0.1 and 10 micron shear-induced diffusion plays a major role and for even larger particles, inertial lift is the main migration phenomenon (Davis 1992). The 'particle' radius (a) (with which we mean any component, not necessary a solid particle), relative to the dimensions of the device (like channel height, h) determines the scale at which migration phenomena play a role (see also next section).

The goal that we set for this chapter is to evaluate experimental methods on their suitability to measure migration phenomena in microfluidic devices based on knowledge about migration phenomena and other characteristics of the techniques.

2.3. Theory

In Poiseuille flow, which occurs when a viscous fluid flows in a channel and a constant pressure gradient over the length is applied, the flow has a characteristic parabolic profile, and this is also expected to be the case in microfluidic devices. For a no slip velocity at the walls (v_{wall} = 0), the velocity at a certain height in the channel (v_x(z) (m/s)) is given by equation 2.1.

$$v_x(z) = \frac{1}{2\eta(\phi)} \frac{\Delta p}{L} \left(\left(\frac{h}{2} \right)^2 - z^2 \right) \tag{2.1}$$

27

Here Δp is the pressure drop (Pa) over the channel length (L (m)), h is the channel height (m), z is the position of the particle relative to the wall (m), $\eta(\phi)$ is the viscosity of the suspension as function of the particle volume fraction (ϕ), which is described by equation 2.2 (Krieger and Dougherty 1959),

$$\frac{\eta(\phi)}{\eta_0} = \left(1 - \frac{\phi}{\phi_{\max}}\right)^{-[\eta]\phi_{\max}}$$

(2.2)

η_0 is the viscosity of the particle-free liquid (Pa·s), ϕ_{max} the maximum random packing density for the suspension (-) (assumed to be 0.64 for monodisperse suspensions of hard spheres), and $[\eta]$ is the intrinsic relative viscosity of the suspension (assumed to be 2.68 as reported by Phillips *et al.* (2006)) (Phillips, Armstrong et al. 1992).

Particles present in Poiseulle flow will experience a velocity gradient, and depending on their size they may migrate to other flow lanes. Viscous forces, combined with inter-particle interactions lead to hydrodynamic diffusion of particles in the range of 0.1-10 micron (shear-induced diffusion), and inertial forces (inertial lift) will act on particles > 10 micron. The importance of these mechanisms can be derived from the ratio between inertial and viscous forces, characterised by the Reynolds number, as discussed in the next section. To be complete, Brownian motion generally leads to random motion of particles, but may lead to separation when an external field is applied, as is the case in field flow fractionation (Schimpf, Caldwell et al. 2000). This latter case, we will not discuss further in this review.

2.3.1. Reynolds number

The Reynolds number defines the ratio of inertial to viscous forces and is shown in equation 2.3.

$$\mathrm{Re}_c = \frac{\rho \bar{v} D_h}{\eta(\phi)}$$

(2.3)

For a rectangular channel, as is mostly the case in microfluidic devices, the hydraulic diameter is described in equation 2.4. For other geometries, different equations are available.

$$D_h = \frac{4wH}{(w+2H)}$$ (2.4)

In which ρ is the density, v is the average velocity in the channel, D_h the hydraulic diameter (equation 2.4), w the channel width (m) and H half the height of the channel (m).

Shear-induced diffusion occurs already at low Reynolds numbers, where inertia is not relevant. As a rule of thumb, inertial lift only takes place in a rectangular channel when the Reynolds number of the particle Re_p (-) defined in equation 2.5 (Altena and Belfort 1984), is larger than 1.

$$Re_p = Re_c \left(\frac{2a}{D_h} \right)^2 = \frac{\dot{\gamma} \rho a^2 (w+2H)}{3\eta(\phi)w}$$ (2.5)

$$\dot{\gamma} = \frac{3\bar{v}}{H}$$ (2.6)

In which, $\dot{\gamma}$ is the shear rate (1/s) given in equation 2.6, a is the particle radius (m), Re_p is the particle Reynolds number and Re_c the channel Reynolds number (as defined in equation 2.3).

2.3.2.   Péclet number

The ratio between convection and diffusion, characterised by the Péclet number, defines the ratio between hydrodynamic forces and Brownian diffusion. It indicates whether hydrodynamic migration or Brownian diffusion is dominant and relates this to dimensions of the device. Transition from mainly Brownian to hydrodynamic migration occurs at a Péclet number of 1, as defined in equation 2.7 (Ackerson 1991). In systems where hydrodynamic migration should be dominant, conditions like channel height, velocity and viscosity should be chosen in such a way that Péclet numbers are larger than 1.

$$\text{Pe} = \frac{\dot{\gamma}a^2}{D} = \frac{6\dot{\gamma}a^3\eta(\phi)\pi}{kT} \qquad (2.7)$$

Where k the Boltzmann constant (1.380×10^{-23} J/K) and T the temperature (K), and D is given by the Stokes-Einstein diffusivity (m^2/s) given in equation 2.8.

$$D = \frac{kT}{6\pi\eta(\phi)a} \qquad (2.8)$$

Hydrodynamic forces in a Poiseuille type flow field cause the particles to concentrate at certain regions, e.g. the centre of the channel in case of shear-induced diffusion or off-axis focusing (i.e. 'tubular pinch') in the case of inertial lift. Brownian motion may counteract these effects, but is mostly much weaker. For example, for a dilute suspension with 1 micron particles in a 100 micron channel, a velocity larger than 4 μm/s already causes the migration effect to surpass Brownian motion.

Besides the Reynolds and Péclet numbers described here, which are really focussing on particle behaviour, there are also other dimensionless numbers expressing the relevance of various physical phenomena in microfluidic devices. For a complete overview, we would like to refer through to the review by Squires *et. al.* (Squires and Quake 2005).

2.3.3.   Channel dimensions

Combining equation 2.6 and 2.7 leads to the conclusion that in microchannels, where the particle to channel ratio (a/H) is comparatively large, the Péclet number is often larger than 1 and that leads to dominance of hydrodynamic diffusion.
The particle Reynolds number increases with a/H ratio, which indicates that the lift effect becomes more pronounced at higher a/H ratio (equation 2.5). The same holds for shear-induced diffusion, where the shear-induced self-diffusion coefficient can be described by equation 2.9.

$$D_{shear} = D(\phi)\dot{\gamma}a^2 \qquad (2.9)$$

The typical average shear rate ($\dot{\gamma}$) in a channel can be estimated from the average flow velocity divided by the half-height of the channel (equation 2.6). $D(\phi)$ is a dimensionless function of the solid volume fraction (ϕ (-)), for which several comparable equations are known in literature. Here we follow the approach by Leighton and Acrivos (Leighton and Acrivos 1987) for spherical-shaped particles.

Chapter

2

$$D(\phi) = \phi^2 \left(1 + e^{8.8\phi}\right) \qquad (2.10)$$

In systems with gradients in concentration, shear rate and/or viscosity, the self-diffusion coefficient cannot be directly taken to describe migration and the shear-induced migration flux under these conditions needs to be taken into account. Phillips *et al.* (1992) proposed a model, described in equation 2.11 (Phillips, Armstrong et al. 1992).

$$J_{mig} = -D_c a^2 \phi \nabla\left(\phi\dot{\gamma}\right) - D_\mu a^2 \phi^2 \dot{\gamma}\nabla\ln(\eta(\phi)) \qquad (2.11)$$

In which D_c and D_μ are dimensionless parameters (possibly linked to the self-diffusion coefficient).

The gradients include the shear rate and the viscosity, which is influenced by the distribution of the particles over the channel. This relation shows that the particles will distribute unevenly when the suspension is subjected to a non-homogeneous shear field (e.g., Poiseuille flow). One can see that since the shear rate at the centre of a flow channel is zero, the equation predicts that particles will move towards the centre of the channel, even against their own concentration gradient.

Particle migration is much more likely to occur in small channels than in traditional process equipment that uses larger dimensions. First of all, the gradients will be larger; second, the distance over which migration has to take place is much shorter. Knowledge about these aspects is expected to drive development of micro-technological devices for e.g. food, biological and chemical applications in which particles from 0.1-10 μm are abundantly available much further.

2.3.4. Suspension characteristics

For shear-induced diffusion the dimensionless diffusion coefficient depends on the particle shape. Non-spherical particles have shear-induced diffusivities up to five times larger than spheres (Lopez 2008), e.g. Rusconi and Stone (2008) found values that were two times higher for plate-like clay particles (Rusconi and Stone 2008). Furthermore natural particles can be deformable. In case of inertial lift in Poiseuille flow, it was demonstrated that under the conditions where rigid particles migrate to an equilibrium radial position in the tube, neutrally buoyant, deformable particles may migrate to the tube axis (Karnis, Goldsmith et al. 1966) depending on the liquid behaviour (Gauthier, Goldsmit et al. 1971). Faivre *et al.* (2006) demonstrated this with deformable blood cells, which causes a larger particle free layer near the wall than found for rigid particles (Faivre, Abkarian et al. 2006).

All presented equations hold for monodisperse suspensions, but can also be applied to other suspensions that tend to be polydisperse due to natural variation. Polydispersity can cause several migration phenomena to be taking place simultaneously or causes a migration effect to be important over a broader range of sizes.

2.3.5. Overview of process conditions in relation to migration phenomena

In Table 2.1, an overview is given of the conditions expressed as dimensionless numbers related to migration mechanisms; please note, these values are indicative. Shear-induced diffusion is dominant in concentrated systems and at low Reynold numbers, while inertial lift is more dominant in dilute suspensions at high Reynolds numbers. Both low and high Reynolds numbers can be applied in microfluidics, which allows a choice in migration mechanism, as for example demonstrated in the work of Di Carlo who showed that inertial lift is abundantly used in microfluidic devices (Di Carlo 2009).

This is the general case, when using polydisperse suspensions, or suspensions with non-spherical or even deformable particles this will lead to extra implications for the technology used to determine concentration or velocity profiles in microfluidic devices. The spatial and temporal resolution of the technique will determine the range of particle Reynolds numbers and Péclet numbers that can be investigated.

For magnetic resonance imaging and ultrasonic pulsed Doppler velocimetry, a survey has been performed by Powell *et al.* (2008), and Aubin *et al.* (2010) discussed measurement techniques for microchannels, mainly focussing on mixing of fluids and measurement of droplets under static conditions (Powell 2008; Aubin, Ferrando et al. 2010).

Chapter

2

Table 2.1. Overview of conditions at which different migration phenomena are dominant.

	Pe	Re	Re$_p$	ϕ	a/h	a
Brownian diffusion	<1	<10	<1	Increase ϕ, decrease Brownian diffusion	N.A.	$a < 0.1 \cdot 10^{-6}$ m
Shear-induced diffusion	>1	<10	<1	Increase ϕ, increase shear-induced diffusion	Large ($a/h \geq 0.1$)	$0.1 \cdot 10^{-6}$ m < $a < 1 \cdot 10^{-5}$ m
Inertial lift	>1	10-1000	1-100	Increase ϕ, decrease inertial lift	Large ($a/h \geq 0.1$)	$a > 1 \cdot 10^{-5}$ m

The objective of this chapter is to evaluate all existing experimental methods which are able to give detailed information about migration phenomena in realistic, flowing suspensions. The evaluation includes optical techniques specifically targeted at confined flow geometries such as microfluidic devices, but also tomography and ultrasound. All methods are evaluated and compared, as presented in Tables 2.2 and 2.3, through which a choice can be made for the most appropriate method to study particle migration in suspensions in microfluidic devices, and an outlook is given on expected developments.

To be complete, modelling can be a useful tool to investigate particle migration, and considerable progress has been made in recent years. Erickson (2005) wrote an extensive review about modelling in microfluidic devices (Erickson 2005). The physics involved are very complex and necessarily 'simplified' systems are used in modelling; a recent review for mainly shear-induced migration in flowing viscous, concentrated particle suspensions is written by Vollebregt *et al.* (2010) (Vollebregt,

van der Sman et al. 2010). Further, it has been reported that entrance / exit effects are difficult to cover as are wall-particle hydrodynamic interactions (Al Quddus, Moussa et al. 2008), especially when differently shaped, deformable, natural particles are used, e.g. blood cells in blood vessels (Longest, Kleinstreuer et al. 2004), or when there is an obstacle in the channel (Roberto G 2000). For this review, we consider modelling techniques outside the scope.

2.4.   Evaluation criteria

The eight measurement techniques are presented in the next chapter, and four dimensionless numbers will initially be used for the evaluation. Two are already mentioned, i.e. Reynolds and Péclet number, and two others will be defined in sections 2.4.2.d and e and Table 2.2. However, there are more specific requirements that we summarized in eleven criteria related to the nature of the suspension, module or measurement parameters (discussed in sections 2.4.2. and Table 2.3). These eleven criteria can be divided into measurement parameters and technique characteristics, which are specific for the method used in relation to measurement of concentrated natural suspensions.

2.4.1.   Measurement parameters

Three quantities need to be measured, preferably simultaneously, all as function of the 3D location in the channel:

(1) The volume fraction of the particles;
(2) The velocity of the particles;
(3) The particle size (distribution) and shape.

A measurement technique is needed that allows for single particle detection in space as well as in time and discriminates between particles. As biological suspensions are often polydisperse, information about *particle size and spatial location* would be a key parameter to investigate.

For most measurement techniques it would be easy if particles of different size or shape have different material properties to distinguish them, or can be labelled with different markers; obviously in a real system this would mostly not be possible. On the other hand, if the size or shape of the particle itself can be

measured with the measurement technique, differentiation becomes more straightforward.

2.4.2. Technique characteristics

Below the list of technical characteristics that we identified as important for the measurement of realistic suspensions.

(a) The technique should not be limited to model suspensions, but should be usable with *practical media*. The fluidic properties of suspensions are dependent on many parameters; simplifying the suspension into a model suspension may well fundamentally change the behaviour of the fluid. Changing particle properties might lead to different migration behaviour and in industrial processes, particles should be traced inline in order to control the process.

(b) Practically relevant media are often *concentrated*, and therefore the technique should be able to measure concentrated systems. High concentrations of suspended particles can influence visibility; therefore, most systems are opaque, and optical measurement techniques are less suited. Often model systems are used in which the optical index of particles and surrounding liquid are matched. The reflection of light at the particle surface is minimized and consequently other properties of particles can be used to determine concentration and velocity profiles, e.g. fluorescently dyed particles under a laser microscope. Additionally, not all techniques are suitable to measure concentrated suspensions, due to scattering and interference, resulting in a low signal-to-noise ratio.

(c) As mentioned, the *signal-to-noise ratio* should be high enough to distinguish signal from noise. When the signal-to-noise ratio is too low, the data become less reliable. We could say that the signal needs to be at least twice as big as the noise, but preferably this ratio is larger. For example, the Péclet number from equation 2.7 should be larger than 1 to have sufficient signal over the noise caused by Brownian diffusion.

(d) The fourth characteristic is *spatial resolution*. Here also the suspension characteristics determine whether the spatial resolution of a technique is sufficient. Suspensions can be distinguished based on particle sizes

present and in this article we focus on suspensions, with sizes typically between 0.1 and 10 micron. Detection of single particles in these size ranges can only be possible in a measurement volume in the order of a few micron cubed. The measurement technique should therefore have a spatial resolution slightly smaller than 1 micron, i.e. $\Delta x/a < 1$.

(e) Besides spatial resolution, *time resolution* is important as well. The temporal resolution should be much smaller than 1 second at high velocities, for tracking particles in the flow, i.e. $\Delta x/v << \Delta t$ or $a/v << \Delta t$.

(f) It is obvious that the measurement technique should *be non-invasive*. If the flow is disturbed, migration of particles will be influenced.

(g) *Data analysis* can be time consuming and rather complicated. Especially for industrial use this should be prevented.

(h) Even though *cost* is not of the utmost importance for an analysis technique, some techniques, such as NMR, require extensive equipment when applied with high resolution. Obviously, a technique that yields the same resolution but is more cost effective is preferred.

2.5. Measurement techniques

2.5.1. Tomographic methods

a. EIT (Electrical Impedance Tomography)

Electrical Impedance Tomography is a technique where the difference in electrical conductivity is measured to determine the distribution of a phase with lower conductivity than the continuous phase. The technique was for the first time used to study the spatial distribution of air and water flow in a pipe (Cheney, Isaacson et al. 1999). Networks of wires were installed in the cross-sectional area; the extremely small diameter of the wires did not disturb the flow. Electrodes can also be installed at the outside of the pipe, thereby preventing any hindrance for the flowing suspension. From the conductance between two parallel wires, the phase distribution or particle volume fraction can be determined via numerical inversion, which is relevant for measurement of two-phase systems (Reinecke, Petritsch et al. 1998).

Advantages and disadvantages

EIT is a technique that can well be used for the measurement of concentration profiles of concentrated suspensions. Although EIT is not a common technique to measure particle migration in pressure-driven flow, it was successfully used by Butler *et al.* (1999), for suspensions up to 0.40 solid volume fraction, with 200 μm particles in a 2 cm channel (Butler and Bonnecaze 1999). Measurement of these concentration profiles can be done for a large range of Reynolds numbers, with velocities up to 3 m/s (Reinecke, Petritsch et al. 1998). However, the velocity profiles and particle sizes as a function of spatial position cannot be measured, while the data analysis is time consuming.

EIT is known to be a relatively inexpensive technique with a good time resolution; data can usually be measured within less than 1 second (Butler and Bonnecaze 1999; Kim, Kim et al. 2004), with a minimum of even 5 milliseconds (Reinecke, Petritsch et al. 1998). The main reason why EIT is not often used for suspension flow is the need for a large difference in electrical conductivity between particles and the fluid (Williams 2003) and its commonly poor spatial resolution (5% of the channel). Although Reinecke *et al.* (1998) showed that 1 μm particles flowing at a velocity of 1 μm/s could be detected in a 100 μm channel (1% spatial resolution), it should be noted that this is on the limit of the technique (Reinecke, Petritsch et al. 1998). Improvements in spatial resolution have mainly been focussed on combination of EIT with other techniques like Nuclear Magnetic Resonance, described in the next section, to create higher resolution conductivity images (Aubin, Ferrando et al. 2010).

Applicability for practical suspensions in microfluidic devices

Only recently EIT has been used in microchannels. Before, EIT was mainly applied to relatively large channels and particles. Measurement of particles smaller than 10 micron is shown to be possible, as long as the difference in conductivity between solvent and particles is sufficient. In milk, for example, the non-fat part of milk has a conductance of 5.40 mS at 100kHz, while addition of 3.6% fat reduces the average conductance to 5.05 mS. The conductance difference can be used to investigate the migration of milk fat globules with EIT, although spatial resolution might be low for 4 micron fat globules (Mabrook and Petty 2003). Ayliffe *et al.* (1999) successfully used microelectric impedance with integrated electrodes in a

Chapter

2

10 micron channel for the detection of biological cells and a polymer dispersion (Ayliffe, Frazier et al. 1999). This technique (sometimes slightly modified) is increasingly used in biological cell characterisation in small chips (Cheung and Renaud 2006). Also Bao *et al.* (2008) have written an extensive review about electric analysis of cells in microfluidic devices (Bao, Wang et al. 2008). The short measurement distance in microchannels improves conductivity measurement, as long as electrodes and no wires are used (Ayliffe, Frazier et al. 1999), and this is a big pro for application of this technique.

    b.   NMR (Nuclear Magnetic Resonance)/ MRI (Magnetic Resonance Imaging)

Nuclear Magnetic Resonance is often used to study migration of particles; the interested reader is referred to a recent review by Powell *et al.* (2008) (Powell 2008). NMR allows the detection of the volume fraction(s), the physical behaviour (physical response) as well as properties (physical system's state). The sample is placed in an external magnetic field and commonly the resonance frequency of protons (1H), as well as the relaxation times of the signal are measured. The amplitude of the signal can be related to proton density, which is related to the amount of a certain component present (Windt 2007).

Advantages and disadvantages

The main advantage of NMR is its versatility: many parameters can be evaluated simultaneously, including concentration distributions, velocity fields, diffusion rates and velocity fluctuation correlations, as well as information on pores and viscosity (Powell, Maneval et al. 1994; Fukushima 1999). Interesting is the possibility to measure size distributions of droplets in an emulsion, based on hindered diffusion of one component in another phase (Packer and Rees 1972; McCarthy and Kerr 1998; d'Avila, Powell et al. 2005). Especially d'Avila *et al.* (2005) studied concentrated emulsions under flow and showed the possibility to measure velocity, droplet size distribution and volume fraction with different techniques within MRI, although the droplet sizes were measured under static conditions (d'Avila, Powell et al. 2005). The NMR technique can measure highly concentrated suspensions without disturbing fluid flow. The range of flow velocities are typically between 10^{-4} and 1 m/s at a velocity resolution of a few tens of µm/s (Kose 1992), and temporal resolutions of 32 ms can be applied (Raguin and Ciobanu 2007). This

implies that both shear-induced diffusion and inertial lift can be monitored. A drawback is that NMR is a relatively specialized technique, with expensive equipment, and the need for trained staff to operate and interpret the results. Another disadvantage is that often many assumptions have to be made on the specific properties of materials. Additionally, the signal-to-noise ratio for an NMR experiment is, amongst others, strongly proportional to the strength of the magnetic field. Thus, from a purely signal over noise (S/N) consideration, NMR should be done in the strongest field possible (B_0), as indicated in equation 2.12.

$$\frac{S}{N} \sim \sqrt{B_0^{\,3}}$$
(2.12)

In which, B_0 is the static magnetic field strength (T), S is the signal (Hz) and N is the noise (Hz) (Hoult, Chen et al. 1986).

However, there is a trade-off between intensity of the magnetic field and the volume of the effective field; it is not so easy to make homogeneous, strong field magnets in a large volume. One should also be aware that there is always an optimisation between spatial and temporal resolution (Powell 2008). Spatial resolutions of up to 10 μm can be obtained for ^{1}H of water, however a spatial resolution of 50-100 μm is more realistic (Lens, Gastesi et al. 2003; Gao, Xu et al. 2009).

Applicability for practical suspensions in microfluidic devices

Various techniques within NMR and MRI are able to measure velocity and concentration profiles, but spatial resolution is relatively low (Altobelli, Givler et al. 1991). The most common method is MRI, where measurement of velocity and concentration profiles in flowing suspensions is done in large devices and with large particles (Majors, Givler et al. 1989; Chow, Sinton et al. 1994; McCarthy and Kerr 1998). More recently smaller dimensions were studied. Brown *et al.* (2009) investigated the migration of 2.5 μm particles in a 1 millimeter channel and Zhang *et al.* (2010) made use of high static magnetic fields generated by microcoils, to study two-phase flows in 400 μm capillaries (Brown, Fridjonsson et al. 2009; Zhang and Balcom 2010). Measurement in microchannels was possible but only in strong fields, which through the use of small coils to drastically improve signal-to-

noise, may be within reach. Developments in this field are going fast, clearly shown by the article of Lee *et al.* (2009), where a new generation of diagnostic magnetic resonance (DMR) sensors was developed, that combines a microprobe with magnetic nanoparticles, to detect cancer cells (Lee, Yoon et al. 2009).

To deal with the relatively low spatial resolution, another option is to not use direct imaging as such but instead measure the distribution of the volume fractions as a function of velocity in the channel. This implies that there is no spatial registration and therefore no spatial resolution limit. The probability distribution of the velocity over a spatial range will be measured and the data give a statistical distribution of the displacement for all particles (Garroway 1974; Fukushima 1999). A distribution curve can be made, in which the chance to find a certain velocity is on the y-axis, and the velocity itself is on the x-axis.

Static conditions in suspensions are relatively easy to measure with MRI, but under dynamic conditions higher temporal and spatial resolutions are needed. Particle size can be derived from hindered diffusion inside the particle (in the case of e.g. emulsion droplets) which is the diffusion perpendicular to the flow, but the signal-to-noise ratio has to be drastically improved when one investigates particle flow in a microchannel. Particle sizes with different material properties can be chosen and major particle components can be distinguished through spectroscopic investigation or by investigation of the relaxation times. Additionally, the relaxation time is strongly concentration dependent; so information about concentration profiles can be obtained. All these possibilities show that NMR can be a very useful tool to study particle behaviour in microchannels.

c.   **PEPT (Positron emission particle tracking) / Neutron and x-ray radiographies/ tomographies**

Neutron and x-ray radiography are imaging techniques, capable of showing particle concentration profiles. Where the x-ray imaging relies on the presence of elements with higher atomic number, neutron scattering imaging depends on the presence of a few specific elements. Neutrons are attenuated by some light materials, i.e. hydrogen, oils, plastics and water, but penetrate many heavy materials, like metals. The neutron beam is recorded after penetrating a sample,

and an image representing the macroscopic structure is obtained; the penetrating radiation has a wavelength less than 10 nm (Prince 1999). As a result the neutron radiography technique can be used to characterize the flow of tracer particles through metal shrouded pipes, as demonstrated by Cimbala *et al.* (1988) (Cimbala and Sathianathan 1988).

Chapter

2

X-ray radiography has been successfully applied for profiles of alumina and glass particles in composite-polymers (Lagasse and Thompson 2002); the x-ray source being poly-energetic (Yaffe and Rowlands 1997). One could see tomography as a more advanced form of radiography, because images are made of one geometric plane of the object, while in general with radiography a kind of 'shadowgram' is made (Novelline 1997).

Advantages and disadvantages

Neutron and x-ray radiography are capable of studying two-phase flows in any geometry, and can penetrate materials often used for equipment; they are non-invasive (Mondy, Graham et al. 1986). At the same time, they are not abundantly used given the expensive equipment, specialized facilities and staff needed (Williams 2003). Further, the spatial resolutions are generally not high (Chaouki, Larachi et al. 1997), as demonstrated in the studies of Lagasse *et al.* (Lagasse and Thompson 2002) and Mondy *et al.* (2008), where a spatial resolution of 0.2 mm was reached for x-ray radiography and particle and bubble sizes were between 1 μm and 1.7 mm (Mondy, Retallack et al. 2008). The temporal resolution was found to be high, namely 66 microseconds. Addition of multiple x-ray source/sensor pairs also improves scan time and reconstruction time (Williams 2003). With neutron and x-ray radiography both concentration profiles as well as velocity profiles can be measured (Mondy, Graham et al. 1986) and velocities in the range of 0-30 cm/s can be used (Mishima and Hibiki 1998).

Applicability for practical suspensions in microfluidic devices

X-ray radiography is often related to metal applications (Saito, Mishima et al. 2005), but in the study of David *et al.* (2008), the concentration of casein micelles was studied above a membrane with small-angle x-ray scattering, having a spatial resolution of 100 micron and a temporal resolution of a fraction of a second (David,

Pignon et al. 2008). Unfortunately, the membrane module material did influence the scattered signal of the beam, but Davit *et al.* (2011) showed that the contrast between particles (biofilm) and surrounding (porous media) could be enhanced with the addition of contrast agents (Davit, Iltis et al. 2011). Further, spatial resolution can be drastically increased to 9 micron with x-ray microtomography and even up to 5 μm per voxel. Suspension particles in microchannels need higher resolution, but the trends towards microtomography show great potential for this technique in natural suspensions. Microfocused small-angle X-ray scattering has been used to study concentration and structure of nanoparticles in space and time with a micron spatial resolution (Merlin, Angly et al. 2011). Further, to trace different sized particles a difference in contrast is needed.

Food systems are sometimes analysed with neutron radiography, e.g. the structure of corn kernels (Cleveland Iv, Hussey et al. 2008), mainly based on the presence and absence of water. X-ray tomography can be used in the study of blood flow with contrast agent in for example a dialyzer (Sakai, Wada et al. 2003) or for the transport of naturally mobile particles, through microchannels in the soil, into the groundwater (Rousseau, Di Pietro et al. 2004).

Positron emission particle tracking or PEPT is used to track a single radioactively labelled tracer particle in food multiphase systems (Fryer, Fairhurst et al. 2000). Since the tracer particles should have a minimum size of around 60 μm to have enough radioactive load, this is beyond the size range of interest of this chapter (Fan, Parker et al. 2006).

2.5.2.   Ultrasonic measurement

d.   UPDV (Ultrasonic pulsed Doppler velocimetry) and UVP (Ultrasonic velocity profile)

The use of ultrasonic waves to determine velocities is very similar to Laser Doppler Anemometry and Laser Doppler Velocimetry. For velocity determination, the Doppler shift in the frequency of an ultrasonic wave scattered from a moving particle is determined at different positions. The acoustic pressure is usually related to the velocity of the particle given in equation 2.13.

$$p = \bar{v} Z \tag{2.13}$$

In which p is the acoustic pressure (kg/m·s²), Z is the characteristic impedance, which is dependent on the material properties (kg/m²·s) (see equation 2.14) and $\bar{v}$ is the particle velocity (m/s).

$$Z = v_{sound} \rho \tag{2.14}$$

where ρ is the density (kg/m³) and v_{sound} the speed of sound (m/s).

When particle-particle interactions are taking place, especially in concentrated systems, the sound attenuation is found to be different and consequently the (particle size) measurement changes (Dukhin, Goetz et al. 1996).

Advantages and disadvantages

UDPV and UVP are both 'light' in equipment, training, and staff costs compared to other techniques. The technique is non-invasive, and non-transparent samples can be measured (Manneville 2008). Spatial resolutions are about 40 μm and the temporal resolution varies between 0.02 to 2 second as shown by Manneville *et al.* (2004) for a dilute oil-in-water emulsion (Manneville, Becu et al. 2004). For concentrated emulsions, multiple scattering and adsorption of ultrasonic waves severely influences the results (Kytömaa 1995). Christopher *et al.* (1997) measured a velocity between 0.5 and 5 mm/s in blood flow, with temporal resolutions between 15 and 100 ms (Christopher, Burns et al. 1997). The technique is therefore well capable of measuring shear-induced diffusion, although for inertial lift, the maximum measurable velocity (which can be derived from the Nyquist theorem; equation 2.15) is probably not high enough.

$$v_{max} = \frac{v_{wave}}{4 t_{prf} F_e \cos(\theta)} \tag{2.15}$$

In which v_{max} is the maximum velocity (m/s), v_{wave} is the sound velocity of the ultrasonic wave in the fluid (m/s), t_{prf} is the time between two emissions (s), F_e the emitting frequency (Hz) en θ the angle between two intersecting waves (°) (Nyquist 2002).

UVP can measure velocity profiles (Yamanaka, Kikura et al. 2003), but concentration profiles are not easy to measure, due to multiple scattering and low spatial resolution (Kytömaa 1995). However, Wang *et al.* (2003) developed a method that allowed measurement of the concentration as well as the location. The spatial location follows from the velocity of an ultrasound wave through the different materials (i.e. the wall, liquid in tube) and the time span between emitting and receiving the pulse. Additionally, the concentration of particles is related to the decrease in received ultrasound intensity as a result of backscatter (Wang, Wang et al. 2003). Measuring spatial orientation of particles in concentrated suspensions is not straightforward due to multiple scattering. To determine the spatial position of large and small particles in a polydisperse suspension is outside the reach of this technique.

Applicability for practical suspensions in microfluidic devices

To distinguish particles from the surrounding fluid and determine the velocity of the particles, the characteristic impedance of materials can be used. In milk for example, the impedance values of water and 9% protein are respectively $1.49 \cdot 10^6$ and $1.83 \cdot 10^6$ kg/m^2·s, while milk itself has a characteristic impedance of $1.56 \cdot 10^6$ kg/m^2·s (Wallhäußer, Hussein et al. 2011). The flow of blood is abundantly studied with ultrasonic techniques, where blood cells have a characteristic impedance of $1.6 \cdot 10^6$ kg/m^2·s and blood vessels of $1.7 \cdot 10^6$ kg/m^2·s. It is however not possible to distinguish the signals in three phase systems; information on bidisperse suspensions and their spatial orientation is therefore outside the reach of this technique. Based on the low spatial resolution of 40 micron (Peters, Lobry et al. 2010), high prevalence of multiple-scattering and the ability to only measure velocity profiles, this method is not a logical choice to measure flow of most practical suspensions in microchannels.

2.5.3. Optical methods

e. LDV (Laser Doppler Velocimetry) and LDA (Laser Doppler Anemometry)

In LDA and LDV, velocity of particles is determined by comparing the interference patterns (fringes) from two laser beams with the scattered light from a crossing particle (Andersson and Rasmuson 2000). Also concentration profiles can be

determined by measuring the time between two particles entering the probe volume (Lyon and Leal 1998).

Advantages and disadvantages

The concentration and velocity profiles can only be measured with LDA when the dispersed phase is dilute enough to have not more than one particle at a given time in the sample volume. The detection volumes should be small, but not smaller than the particles. The fringe spacing of the lasers determines the particle sizes that can be measured, as described in equation 2.16.

$$d_f = \frac{\lambda_{wave}}{2\sin(\theta/2)}$$ (2.16)

In which d_f is the fringe spacing (m), λ_{wave} the wavelength (m) and θ the angle between two intersecting waves of beam light (°) (Ayranci, Pinguet et al. 2007).

Durst *et al.* (1981) concluded that a particle diameter to fringe ratio of 0.5-2.0 gives the highest signal-to-noise ratio, which implies (taking the wavelength into account) that a range of particle sizes between 0.3 and 16 μm is within reach, which makes this technique suitable for most natural systems (Durst, Melling et al. 1981). The overall signal-to-noise ratio is not very high, due to a generally weak light intensity due to scattering (Ayranci, Pinguet et al. 2007); the signal can also be influenced by the wall (Koh, Hookham et al. 1994). LDV and LDA do not disturb the flow (Bachalo 1994) and have good spatial resolution, first reported from 20 μm to several mm (Koh, Hookham et al. 1994) and more recently down to 1.6 μm (Voigt, Bayer et al. 2008). Three velocity components, ranging from 10^{-5}-10 m/s (broad range of Pe and Re), can be measured with wide range and high-resolution sensors (Havelock 1996). However, it is not possible to discriminate on particle size with either technique (Bachalo 1994), but Phase Doppler Anemometry, might be a solution to this. PDA is an extension of LDA (Voigt, Bayer et al., 2008), not only using the Doppler shift frequency to determine velocity, but also the phase shift at three different receiving locations to derive the diameter of the scattering particle (Ayranci, Pinguet et al. 2007). It should be mentioned that scattered light intensity and polarization depend strongly on the viewing angle and the refractive indexes

of the continuous and dispersed phase. The costs of these techniques are still fairly high due to the lasers as well as the processing equipment. There is a trend towards cheaper semi-conductor lasers, although some issues still need to be resolved (Maru and Fujii 2010).

Applicability for practical suspensions in microfluidic devices

In microchannels the signal-to-noise ratio near the wall is low, as a result of a high surface to volume ratio, and this leads to a bias in the data. For the measurement of concentrated suspensions with LDA and LDV, the refractive index of particles and fluid needs to be matched, which often leads to the use of model suspensions. It is a challenge to translate data from model systems to realistic products and therefore measurement of real media is preferred. Although the spatial resolution can go down to 1.6 micron, mostly micro-PIV is used when microchannels are concerned and this technique is described in section 2.5.3g (Di Leonardo, Leach et al. 2006). The main advantage of PDA is that particle size, velocity and concentration can be obtained simultaneously. The other pros and cons, as well as the applicability for realistic suspension in microchannels are similar to LDV an LDA.

f. **PTV (Particle Tracking Velocimetry)**

With Particle Tracking Velocimetry, particle behaviour in flow can be visualized by two cameras, creating a 3D image (see Figure 2.1). Particles are fluorescently labelled and are individually tracked in consecutive images. Afterwards the directionally resolved vector is computed for each pair of matched particle-images.

Advantages and disadvantages

The PTV technique allows analysis over the whole volume during the whole time, rather than point-by-point, as is the case with other anemometric techniques (Durst 1980). The limitation of PTV is the gathering of large amounts of data about the flow field, which requires extensive analysis of multiple images (Adamczyk 1988). The spatial resolution of PTV is generally not so high, and depends on the resolution of the camera and on the observation volume. In the article of Maas (1993), the spatial resolution was in the order of millimetres, with 1000 particles in a flow field at a time resolution of 40 ms (Maas 1993).
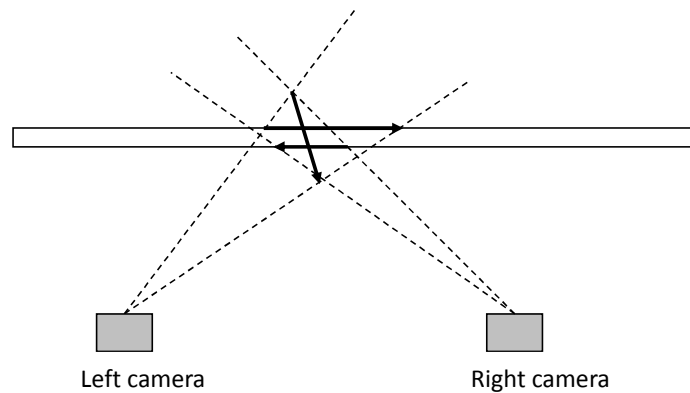
Figure 2.1. Two cameras to create a 3D view.

In the last years this technique has improved and is now able to measure length scales from 0.1 to 100 μm (Williams, Park et al. 2010) and a temporal resolution of 10 ms (Lima, Ishikawa et al. 2009). To improve visualisation of the particles, they need to be at least in the nanometre range (Kikura, Matsushita et al. 2004). The concentration is limited to allow identification of single particle trajectories, which may be improved by creation of a vector for each particle as discussed in the next section.

Applicability for practical suspensions in microfluidic devices

Velocity and concentration gradients as well as particle size can be determined with PTV, although as with all optical methods, refractive index matching has to be done for concentrated systems. Spatial resolution of PTV has been improved, but for the measurement of particles between 0.1 and 10 micron in microchannels, the technique should be combined with a more sophisticated, sensitive method like micro-PIV as described next, similar to micro-PTV.

g.   Micro-PIV (Micro Particle Image Velocimetry)

Particle Tracking Velocimetry is actually a low-image-density PIV method (Keane 1995). To investigate fluid flow in a micro-fluidic device, micro-PIV is an option. Fluorescent, neutrally buoyant tracer particles that are large enough to minimize the influence of Brownian motion (Pe > 1) are added to the fluid (Meinhart, Wereley et al. 1999). Two lasers are used and images are recorded using a high-speed CCD camera. From the spatial correlation of the position of the particles in

different images, velocity gradients of the fluid can be derived. Statistical analysis is used to evaluate the particle-image displacement as a function of the spatial resolution (Westerweel 1997). When PIV is combined with PTV, two cameras detect the light which yields a   3D velocity image with high spatial resolution. PTV creates a vector for each particle, while PIV creates one vector for each window (Stitou and Riethmuller 2001). Micro-PIV has been combined with confocal scanning laser microscopy (CSLM) (Park 2004); Lindken *et al.* (2006) used stereo micro-PIV, where two cameras are detecting fluorescence from particles illuminated by a double pulse laser and viewed by a stereomicroscope (Lindken, Westerweel et al. 2006).

Advantages and disadvantages

The main advantage of PIV over other techniques is that PIV produces detailed information on the spatial distribution. The analysis is however time intensive, leading to a limited amount of data (Bachalo 1994). The spatial resolution of PIV is strongly dependent on the optics and co-determined by the size of the measurement volume, which is typically a fraction of a mm (Keane 1995). For sufficient resolution the smallest particles span at least 3-4 pixels in diameter. Increasing the spatial resolution to 1 μm has recently been shown possible in so-called super-resolution PIV, with observation volumes of 13.6 by 0.9 by 2.2 μm^3 (Santiago, Wereley et al. 1998; Aubin, Ferrando et al. 2010). The temporal resolution may range from tens of nanoseconds up to a few seconds. This interval can be reduced to nanoseconds by changing the camera resolution, illustrating the dependency of both time and spatial resolution on camera characteristics (Meinhart, Wereley et al. 1999). Typical velocities that can be measured are from μm/s to cm/s, e.g. 3.3 cm/s for 80 μm particles (Willert 1991).

The amount of fluorescent particles in the observation volume should be at least 2-3, which implies that the concentration of fluorescent particles in the suspension should be sufficiently high, while fluorescent light scattering at high concentrations should be prevented. PIV was initially developed for the measurement of velocity profiles, but concentration profiles are within reach by combination with PTV or CSLM.

Applicability for practical suspensions in microfluidic devices

In concentrated systems, particles need to be optically matched with the carrier fluid. The particle size needs to be larger than the wavelength of the laser light, which is usually 532 nm; micron-sized particles can be measured. The velocities are mainly in the μm/s range (low Re) when micro-PIV is used in combination with CSLM (Park 2004). Increasing the velocity will lead to streaks, and less reliable results (Santiago, Wereley et al. 1998). Since high spatial resolutions can be obtained with micro-PIV, it can be applied for flowing suspensions in microchannels without any problem, albeit that model systems are needed.

Chapter

2

h. CSLM (Confocal Scanning Laser Microscopy)

Confocal scanning laser microscopy receives the emitted light from a fluorescent sample that was excited with laser light, by optically focusing on a small volume in the channel. Although for CSLM, concentrated suspensions should have particles where the refractive index is matched with the surrounding liquid, this technique can eliminate out-of-focus parts and select an optical section from a thick sample much easier than the conventional microscope (Prasad, Semwogerere et al. 2007). An extensive study by Sandison and Webb (1994) showed that the signal-to-noise ratio obtained with a confocal microscope can be more than 100 times greater than with a conventional microscope (Sandison and Webb 1994). Rusconi and Stone (2008) showed that with a conventional fast-scanning microscope measurement of particle suspensions up to solid volume fractions of 1% is possible, but for concentrated systems this technique becomes limited (Rusconi and Stone 2008).

Advantages and disadvantages

For microscopy, there is always a balance between number of pixels of the image, speed of the pictures taken, magnification used, thickness of the measured area, etc., comparable to PTV and micro-PIV. At high particle concentration, a lower signal-to-noise ratio is obtained, which influences velocity calculations when combined with PIV analysis (Park 2004). Additionally, refractive index matching of the particles with the surrounding solution is needed, as is the case for all optical methods, which limits the type of systems that can be studied. Maximum velocities that can be measured are dependent on the optical system (camera, objective) and

observation volume chosen. With a field of view of 55 by 55 µm², and a 100·1.35 numerical aperture objective, the temporal resolution is 11 ms and particles can flow with velocities up to 5 mm/s (Semwogerere, Morris et al. 2007). In the article of Frank *et al.* (2003), even speeds up to 8 mm/s were measured, similar to the velocities mentioned by Besseling *et al.* (2009) (Frank, Anderson et al. 2003; Besseling, Isa et al. 2009).

Applicability for practical suspensions in microfluidic devices

CSLM can focus on an image at a specific height in the channel and combined with refractive index matching (model suspensions), gives the possibility to look at relatively concentrated suspensions. An illustrative example is given in the study of Isa *et al.* (2006), where concentrated suspensions with particles of around 1 µm were flowing through microchannels (Isa, Besseling et al. 2006). Concentration profiles, as well as velocity profiles can be determined, although this has not yet been published for polydisperse suspensions. This is possible using different fluorescent dyes and following the particle movement by taking successive images (comparable to PTV).

In the paper of Park *et al.* (2004) both CSLM and micro-PIV have been applied to creeping Poiseuille flow in microchannels of 99 µm internal diameter and several other authors have used CSLM as well to investigate particle behaviour in microchannels as the technique is able to focus on small volumes (Dinsmore, Weeks et al. 2001; Frank, Anderson et al. 2003; Derks, Wisman et al. 2004; Park 2004; Isa, Besseling et al. 2006; Prasad, Semwogerere et al. 2007; Wu, Brand et al. 2007; Conrad and Lewis 2008; Semwogerere and Weeks 2008).

i.   FCS (Fluorescence Correlation Spectroscopy)

The concept of FCS was introduced in the early 1970s (Magde, Webb et al. 1972) in biological and chemical research. The technique is based on fluctuation measurement of a fluorescence signal from a particle in a voxel (Figure 2.2a) (Thompson 2002); combined with a high-speed camera it enables visualization of the flow. The length of each track in an observation volume corresponds to the particle velocity (Hashmi, Loewenberg et al. 2007). Further the fluorescent signal can be plotted against time, from which an autocorrelation function can pick up

very subtle changes in fluorescence intensity (Figure 2.2b), related to diffusion coefficients and average number of particles.

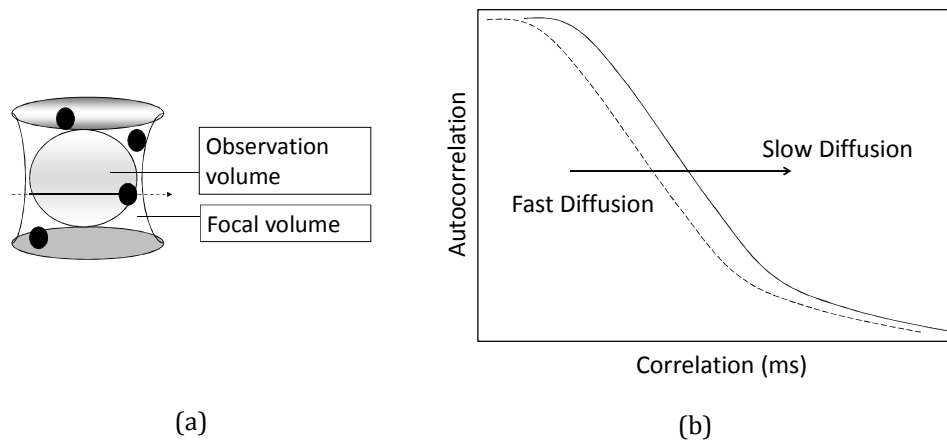(a)   (b)

Figure 2.2: FCS. (a) Focal and observation volume; (b) Autocorrelation curve obtained from fluorescence signal that is converted to average fluorescence.

Advantages and disadvantages

Spatial resolutions of FCS are in the order of microns, as shown by Brister *et al*. (2005), where the length-scale covering the x-axis of the detection volume was around 0.3 to 0.5 μm and the length-scale covering the z-axis was 1.5 to 3 μm (Brister, Kuricheti et al. 2005). Temporal resolutions are from 1 ms to more than 10 seconds in an observation volume of around 10^{-6} μm^3, for velocities of 1 to 200 mm/s and particle concentrations of $2 \cdot 10^6$ to $1000 \cdot 10^6$ particles/μL (Brister, Kuricheti et al. 2005). Generally, the signal-to-noise ratio is high: $1 \cdot 10^5$ photons for the signal, compared to less than 20 photons for the background (Kunst, Schots et al. 2004). Further, the required instrumentation and data analysis method are relatively simple. The technique works well for 2D systems, and in combination with confocal microscopy techniques, 3D systems can be analysed (Berland, So et al. 1995). The data that can be derived from FCS are concentration and velocity profiles as well as particle sizes, when different particle sizes contain different dyes. In very concentrated suspensions, scattering cannot be neglected, and this limits the applicability of the technique.

Applicability for practical suspensions in microfluidic devices

The FCS technique is suitable to derive information from flow in microchannels, as illustrated in the article of Lumma *et al.* (2003), where the entire velocity profile was directly probed within a 110 μm wide channel (Lumma, Best et al. 2003). The small focal volume is an advantage, although it might be even too small for some natural suspensions. FCS is a very good technique to analyse diluted suspensions (of nanoparticles) in microchannels.

2.6.   Comparison and future developments

In the former sections, optical, tomographic and ultrasonic methods were described, and information was given on their applicability for the study of suspension flow in microfluidic devices. In Table 2.2 the techniques are evaluated on the basis of four dimensionless numbers: the table indicates at which Reynolds numbers and Péclet number the technique is able to operate and the range of velocity, spatial and temporal resolutions. Table 2.2 shows that all techniques have different ranges of operation as illustrated by the values of the dimensionless numbers, but based on this table a technique to measure suspension flow in microchannels cannot be selected. In order to come to a conclusion about the applicability of the technique for particle flow in microchannels, the criteria mentioned in section 2.4.2. are needed and table 2.3 elaborates on the suitability of the techniques for suspensions in microchannels. In the table, an overview is shown of all methods, and + and – signs are used to indicate the suitability of a technique concerning different evaluation characteristics. For measurement of concentrated suspensions in microchannels, none of the methods satisfies all requirements, and compromises have to be made. If we assume that realistic suspensions behave like suspensions of hard spheres, one can use model systems of refractive index-matched fluid and microparticles, as used in CSLM and a realistic image of a flowing suspension in a microchannel can be obtained, because CSLM can focus on one specific height in the sample. Optical techniques have improved considerably in the last years, e.g. high resolution stereo micro-PIV. These improvements are related to improved spatial resolution and combinations of techniques (e.g. PTV with micro-PIV and CSLM, FCS with CSLM), which makes them suitable for measurements at small scale. UDPV, UVP, EIT as well as neutron and x-ray radiographies have low spatial resolution and measurement of realistic

suspensions in microchannels is difficult. NMR may have low spatial resolution for microchannels, but distribution analysis might be a solution for this. Besides, NMR allows visualisation of migration in real systems at higher velocity. Clear improvements of NMR systems were made in the last years, e.g. smaller probes and stronger magnets give increased sensitivity and spatial resolution (Wolters, Jayawickrama et al. 2002). Additionally, NMR enables the measurement of highly concentrated suspensions, which is not straightforward with optical methods. Recently, it even has been demonstrated that MRI can be used to investigate flow properties and measure local flow phenomena (Bonn, Rodts et al. 2008); all these developments make us conclude that NMR has considerable potential for registration of flow of micro-sized particles in microchannels. Regarding FCS, micro-PIV combined with PTV and LDA/PDA, these optical techniques have a great potential for measurement in microchannels; however, their major drawback is, besides the need for refractive index matching, that micro-PIV and PTV are mainly developed to measure velocities and are not able to determine size of the particles directly. Further, wall effects influence the results for micro-PIV and LDA/PDA, and FCS could be interesting for particles in the range of nanometres, but becomes less sensitive when larger particles are used.

In section 2.3.1. we started with defining the Reynolds number for a rectangular channel, although migration phenomena also occur in tubes. All measurement techniques can measure flow in tubes as well, although the curvature of the walls might affect the laser beam for optical techniques. The tube can be placed in a solution with the same refractive index as the channel wall to minimize this effect. Furthermore, although no attention has been paid to transient effects, such as wall slip or transient clogging, which can have large effects on migration of microparticles, it would be very interesting to select a method that would be suitable to measure these effects.

2.7. Conclusions

In this review chapter optical, tomographic and ultrasonic methods were evaluated for the study of the behaviour of practical suspensions flowing through microfluidic devices. The focus was on (concentrated) natural suspensions, typically having particle sizes between 0.1 and 10 micron and under these

circumstances, shear-induced diffusion seemed the most dominant migration mechanism. To measure migration under these conditions, NMR and CSLM seem to be the most promising methods, in spite of the related costs. NMR allows differentiation of real particles based on material characteristics at high concentration. Even though imaging is not possible, because of the general low spatial resolution, there is still a lot of potential in its use for distribution analysis. CSLM allows measurement in microchannels by focussing on one height, but matching of refractive indices of the fluid and the particles is needed, which results in analysis of model suspensions. The most direct method for a realistic suspension appears to be NMR, where limitations may occur regarding channel size. CSLM, on the other hand, is very suited to show migration phenomena of particle sizes that are relevant in natural systems, with model suspension in microchannels. A combination of results obtained with these two techniques is expected to be useful in the design of devices that use microchannels for all types of natural occurring suspensions.

Table 2.2. Overview of scores on dimensionless numbers for different techniques.

| Method | Tomographic methods | | | Neutron and x-ray radiographies | Ultrasonic methods | Optical methods | | | |
	EIT	MRI	NMR (no imaging)		UPDV/ UVP	(μ)-PIV + PTV	LDV/ LDA/ PDA	CSLM	FCS
Péclet number (>1)	>>1	>>1	>>1	>>1	>>1	>>1	>>1	>>1	>>1
$\Delta x/a$ (<1)	<10	<100	N.A.	<100	>100	<10	<100	<10	<1
$v\Delta t/\Delta x$ (<1)	<10	<10	N.A.	<1	<1	<<1	<10	<10	<10
Reynolds number	>10	<100	<100	<100	<10	<100	<100	<10	<10

Péclet number: The ratio between hydrodynamic forces and Brownian diffusion.

Reynolds number: The ratio of inertial to viscous forces.

Chapter

2

Table 2.3. Overview of scores on evaluation criteria for different techniques.

	Method	Tomographic methods				Ultrasonic methods	Optical methods			
		EIT	MRI	NMR (no imaging)	Neutron and x-ray radiographies	UPDV/ UVP	(μ)-PIV + PTV	LDV/ LDA/ PDA	CSLM	FCS
Measurement parameters	Velocity profile	- -	++	++	++	++	++	++	++	+
	Concentration profile	++	++	++	++	+	++	++	++	++
	Bidisperse / polydisperse system	+ (constrast conductivity)	+ (difference material properties)	+ (difference material properties)	+ (contrast neutron/x-ray signal)	- -	- - (different labelling)	++ (PDA)	++	+ (different labelling)
Technique characteristics	Measure real media	+ (contrast conductivity)	++ (amount protos)	++ (amount protons)	+ (contrast neutron/ x-ray signal)	+	- (fluorescent)	- (fluorescent)	- (fluorescent)	- (fluorescent)
	Concentrated suspensions	+ + (up to 0.4)	++ (higher ϕ, more signal)	++ (higher ϕ, more signal)	+	- - (scattering)	- - (scattering)	- - (scattering)	+	- - (scattering)
	Signal-to-noise (S/N)	- -	-	-	-	-	-	-	+	++
	Spatial resolution	+ (1-5% of tube)	- (10 μm)	N.A.	+ (1 μm)	- - (40 μm)	+ (1 μm)	+ (1.6 μm)	+ (1 μm)	++ (0.1 μm)
	Time resolution	+ (5 ms-1 s)	+ (32 ms)	+ (32 ms)	++ (66 μs)	+ (0.015-2 s)	++ (0.1 ns-1 s)	+	+ (11 ms)	+ (1 ms-10 s)
	No disturbance flow and non-invasive	+ (invasive)	++	++	++	++	++	++	++	++
	Data analysis	- -	-	-	-	+	- -	+	+	-
	Costs	+	- -	- -	- -	++	- -	- -	- -	- -
Total		4+	7+	8+	7+	3+	2+	5+	10+	5+

Chapter 3

Flow-induced Particle Migration for improved Membrane Microfiltration and Fractionation Processes

3. Flow-induced Particle Migration for Improved Membrane Microfiltration and Fractionation Processes

3.1. Abstract

Chapter

3

Microfiltration is commonly designed for maximum flux. We here show that different options are available when starting the design at the particle level. The behaviour of suspensions between 9 and 38 volume% was studied by CSLM; migration as a result of shear-induced diffusion was observed in a rectangular closed channel. Under all investigated conditions, particles segregated on size within the first 10 centimetres of the channel (an entrance length of 1000 times the channel height). To illustrate this, at around 20 volume% of small (1.53 μm) and large (2.65 μm) particles each, the larger particles migrate to the middle of the channel, while the small particles have high concentrations near the walls. This also implies that the small particles can be collected from their position close to the wall in case of permeable walls, e.g. membranes, and that the pore size of the membrane is no longer the determining factor for separation.

Guidelines for using this phenomenon in a microfiltration process were derived and the selectivity of the process was experimentally evaluated in proof of principle experiments. The small particles could be removed from the mixtures with a membrane having pores 3.7 times larger than the particles, thereby minimizing accumulation of particles in and on the membrane. As long as the process conditions are chosen appropriately, no particle deposition takes place and high fluxes ($4.4 \cdot 10^4$ L·h^{-1}·m^{-2}·bar^{-1}) can be maintained.

3.2. Introduction

Microfiltration is mostly used to remove particles from a liquid stream. It is carried out in many industries and for different applications (Strathmann 2001), for example to remove bacteria from liquid foods, and is optimised for high trans-membrane flux. For this, membrane fouling and flux reduction as a result of (temporary) particle accumulation are mostly taken for granted, and for example high frequency back-pulsing may be used to temporarily remove the particles from the membrane and keep the membrane flux at acceptable levels.

As the design of such processes mostly revolves around obtaining as much permeate as possible, the neglect of the dynamics of the suspension on the particle level leads to fouling and therefore stresses the importance to use particle behaviour as an alternative design parameter. When starting from the behaviour of the particles themselves, a different process that operates without fouling or flux reduction may be the result, and this could revolutionise membrane process design. The pioneering work of Belfort who described the effect of inertial lift is exemplary for this (Belfort 1989); in this chapter we focus on shear-induced diffusion as migratory mechanism, but we also cover other mechanisms.

For microfiltration, the influence of process conditions on particle behaviour is of eminent importance (Belfort, Davis et al. 1994). When particles can be kept away from the membrane by adjustment of the process conditions, the trans-membrane flux and retention can be constant in time, as was illustrated in a recent publication from our lab (van Dinther, Schroën et al. 2011). Even though Field *et al.* (1995) already introduced the importance of a steady flux by introducing the critical flux, understanding particle migration not only in the concentration polarization layer, but also in the bulk, can even further improve the process (Field, Wu et al. 1995). We would like to stress that the new process concept presented here is different from regular practice, in which flux and retention generally change in time (Fillaudeau and Carrere 2002; Abbasi, Sebzari et al. 2011; El Rayess, Albasi et al. 2011; Nandi, Uppaluri et al. 2011; Rezaei, Ashtiani et al. 2011).

A flowing fluid exerts forces on a moving particle and this may lead to migration of particles from their streamlines (Belfort, Davis et al. 1994). Particles of different sizes are affected differently, and this may ultimately lead to a segregation of particles in the bulk of the liquid flowing over the membrane, which is useful in microfiltration. When particles segregate in the liquid before approaching the membrane surface, separation and fractionation will no longer be based on membrane pore size only (Kromkamp, Faber et al. 2006; van Dinther, Schroën et al. 2009). As a result the membrane pores can be much larger and accumulation of particles on the membrane surface or in the membrane pores is prevented, as long as the process conditions remain appropriate. Such process is expected to operate much more efficiently at acceptably high fluxes, without fouling, and with less need for long and aggressive cleaning. In a flowing suspension, hydrodynamic, lift and body forces are dominant. The migration of particles is a result of the force balance on a particle and which forces are dominant depends on the process conditions,

indicating that various migration phenomena may be observed during membrane filtration (Belfort, Davis et al. 1994). In the following sections we ignore body forces, by assuming hard sphere behaviour and preventing (large) density differences between particles and the surrounding fluid. By choosing the right process conditions, the effect of Brownian motion, also a body force, is negligible compared to other mechanisms. The two main particle migration effects under the conditions relevant to microfiltration, are inertial lift and hydrodynamic shear-induced diffusion and these are now discussed in more detail; the actual window of operation is given in the next section.

Lift forces are induced by shear, viscosity and inertia. The shear created when fluid flows through a channel results in a lift force causing the particle to migrate towards the wall (Eckstein, Bailey et al. 1977); however, at the same time the wall-induced inertial lift force directs the particles away from the wall (McLaughlin 1993; Zeng, Balanchandar et al. 2005). As a result the particles migrate to a certain equilibrium position (Eloot, De Bisschop et al. 2004); this is called the Segré-Silberberg effect or 'Tubular Pinch'.

Velocity gradients can also lead to shear-induced migration of particles. Particles rotate with an angular velocity and circulatory fluid motion is established around the particle creating a velocity field that exerts drag on neighbouring particles (Piron, Rene et al. 1995). Besides this, particles pass other particles in slower-moving fluid streamlines, thereby causing 'collisions' based on excluded volume, usually without contact, which causes particles to move to other streamlines (Eckstein, Bailey et al. 1977). When three or more particles are involved simultaneously, the net displacement is random, resulting in a diffusion-type behaviour of the particles.

Phillips *et al.* (1992) estimated the total flux due to shear-induced diffusion in a straight channel with equation 3.1 and 3.2 (Phillips, Armstrong et al. 1992):

$$J_{mig} = -D_{shear} \nabla \left(\ln \left(\dot{\gamma} \phi \eta^{\lambda} \right) \right)$$

(3.1)

In which

$$D_{shear} = K \dot{\gamma} a^2 \phi^2$$

(3.2)

With a the particle size (m), ϕ the solid volume fraction (-), $\dot{\gamma}$ the shear rate (1/s), η the viscosity (Pa·s), λ a constant (-), D_{shear} the shear-induced diffusion coefficient (m²/s) and K a constant (-) that may be dependent on the volume fraction (Leighton and Acrivos 1987; Leighton and Acrivos 1987). Gradients in shear rate, concentration and in viscosity all give rise to migration.

Chapter

3

The migration thus depends on particle size (via D_{shear}) and concentration (via the driving forces and D_{shear}) and it is therefore clear that particles with different sizes and concentrations will have different migration velocities. Larger particles interact more easily with streamlines of neighbouring particles due to their size and thereby easily move to other streamlines, leading to faster migration (Eloot, De Bisschop et al. 2004). As a result, larger particles will concentrate towards the middle of the channel while smaller particles are in the region close to the wall (Leighton and Acrivos 1987; Graham, Altobelli et al. 1991; Lyon and Leal 1998; Lyon and Leal 1998; Breedveld, van den Ende et al. 2001; Tan 2003). This explains why in general cake layers tend to consist mostly of smaller particles. One may also make good use of this segregation as is done in this chapter. Shear-induced diffusion is especially dominant in concentrated suspensions, which easily leads to fouling in and on the membrane during regular microfiltration, due to the large amount of particles present. We will show that shear-induced diffusion can be used to enhance membrane processes.

Although research has been done on migration phenomena in closed channels and Couette devices (Abbott, Tetlow et al. 1991; Graham, Altobelli et al. 1991; Acrivos, Mauri et al. 1993; Chow, Sinton et al. 1994; Tetlow, Graham et al. 1998; Shakib-Manesh, Raiskinmaki et al. 2002; Yu, Shao et al. 2007), as well as on particle migration in membrane microfiltration (Belfort 1989; Belfort, Davis et al. 1994; Kromkamp 2005; Vollebregt, van der Sman et al. 2010), it has never been investigated how particle migration in a channel may be utilised for microfiltration. Additionally, there is a lack of information about the influence of most parameters needed in membrane filtration.

Semwogerere *et al.* (2007, 2008) summarized the influence of the ratio of particle sizes on the development of the concentration profile in concentrated suspensions, into an evolution parameter (Semwogerere, Morris et al. 2007; Semwogerere and Weeks 2008). From this parameter, the evolution length can be calculated, which is related to the point where the concentration profile is completely developed. Even

though also partially developed profiles show segregation, this evolution length may be used as a guideline to identify process conditions of interest.

In this chapter, we experimentally determine the concentration profiles by CSLM in bi-disperse suspensions flowing in closed channels which have dimensions similar to the ones used for membrane separation. This yields insight in the most important process parameters for particle migration in fluid flow and the ones resulting in segregation of particles on size, thereby giving guidelines to use shear-induced migration for fractionation purposes in new separation processes. At the end of the experimental section, a proof of principle is shown in which a membrane process is designed around these new insights.

Chapter

3

3.3. Window of operation

3.3.1. Brownian motion

Brownian motion is a body force which leads to random motion of particles. The Péclet number (equation 3.3) gives the relative importance of hydrodynamic to Brownian forces (Ackerson 1991); at a Péclet number < 1, the hydrodynamic forces dominate Brownian motion.

$$\text{Pe} = \frac{\dot{\gamma} a^2}{D} \tag{3.3}$$

In which D is defined by the Stokes-Einstein diffusivity (m^2/s) given in equation 3.4.

$$D = \frac{kT}{6\pi\eta a} \tag{3.4}$$

Where k is the Boltzmann constant (1.380×10^{-23} J/K), T is the temperature (K), and η is the viscosity of the suspension (Pa·s).

The shear rate is related to the flow velocity. In equation 3.5 one can see the relation for Poisseuille flow:

$$\dot{\gamma} = \frac{3\bar{v}}{h} \tag{3.5}$$

where $\bar{v}$ is the average velocity (m/s), and H is half the channel height (m). We only consider a laminar regime here, since turbulence would disturb particle migration.

From equation 3.3, the minimal shear rate needed to circumvent the influence of Brownian diffusion is derived and subsequently we can derive the minimal velocity (v_{min}) using equation 3.5. For dimensionless channel lengths (length in the channel divided by half its height) of 2400 and 4800, the minimum velocity is 3.30 and 0.63 μm/s, for 1.53 and 2.65 μm particles respectively (Pe<1). In all our experiments the velocity is above v_{min}, indicating that Brownian diffusion of suspension particles is not important.

3.3.2. Shear-induced migration

Shear-induced diffusion is dominant in concentrated suspensions, and if membrane fractionation is aimed for, particles should have sufficient time to migrate. This means that the time scale for migration, i.e. shear-induced diffusion, should be smaller than that for convection, and this can be related to an evolution length for the CSLM experiments (Nott and Brady 1994). The time scale of convection τ_{con} (s) is given by equation 3.6.

$$\tau_{conv} = \frac{L}{\dot{\gamma}H} \tag{3.6}$$

where L is the channel length (m).
The average distance travelled by the particles perpendicular to the flow (y (m)) is described in equation 3.7.

$$y = 2\left(D_{shear}t\right)^{\frac{1}{2}} \tag{3.7}$$

with t the time (s). This leads to the time scale for migration (τ_{dif} (s)), defined in equation 3.8.

$$\tau_{dif} = \frac{H^2}{D_\phi \dot{\gamma} a^2}$$ (3.8)

With D_ϕ the dimensionless diffusion coefficient, defined as (Leighton and Acrivos 1987).

$$D_\phi = \frac{1}{3}\phi^2\left(1 + 0.5e^{8.8\phi}\right)$$ (3.9)

The evolution length (see section 3.3.3.) is defined as the length at which the particles have migrated a pre-set distance, in our Péclet number half the channel height. It must be noted that estimates based on this are conservative; not all particles have to travel half the channel height. In a membrane process the large particles would need to move thus far that they are not incorporated in the permeate, while the small ones can stay close to the walls. The ratio between the time scales is a Péclet number defining the ratio of convective and diffusive processes (equation 3.10). This number is different from the one described in equation 3.3, and therefore we use a star to signify the difference.

$$Pe* = \frac{\tau_{dif}}{\tau_{con}} = \left(\frac{H}{a}\right)^2 \frac{1}{12D_\phi}\frac{H}{L}$$ (3.10)

3.3.3.   Evolution length

The evolution length is the channel length necessary to establish migration patterns and it can be calculated for different degrees of migration (fully or partially developed). For membrane microfiltration, sufficient migration of particles needs to take place, but the concentration profile does not need to be completely developed as mentioned before. Additionally, if a closed channel is used prior to a channel with porous walls, the total length of the module should be kept as short as possible, mainly to prevent unacceptable pressure drops. The pressure drop over the length of the closed channel was in the experiments described here in the order of millibars.

The size and concentration distribution at different positions in the channel was analysed with confocal scanning laser microscopy (CSLM). The evolution length, i.e.

length at which the concentration profile is completely developed, could be evaluated from the so-called evolution parameter ($E_p(x)$), introduced by Semwogerere *et al.* (2008). This parameter determines the degree of development of the concentration profile (with particles) and is described in equation 3.11 (Semwogerere, Morris et al. 2007; Semwogerere and Weeks 2008).

$$E_p(x) = \frac{1}{2H} \int_0^{2H} \left| \frac{\phi(x,z)}{\langle \phi(x,z) \rangle_z} - \frac{\phi_{ref}(z)}{\langle \phi_{ref}(z) \rangle_z} \right| dz \tag{3.11}$$

In the equation $\phi(x,z)$ is the concentration profile of particles at a certain distance in the channel (-), $\phi_{ref}(z)$ is the concentration profile at the inlet (-), $<\phi(x,z)>_z$ is the cross-sectional average volume fraction (-) and $<\phi_{ref}(z)>_z$ is the cross-sectional average volume fraction at the inlet (-).

The evolution parameter is fitted with an exponential function (equation 3.12), for which we have used a simplified fit with two variables.

$$E_p^{fit}(X) = b\left(1 - e^{-cX}\right) \tag{3.12}$$

X is the dimensionless distance from the inlet and defined as x/H (-), b and c are fitting parameters, with c defined as E_L^{-1} (E_L is the dimensionless evolution length (-)). The fit is normalized using the value for b (equation 3.13), after which the curves can be compared directly.

$$E_p^{fit}{}_{norm}(X) = E_p^{fit}(X)/b \tag{3.13}$$

3.3.4.   Inertial lift

Inertial lift is exerted on a particle by the fluid, due to the flow profile and the proximity of a wall. It is dependent on the particle Reynolds number, as given by equation 3.14, which in turn is a function of the channel Reynolds number (equation 3.15) (Park, Song et al. 2009). Whether inertial lift plays a role depends on the ratio between inertial and viscous forces; generally at particle Reynolds

numbers > 1 (Asmolov 1999), inertial lift is relevant. In all experiments the particle Reynolds numbers were below $9 \cdot 10^{-7}$, indicating that inertial lift did not play a role.

$$\text{Re}_p = \text{Re}_c \left(\frac{2a(w+2H)}{4wH} \right)^2 = \frac{\dot{\gamma} a^2 \rho (w+2H)}{3\eta(\phi)w} \qquad (3.14)$$

With

$$\text{Re}_c = \frac{4wH}{(w+2H)} \frac{\bar{v} \rho}{\eta(\phi)} \qquad (3.15)$$

where Re_c is the channel Reynolds number defined in equation 3.15, ρ is the density of the suspension (kg/m^3), w is the channel width (m) and $\eta(\phi)$ is the viscosity as a function of the solid volume fraction of the suspension (Pa·s).

3.4. Experimental

3.4.1. Particle migration in closed channel

The experiments were carried out with a confocal scanning laser microscope (Leica SP2, Germany), with a 63 x 1.4 numerical aperture oil immersion objective and laser light with a wavelength of 543 and 488 nm. The height of the focal plane could be positioned with a piezo-focusing drive (P-721, Physik Instrumente, Germany).

Two types of PMMA (polymethyl methacrylate) particles were made by dispersion polymerization and fluorescently labelled with NBD (7-nitrobenzo-2-oxa-1,3-diazol) and rhodamine B fluorescent dye, respectively (Bosma, Pathmamanoharan et al. 2002). The smallest particles had an average size of 1.53 micron and the larger ones a size of 2.65 micron. The particles were dispersed in a mixture of 72.8% cyclohexylbromide and 27.2% cis-decalin to match the refractive indices of particles and surrounding liquid. The solvent was saturated with tetrabutylammoniumbromide (TBAB) to screen any small particle charges, and make them behave like hard spheres. Stock suspensions were mixed in the desired ratio, and pumped through a glass rectangular channel with a syringe pump (Pico Plus, Harvard Apparatus, USA). The channel was 30 cm by 2 mm by 100 μm (length,

width, height respectively) (Friedrich & Dimmock Inc., USA). A holder was constructed in order to prevent the glass channel from breaking and to make the connection to the syringe (Fine-mechanical workshop, Wageningen University). For the velocities investigated in our experiments we only need $2H$ length to establish a fully developed *fluid* velocity profile (Shah and London 1979) (please note that this does not coincided with the particle concentration profile), and therefore the 0.3 meter long closed channel was more than long enough; also the membrane module satisfies this prerequisite.

The pictures taken (at 12 and 24 cm from the entrance of the channel) consisted of 512 by 64 pixels, corresponding to a field of view of 59.52 by 7.44 micron with a depth of ∼250 nm. The system was operated in the xyt-mode, with a zoom of 4 and a scanning frequency 400 Hz. Here, *x* is oriented along the channel length and y along the width. The frame rate used was 10 frames/s. Under these circumstances velocities up to 590 μm/s can be measured; experimental velocities are always lower. The pictures were analysed with the image processing toolbox in MATLAB (Mathworks, US) to determine particle number, type and velocity.

Table 3.1. Minimal solid volume fraction for migration of 1.53 μm and 2.65 μm particles as a function of dimensionless length in the rectangular channel.

	1.53 μm particles	2.65 μm particles
L/H (-)	ϕ_{min} (-)	ϕ_{min} (-)
2400	0.27	0.20
4800	0.23	0.16

From equation 3.9 and 3.10 in the former section, the minimal solid volume fraction (ϕ_{min}) for migration for shear-induced diffusion to be relevant (Pe*<1), can be derived and the results are presented in table 3.1. For these data, it is assumed that the dimensionless diffusion coefficient is given by the relation derived by Leighton and Acrivos (equation 3.9)(Leighton and Acrivos 1987). These values are valid for a monodisperse suspension, where the Péclet number is determined on the basis of the total volume fraction of the suspension. From this it can be concluded that 1.53 μm particles are expected to show significant migration behaviour at total solid volume fraction > 0.23 at a given channel length. For the 2.65 μm particles, migration is expected at volume fractions > 0.16. For

fractionation purposes, migration of the small particles to the middle is not preferred and in the experiments the solid volume fraction of the small particles does not exceed 0.19. The solid volume fractions of the large particles range from 0.09 to 0.36.

3.4.2.   Membrane microfiltration

For the membrane microfiltration experiments a nickel sieve with spherical pores of 20 micron was used to fractionate the suspensions (Veconic sieve, Stork Veco BV, the Netherlands). The sieve was placed in a module with a length of 40.5 cm, of which the first 34.5 cm was a closed channel to establish a fully developed velocity profile. Within this length, the concentration profiles are also well established, as concluded based on the calculated evolution lengths (section 3.3.3.). In our experiments we used a sieve, which was placed after 34.5 cm and had an area of 1.39 cm^2. The height of the channel could be changed, but was kept at its minimum of 200 micron. The emulsion was fed to the system with a positive displacement pump (VG1000digit, Verdergear, Germany).

Pressure sensors (EL-PRESS P-502C, Bronkhorst High-Tech B.V., the Netherlands) were installed at the beginning and the end of the module, and after the membrane. The pressure data were recorded with Bronkhorst High-Tech software. The trans-membrane flux was measured with a balance (CP4202S, Sartorius, Germany) connected to a computer (Memfill-Lite software, Wageningen University, the Netherlands). The permeate flow was set at a specific value with a peristaltic pump (series 205U, Watson Marlow, England). The measured flux was constant in time, which indicates no accumulation of particles on/in the membrane.

Membrane microfiltration experiments were performed with two emulsions that were mixed in a pre-determined ratio; the oil phase consisted of silicone oil with a density of 1.01 g/cm^3 (silicone oil AR 20, Sigma Aldrich, Germany). In the experiments, two oil volume fractions of 0.27 and 0.36 were used, both consisting of mixtures of two individually prepared emulsions.

For the 0.36 solid volume fraction emulsion, 36 % (w/w) silicone oil, was added to 62 % (w/w) water and 1 % (w/w) span80 (Sigma-Aldrich, Germany) as well as 1 % (w/w) Tween80 (Sigma-Aldrich, USA). A pressure vessel was filled with the mixture, which was then pressed six times through a 5 micron filter (PVDF Durapore, Millipore Corporation, Bedford USA) at 0.5 bar, which resulted in a droplet size of 5.15 micron (emulsion 1). This emulsion was further refined by pressing it six times through a 2.7 micron filter under 2 bars (Glass microfiber

GD/X, Whatman, GE, USA). The typical size of this emulsion was 2.40 micron (emulsion 2); for the separation experiments emulsions 1 and 2 were mixed at set ratios.

The emulsion with a solid volume fraction of 0.27, was prepared with 24% (w/w) silicone oil and was added to 74% (w/w) water and 1% (w/w) span80 (Sigma-Aldrich, Germany) as well as 1% (w/w) Tween80 (Sigma-Aldrich, USA). Again two emulsions were made, similar to the procedure described above. The typical size of the first emulsion was 2.40 micron, while the second had a size of 5.36 micron.

Particle sizes of initial emulsions, mixtures and permeate were measured in the Malvern Mastersizer (Malvern Instruments Ltd, UK). The ratio between large and small droplets was determined by analysis of the Malvern Mastersizer data. The total amount of oil droplets was determined by a dry weight measurement, for which the samples were stored overnight in an oven at 80 degrees Celsius (Memmert, Germany).

3.5. Results

For the investigated process conditions, shear-induced diffusion was the dominant particle migration mechanism and neither inertial lift nor Brownian diffusion was expected to influence the results as described in section 3.3. From the calculated evolution lengths (equation 3.11 and 3.12) of particle suspensions for the investigated conditions, we concluded that the concentration profiles are well established within our module length. We have checked that the concentration profile develops very fast within the first 0.1 meter of the module, which implies that in order to make use of these effects in membrane microfiltration only 0.1 meter of non-porous channel is needed to allow for sufficient particle migration to take place. In this section, first the results obtained with the CSLM will be described followed by an evaluation of the options for membrane separation, which are subsequently experimentally determined.

3.5.1. CSLM

The results are shown at different positions in the channel expressed as x/H, the distance x relative to the entrance of the channel over half-channel height H. This distance was 12 and 24 cm from the entrance length and therefore longer than the

first 10 cm in which the concentration profile develops. On the x-axis of the graphs, the dimensionless height $z/2H$ is used, with z the position of the particle relative to the reference wall (m). Further, the total particle fraction ϕ_{tot}, and the fraction of small particles ϕ_s is indicated.

The concentration profiles of large and small particles develop in the channel, and a striking example can be seen in Figure 3.1. Large particles are migrating to the middle, while small particles have higher concentrations near the wall, and this 'pre-fractionation' of particles in the liquid will later be used to facilitate particle separation. The effect is caused by shear-induced diffusion that causes particles to migrate away from the walls. Larger particles experience a much stronger driving force so that they probably displace the smaller ones to the walls.

In the next sections, we will discuss the influence of process conditions on the concentration profiles of the two particles sizes, to derive guidelines for membrane microfiltration processes.
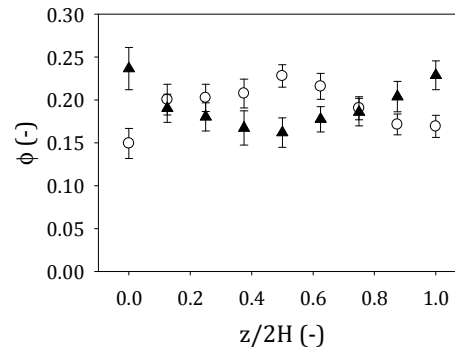

Figure 3.1. Concentration profile for 2.65 μm (○) and 1.53 μm (▲) particles. ϕ_{tot} is 0.38, x/H is 4800, v is 20.8 μm/s and ϕ_s is 0.19.

3.5.2.   Velocity

Two flow velocities, 8.3 and 20.8 μm/s, were used at a total volume fraction of 0.19. The solid volume fraction of small particles relative to the total sold volume fraction was 0.1 and 0.5 (with a small particle solid volume fraction ϕ_s of 0.02 and 0.09) (Figure 3.2a and b), and in both cases, no difference in concentration profile of the large particles was seen for the two different velocities, as was expected. The velocity, and therewith, the shear rate, is not in the Péclet number (equation 3.10),

which implies that shear-induced diffusion and convection change in similar fashion. The concentration profile will only change when the velocity is below a minimum velocity related to Brownian diffusion (Table 3.1) or a maximum velocity that induces inertial lift. We concluded that the measuring system was suited to investigate shear-induced diffusion effects.
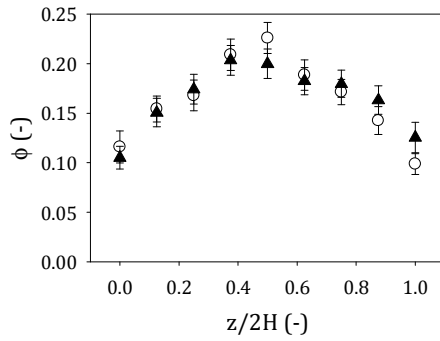
Chapter

3

Figure 3.2a. Influence of velocity on concentration profile of 2.65 μm particles. Velocities 8.3 μm/s (○) and 20.8 μm/s (▲) for x/H is 4800, ϕ_s/ϕ_{tot} is 0.10, ϕ_{tot} is 0.19.
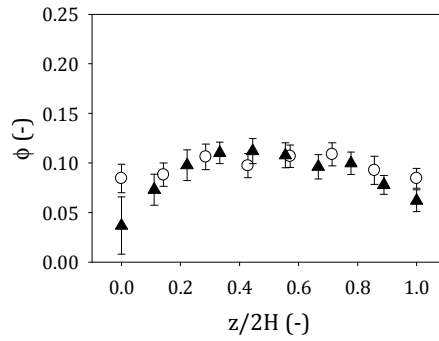
Figure 3.2b. Influence of velocity on concentration profile of 2.65 μm particles. Velocities 8.3 μm/s (○) and 20.8 μm/s (▲) for x/H is 2400, ϕ_s/ϕ_{tot} is 0.50, ϕ_{tot} is 0.19.

3.5.3.   Total solid volume fraction

The influence of the total solid volume fraction on migration behaviour is expected to be strong (equation 3.2). In Figure 3.3, the concentration profiles are shown for 0.38, 0.19 and 0.09 total volume fraction, and a relative fraction of small particles of 0.04. From Figure 3.3, it is clear that higher concentrations lead to steeper profiles caused by increased migration. For a low concentration of 0.09, the concentration profile is relatively flat, and it develops further with increasing concentration, with the highest concentrations in the middle of the channel.

3.5.4.   Relative solid volume fraction of 1.53 micron particles

The concentration profile of the large particles is influenced by the presence of small particles. In Figure 3.4, the profiles are shown for total volume fractions of 0.38, and relative solid volume fractions of small particles equal to 0.50 and 0.04 (absolute volume fraction of small particles is thus 0.19 and 0.02 respectively).
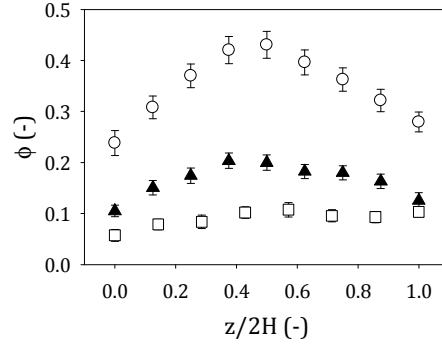
Figure 3.3. Influence of total concentration on concentration profile for 2.65 μm particles. ϕ_{tot} is 0.38 (○), 0.19 (▲) and 0.09 (□) for x/H is 4800, v is 20.8 μm/s and ϕ_s/ϕ_{tot} is 0.04.
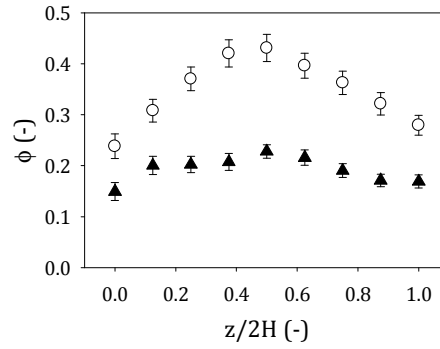
Figure 3.4. Influence of relative volume fraction of small particles (0.50 (▲) and 0.04 (○)) on concentration profile of 2.65 μm particles, x/H is 4800, v is 20.8 μm/s and ϕ_{tot} is 0.38.

The concentration profile of the large particles is more pronounced when the fraction of small particles is lower. This can be related to two effects. The first one is that the large particles are known to be hindered in their movements due to the presence of small particles, therefore the black triangles in Figure 3.4 do not show high values at *z/2H* is 0.5. At the same time, the relative fraction of large particles is also higher for ϕ_s/ϕ_{tot} is 0.04 than for ϕ_s/ϕ_{tot} is 0.50, leading to more shear-induced diffusivity. The absolute solid volume fraction of large particles is namely 0.19 and 0.36 respectively. When the solid volume fraction of large particles exceeds a certain value (dependent on total concentration and fraction of small particles), shear-induced diffusivity is totally determined by the large particles (Lyon and Leal 1998).

3.5.5. Migration of small particles

Until now we mainly focused on the behaviour of the large particles, which primarily accumulated in the middle of the channel. This effect is only beneficial for separation if the profile of the small particles develops differently. Migration of large particles to the middle is preferred since large particles are more difficult to remove from smaller ones than *vice versa*, and at the same time, small particles should move towards the wall.

For a solid volume fraction of small particles equal to 0.19 (ϕ_s/ϕ_{tot} equal to 0.50) (Figure 3.5a), the small particles have a tendency to migrate towards the wall for both velocities investigated (8.3 and 20.6 micron per second). The opposite occurred when the solid volume fraction of small particles was equal to 0.02 (ϕ_s/ϕ_{tot} is 0.04) (Figure 3.5b). The large particles did not show a distinct concentration profile under the circumstances where ϕ_s/ϕ_{tot} is equal to 0.50, as shown in Figure 3.4. The migration of large particles towards the centre might cause exclusion of small particles, although the maximum packing density of particles is never reached in the centre. Based on the Péclet number of the small particles we would expect migration in Figure 3.5a and b. Probably the interaction between differently sized particles which are present in large quantities causes the large particles to be hindered in their migration, while the small particles are being excluded. Please note that the standard deviations in Figure 3.5b are relatively large, due to the small amount of small particles present.

When the solid volume fraction of small particles is 0.09 (ϕ_s/ϕ_{tot} is 0.50) (as shown in Figure 3.6), no particle migration was observed and this was also expected from the Péclet number. The results show that for fractionation purposes, the solid volume fraction of the suspension is preferably high (e.g. 38%), with equal solid volume fractions of small and large particles. Under these circumstances large particles migrate to the middle of the channel, while small particles are present in higher concentrations at the wall. Also Lyon *et al.* (Lyon and Leal 1998) described that the solid volume fraction of the small particles should be around 0.20 to deliver a non-uniform concentration profile.

Even though migration of large particles is more pronounced at smaller relative volume fractions of small particles, the selectivity of the process will be lower as a result of the simultaneous migration of small particles to the middle. Based on our results, equal solid volume fractions of large and small particles in combination

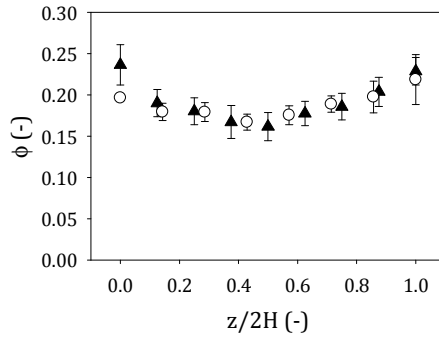with high total concentrations (e.g. 38%; Figures 3.4 and 3.5a.), are most suited for fractionation purposes.

Figure 3.5a. Concentration profile of 1.53 μm particles. Velocities 8.3 μm/s (○) and 20.8 μm/s (▲) for φ$_{tot}$ is 0.38, φ$_s$/ φ$_{tot}$ is 0.50 and x/H is 4800.
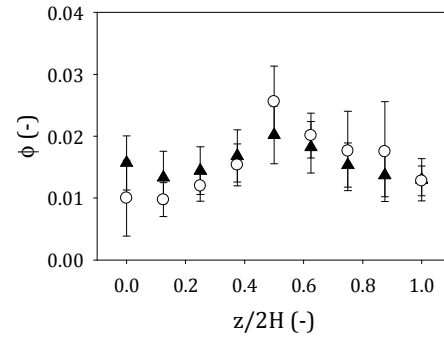
Figure 3.5b. Concentration profile of 1.53 μm particles. Velocities 8.3 μm/s (○) and 20.8 μm/s (▲) for φ$_{tot}$ is 0.38, φ$_s$/ φ$_{tot}$ is 0.04 and x/H is 4800.
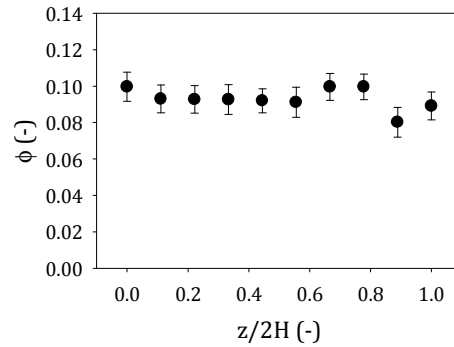

Figure 3.6. Concentration profile of 1.53 μm particles at velocity of 8.3 μm/s, φ$_{tot}$ is 0.19, x/H is 2400 and φ$_s$/ φ$_{tot}$ is 0.50.

A summary of the conditions and particle behaviour of the small and large particles is shown in the schematic overview in Figure 3.7. For concentrations of 38% (top right graph) and equal solid volume fractions of small and large particles the large particles migrate to the middle, while the small ones are mainly present at the sides. The migration of the large ones is hindered by the presence of the small ones and therefore more entrance length is needed for the profile to develop, which is not shown in the Figure. As soon as the relative solid volume fraction of the small ones decreases (bottom right Figure), they migrate to the middle of the

channel, although this effect is rather small. At lower concentration of particles (0.09 or 0.19; as depicted on the left of the Figure) the small particles show a flat concentration profile irrespective of the volume fraction at which they are present (0.004 up to 0.09), while migration of large particles was always seen.
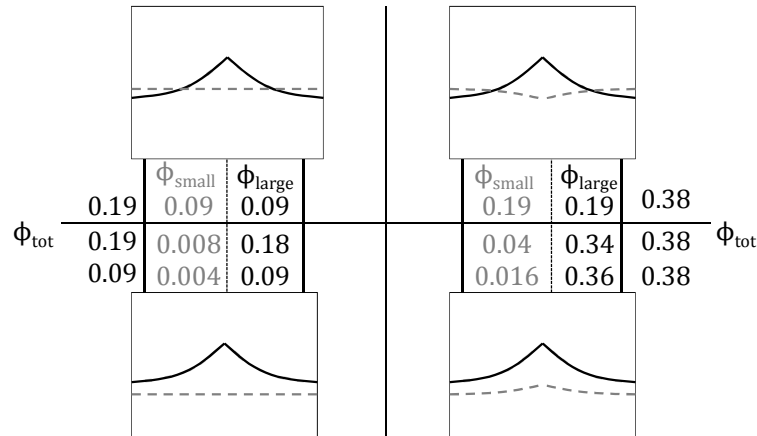

Figure 3.7. Schematic overview of concentration profiles of small (grey, dashed lines) and large (black lines) particles for different conditions; interpretation of the graphs is given in the last part of section 3.5.5.

3.6.   Predictions for membrane microfiltration

In this section, we translate the CSLM results into predictions for membrane filtration. We take the measured concentration profiles as a starting point, and assume that we take a certain amount of the liquid out through a membrane at a fixed position. Permeate is taken from the liquid close to the walls of the channel and the process is operated at a flux of $4.4 \cdot 10^{-11}$ m$^3 \cdot$m$^{-2} \cdot$s^{-1}, which corresponds to membrane fluxes of $4.4 \cdot 10^4$ L$\cdot$h$^{-1} \cdot$m$^{-2} \cdot$bar^{-1} (see appendix for detailed information on process conditions), due to the large pores in the membrane.

When assuming that the liquid close to the wall will form the permeate in a filtration experiment, the resulting concentrations in permeate and retentate can be calculated from the ratio between cross-flow velocity and permeate flux, as shown in Figure 3.8 for a total concentration of 0.38, and equal fractions of small and large particles. The concentration of small particles increases with 20.8%, while the concentration of large particles decreases with 17.3%.
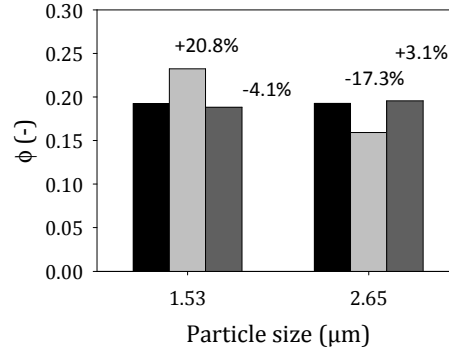
Figure 3.8. Calculated volume fraction in the bulk (black), the permeate (light grey) and the retentate (dark grey) for two different particles sizes. Velocity is 20.8 μm/s, φ$_S$/ φ$_{tot}$ is 0.50 and φ$_{tot}$ is 0.38.
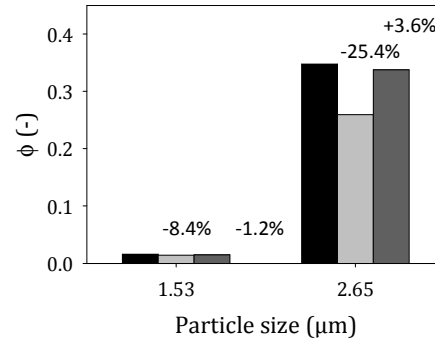
Figure 3.9. Calculated volume fraction in the bulk (black), the permeate (light grey) and the retentate (dark grey) for 1.53 μm particles. Velocity is 20.8 μm/s, φ$_S$/ φ$_{tot}$ is 0.04 and φ$_{tot}$ is 0.38.

The selectivity (α(-)) of this process is defined in equation 3.16, and is 1.47 for this specific example.

$$\alpha = \frac{\phi_{S,p}}{\phi_{L,p}} \frac{\phi_{L,b}}{\phi_{S,b}}$$

(3.16)

Where $\phi_{S,p}$, $\phi_{L,p}$ are the solid volume fractions of the small particles in the permeate (-) and the large ones respectively, and $\phi_{L,b}$, $\phi_{S,b}$ are the solid volume fractions of the large particles in the bulk (-) and of the small ones respectively.

77

At low relative solid volume fraction of small particles (0.04) and a concentration of 38%, both concentrations of particles decrease in the permeate (Figure 3.9), which may lead to options for overall concentration of particles. The concentration of the large and small particles decreases with 8.4% and 25.4% respectively, which still leads to a selectivity of 1.25.

3.6.1. Proof of principle through membrane microfiltration

We now evaluate whether the measured and predicted effects can be used in microfiltration. A concentrated emulsion of 0.36 volume fraction and equal fractions of 2.40 and 5.15 micron (d_L is $2.15 \cdot d_S$) particles was filtered in a cross-flow membrane set-up (ϕ_S / ϕ_{tot} is 0.50). The height of the channel was 200 micron, the cross-flow velocity was 0.59 m/s, and the trans-membrane flux was $1.1 \cdot 10^{-5}$ m/s. The velocity is chosen much higher than applied in the CSLM and that has to do with the time needed to collect a reasonable amount of sample from the set-up. For this we need to operate the set-up at the indicated flux, and in order to prevent particle accumulation the velocity needed to be chosen as indicated. The channel height was 200 micron to prevent severe pressure drops, and the membrane had pores of 20 micron, being 3.9 times larger than the size of the large particles. Even though the conditions are slightly different from the CSLM experiments, inertial lift and Brownian diffusion can still be neglected, i.e. maximum Re_p is 0.01 (equation 3.14) and Pe is smaller than 10^{-5} (equation 3.3). When assuming monodisperse samples, the time scale for convection is also longer than the time scale for shear-induced diffusion (Pe*<1, equation 3.10), although this requirement is not met for the 2.40 micron particles in the second experiment with 0.27 oil volume fraction.

In Figure 3.10 the particle size distribution (volume percentage) of the bulk and the permeate are shown (there was no change in size distribution as function of time in any of the membrane experiments, indicating that no particle accumulation takes place). A clear shift towards smaller particles in the permeate is seen. The actual increase in small particles is around 30% and the decrease of large particles in the permeate is 29%, which leads to a change in ratio small to large of 1.78 in the permeate (in the bulk this ratio is 1.03). The values found here are slightly better than found in the CSLM experiment (selectivity 1.47), but it clearly shows that segregation in the channel leading to the membrane was achieved.
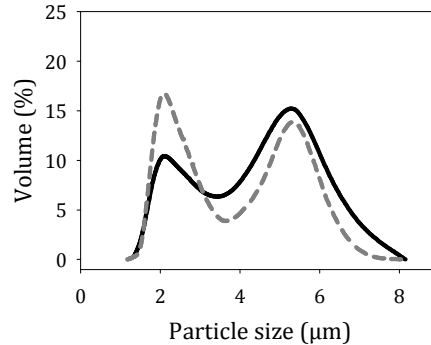
Figure 3.10. Particle size distribution for bulk (solid line) and the permeate (dashed line). Bulk consists of 2.40 micron and 5.15 micron particles. ϕ_{tot} is 0.36, ϕ_S/ϕ_{tot} is 0.5, v is 0.59 m/s, flux is $1.1 \cdot 10^{-5}$ m/s.

A second experiment was performed to maximise the effects and for this an emulsion of 0.27 volume fraction and particles of 2.40 and 5.36 micron (d_L is $2.23 \cdot d_S$) was filtered in a cross-flow membrane set-up (ϕ_S/ϕ_{tot} is 0.89). The trans-membrane flux was $9.3 \cdot 10^{-6}$ m/s. The other conditions were as described before. In Figure 3.11, the particle size distribution (volume percentage) of the bulk and the permeate are shown, and in this case particles > 4 μm did not end up in the permeate, and the number of small particles in the permeate increased with 12%. Since the flux is constant in time, it is clear that the observed effects can be attributed to particle migration and not to particle accumulation; which may lead to a very sharp size segregation as indicated in Figure 3.11.

The difference between Figure 3.10 and 3.11 is probably caused by the difference in ϕ_S/ϕ_{tot} ratio. When the ratio is close to 0.50 (Figure 3.10), large particles migrate to the middle and small ones are present in higher concentrations at the walls; segregation is taking place. However, migration is not strong and therefore the selectivity of the process is not very high. When the fraction of small particles is increased to ϕ_S/ϕ_{tot} is 0.89 (Figure 3.11), the large particles migrate sufficiently away from the wall. The small particles are not really migrating; a similar trend was also observed in the article of Lyon and Leal (Lyon and Leal 1998). More importantly, the increase in small particle concentration in the permeate may only be 12%, but the permeate is free of large particles, leading to very high selectivity. This striking example signifies the importance of knowledge on particle migration for design of membrane fractionation processes.
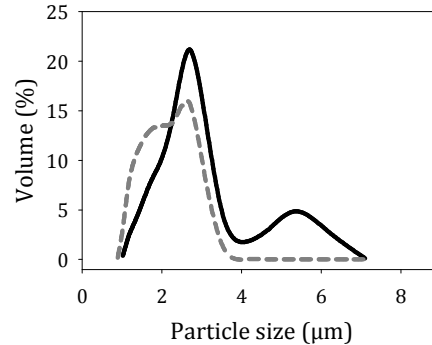
Chapter

3

Figure 3.11. Particle size distribution for bulk (solid line) and the permeate (dashed line). Bulk consists of 2.40 micron and 5.36 micron particles. ϕ_{tot} is 0.27, ϕ_S/ϕ_{tot} is 0.89, v is 0.59 m/s, flux is $9.4\cdot10^{-6}$ m/s.

In summary, the experimental results show that microfiltration can benefit from flow-induced fractionation, when operated under appropriate process conditions. The major advantage of such approach is that separation can be achieved while avoiding process deterioration due to membrane fouling. Since the pore size is no longer the determining factor for separation, the pore size can be chosen at will, while allowing high fluxes. One should note that this mechanism can be most efficiently used at high concentrations. This means, that processes may be relatively compact, while the conditions are very mild (laminar flow).

The CSLM measurements, while not in quantitative agreement with the filtration results, show that shear-induced migration in these concentrated emulsions, is probably the underlying mechanism. It is expected that fractionation can be further optimised when the permeate flux and channel height of the module are decreased, thereby increasing shear-induced diffusion and making optimal use of the separation close to the wall. This may be a challenge for membrane module manufacturers, but obviously the rewards can be great.

3.7. Conclusions

The new approach presented here for microfiltration uses shear-induced migration of particles to facilitate membrane fractionation. Particles migrated well within the first 0.1 meter of the closed rectangular channel used in CSLM analysis and the concentration profiles were measured as function of the particle volume fractions (profiles are more pronounced at higher concentration) and ratio between large and small particles. When the solid volume fractions of small and

large particles (1.53 and 2.65 µm in size respectively) were equal at a total concentration of around 40%, large particles migrated to the middle of the channel, while smaller ones moved closer to the wall. This was experimentally verified for emulsions of 36% and 27%, leading to significant selectivity in membrane separation and in one case even exclusion of large particles from the permeate. The processes were carried out at fluxes up to $4.4 \cdot 10^4$ L·h^{-1}·m^{-2}·bar^{-1} and no flux reduction took place in time, indicating no particle deposition during operation. To make optimal use of particle migration, the membrane module should start with a closed channel where particles have time to migrate, followed by a separation area where the permeate is collected, and this should be feasible to implement in practice.

Chapter

3

3.8. Appendix

$$J = \frac{\Delta P}{\eta R_m}$$
(A3.1)

Where J is the permeate flux ($m^3 \cdot m^{-2} \cdot s^{-1}$), ΔP is the trans-membrane pressure (Pa), η is the viscosity (Pa·s) and R_m the membrane resistance (m^{-1}).

Table A3.1. Summary of process conditions and membrane characteristics to predict fractionation in a membrane microfiltration experiment.

Fluid velocity in channel	$5.9 \cdot 10^{-1}$	m/s
Channel width	$1.6 \cdot 10^{-2}$	m
Channel height	$2.0 \cdot 10^{-4}$	m
Volumetric flow rate through channel	$1.9 \cdot 10^{-4}$	m^3/s
Volumetric permeate flow	$1.4 \cdot 10^{-9}$	m^3/s
Thickness fluid layer for permeate	$1.5 \cdot 10^{-7}$	m
Membrane area	$1.4 \cdot 10^{-4}$	m^2
Permeate flux	$1.0 \cdot 10^{-5}$	$m^3 \cdot m^{-2} \cdot s^{-1}$
Viscosity	$2.5 \cdot 10^{-3}$	Pa·s
Membrane resistance	$3.3 \cdot 10^{-9}$	m^{-1}
Trans-membrane pressure	$8.3 \cdot 10^{-4}$	bar
Permeate flux	$4.4 \cdot 10^{4}$	$L \cdot h^{-1} \cdot m^{-2} \cdot bar^{-1}$

Chapter 4

Particle Migration leads to Deposition-free Fractionation

4. Particle Migration leads to Deposition-free Fractionation

4.1. Abstract

In membrane separation, the pore size is a crucial choice, since it determines the size of 'particles' that should be rejected when they reach the membrane surface. This 'gate keeper' function of the membrane, whereby components are rejected, leads to their accumulation on the membrane surface. Besides, accumulation leads to changed component retention in time. A process without accumulation would therefore be very advantageous since it intrinsically would also have a constant retention as function of time and be very suited for fractionation of components close in size.

In this research, emulsions consisting of small droplets (~2.0 micron) and large droplets (~5.5 micron) with total concentrations between 10 and 47% and $\phi_{large}/\phi_{total}$ ratios between 0.05 and 0.75 were fractionated. The membrane had 20 micron pores, and was used in a cross-flow module that consisted of a closed channel to allow particles to migrate due to shear-induced diffusion, followed by a filtration area where fractions of these emulsions could be removed. Under appropriate process conditions, the permeate consisted only of small droplets, and on top of that their concentration was higher than in the original emulsion, leading to very high selectivity. As expected, the size of the emulsion droplets in the permeate was a function of trans-membrane pressure and oil volume fraction. Especially at high concentrations of droplets (which is known to cause severe fouling in regular membrane filtration), these effects were occurring as a result of shear-induced diffusion of the droplets. If only small particles are targeted in the permeate, the module can be operated at fluxes of 40 L/(m²/h); if fractionation is targeted the fluxes can be considerably higher. Please note, these fluxes are comparable to operational fluxes of current microfiltration processes, but here we operate at much lower cross-flow velocity and trans-membrane pressure (corresponding to fluxes of 1-4 m³/(m²/h/bar)) with stable retention as function of time, indicating that no accumulation took place.

Chapter

4

4.2. Introduction

Membrane microfiltration of concentrated emulsions or suspensions usually leads to severe accumulation of components on the membrane. The suspension particles or oil droplets are dragged towards the membrane surface and give concentration polarisation in first instance, followed by pore blocking and cake layer formation (Strathmann 1981). Besides a sharp decrease in flux often occurring in the initial stage of operation, also the rejection is influenced by the accumulating components, leading to different separation characteristics. If an absolute separation is targeted, as is the case for removal of bacteria, increased rejection is positive, but if fractionation is targeted, in which components close in size need to be separated, this is not desirable. For example, to produce a dairy dessert, for which not all milk ingredients are needed, the milk is currently fractionated in its constituent components and later reconstituted in a ratio needed for the product. If a process with constant rejection would be available, this would allow for direct preparation of the required mix for the product, e.g. enrichment in cream (Brans, Schroën et al. 2004; Kromkamp, Faber et al. 2006).

When considering a standard membrane filtration process, the accumulation of the dispersed phase will reduce flux and increase the selectivity over time. This can be kept in check by gradually lowering the trans-membrane pressure, and hence the flux. In other words, the critical flux, introduced by Field *et al.* (1995), is low (Field, Wu et al. 1995). There are several ways to influence the concentration build-up above the membrane by increasing the mass transfer towards the bulk, for example by back-flushing or creating turbulence (Sherwood, Brian et al. 1965; Schneider and Klein 1982). However, these methods are complex, and more alleviation of a remaining problem, than elimination of the cause.

In earlier work on dilute suspensions (van Dinther, Schroën et al. 2011), it was shown that particle behaviour can be used very effectively in membrane processes. When influencing the particle trajectories by adapting the fluid flow, accumulation of particles on the membrane can be prevented completely and more importantly, fractionation of particles could be obtained, even with membranes having larger pores than the retained particles. In the right flow regime, particles of different size segregate in the fluid flow above the membrane, and the membrane does not

have its classic 'gate keeper' function. If this segregation effect can be further exploited, membrane (process) design could eventually become totally different. In this chapter, we extend the application of this principle to concentrated emulsions (being a specific type of suspension). In their reviews, Belfort *et al.* (1994) and Bowen *et al.* (1995) gave good insights in particle migration during membrane microfiltration, with emphasis on inertial lift effects and shear-induced diffusivity (Belfort, Davis et al. 1994; Bowen and Jenner 1995). Piron *et al.* (1995) showed that these back-transport mechanisms can be used to reduce cake layer formation (Piron, Rene et al. 1995). From earlier experimental work we suspected that particle migration can be used in microfiltration to prevent particle accumulation (Kromkamp, Faber et al. 2006; van Dinther, Schroën et al. 2011). We found that the size and concentration of particles in the permeate could be adjusted through the cross-flow velocity and trans-membrane pressure without having any particle accumulation on the membrane. For dilute suspensions we demonstrated that membranes with pores much larger than the particles present could be used (van Dinther, Schroën et al. 2011), however, this was not yet applied to concentrated systems. In this chapter, we will eventually design fractionation processes for concentrated systems starting from the fundamental behaviour of particles in a (concentrated) suspension or emulsion.

4.3.   Theory

It is known that different particle migration mechanisms can be relevant in flowing suspensions, being Brownian motion, inertial lift and shear-induced diffusion (Altena and Belfort 1984; Davis and Leighton 1987; Belfort, Davis et al. 1994), and here we specifically use shear-induced diffusion under conditions at which the other two mechanisms are not relevant. Brownian diffusion always takes place, but is less relevant for larger particle size – the typical estimate is that for particles larger than 100 nm, Brownian diffusion is no major migratory mechanism. Besides, from the article of Ackerson *et al.* (1991), it is clear that a minimal shear rate is needed to circumvent Brownian diffusion, which we took as a guideline for our experiments (Ackerson 1991).

Inertial lift occurs due to inhomogeneity of a flow around a particle, and is strongest in the proximity of a wall. Generally at particle Reynolds numbers < 1

Chapter

4

(Asmolov 1999), inertial lift is irrelevant, as is the case in our experiments (Re_p<0.02).

$$\text{Re}_p = \frac{\dot{\gamma}a^2\rho(w+2H)}{3\eta(\phi)\,w} \qquad (4.1)$$

Further it is worth mentioning that in concentrated systems it is very unlikely that lift is a dominant migration force due to the increased viscosity (see equation 4.1). The viscosity as function of particle volume fraction can be defined in several ways of which the one of Krieger and Dougherty (1959) is commonly used, as expressed in equation 4.2 (Krieger and Dougherty 1959).

$$\frac{\eta(\phi)}{\eta_0} = \left(1 - \frac{\phi}{\phi_{\max}}\right)^{-m} \qquad (4.2)$$

η_0 is the viscosity of the particle-free liquid (Pa·s), ϕ the oil volume fraction of the suspension (-), ϕ_{max} is the maximum random packing density for the suspension (-), which is assumed to be 0.64 for monodisperse suspensions of hard spheres and m = 2.

Shear-induced diffusion occurs when particles disturb the flow field around another particle; either by their rotation in shear flow, or since they move in a slower or faster-moving streamline. When three or more particles are involved simultaneously, the net displacement is random, resulting in a diffusion-type behaviour of the particles. Being a diffusive effect, shear-induced diffusion needs time to lead to translation of particles. The typical residence time in Poiseuille flow through a channel is given by equation 4.3.

$$\tau_{con} = \frac{3L}{\dot{\gamma}H} \qquad (4.3)$$

where L is the channel length (m). The shear rate $\dot{\gamma}$ (1/s) for Poisseuille flow is given in equation 4.4.

$$\dot{\gamma} = \frac{3\bar{v}}{H} \tag{4.4}$$

The average translation of particles perpendicular to the flow y due to shear-induced diffusion is described in equation 4.5.

$$y = 2\left(D_{shear}t\right)^{1/2} \tag{4.5}$$

with t the time (s) and D_{shear} the shear-induced diffusion coefficient (m²/s).

In many papers it is assumed that shear-induced diffusion is an ideal process. However, Phillips *et al.* (1992) already indicated that there are more driving forces (Phillips, Armstrong et al. 1992). Generally, particles tend to move towards regions with lower volume fraction, lower shear rate and lower viscosity (equation 4.6).

$$J_{mig} = -D_{shear}\nabla\ln\left(\dot{\gamma}\phi\eta^{\lambda}\right) \tag{4.6}$$

In which

$$D_{shear} = K\dot{\gamma}a^2\phi^2 \tag{4.7}$$

with η the viscosity (Pa·s), λ a constant (-) and K a constant (-) that may be dependent on the volume fraction (Leighton and Acrivos 1987; Leighton and Acrivos 1987).

Combining these equations and using half the channel height (H) for y, leads to the time scale for migration (τ_{dif} (s)) defined in equation 4.8.

$$\tau_{dif} = \frac{H^2}{4K\phi^2\dot{\gamma}a^2} \tag{4.8}$$

The ratio between these two time scales can be seen as a Péclet number defining the ratio of convective and diffusive processes (equation 4.9).

Chapter

4

$$\text{Pe}^* = \frac{\tau_{dif}}{\tau_{con}} = \frac{1}{12K\phi^2}\left(\frac{H}{a}\right)^2\left(\frac{H}{L}\right) \qquad\qquad (4.9)$$

The migration depends on particle size (via D_{shear}), particle volume fraction and the viscosity (via the driving forces incorporated in the logarithmic part of equation 4.6 and D_{shear}) and therefore particles with different sizes and concentrations have different migration velocities. Larger particles create much larger disturbances in the flow field, and interact over larger distances with streamlines of neighbouring particles due to their size, leading to faster migration (Eloot, De Bisschop et al. 2004). The net result is that larger particles will migrate faster than smaller ones, leading to size segregation.

Graham *et al.* (1991) and others showed that mono- and bidisperse suspensions migrated in a shear-field as function of shear rate (Abbott, Tetlow et al. 1991; Graham, Altobelli et al. 1991; Krishnan, Beimfohr et al. 1996). Size segregation was also demonstrated by Husband *et al.* (1994), who used two concentric pipes to separate particles (Husband, Mondy et al. 1994). Hampton e*t al.* (1997) showed that the ratio between particle size and channel or gap determines the degree of migration (Hampton, Mammoli et al. 1997). Later Lyon and Leal (1998) visualized concentration profiles for different flow conditions and suggested that small and large particles seemed to influence each other (Lyon and Leal 1998). Semwogerere *et al.* (2008) showed development of the profiles in a closed channel towards a steady-state concentration profile, which is dependent on process conditions (Semwogerere and Weeks 2008) (Lyon and Leal 1998). While the phenomenon of shear-induced migration and segregation is therefore known, it has to our best knowledge, never been applied to (re)design a separation process, such as cross-flow microfiltration. In a previous publication, we have shown with CSLM that migration in concentrated systems already occurs within the first 10 cm of a closed channel (van Dinther, Schroën et al. 2012). Here we report the direct use of these observations to the design of a cross-flow microfiltration process, in which we use the flow field, and not the membrane to create segregation. For this we use a purpose-built membrane module containing a membrane with pores much larger than the particles present and sufficient entrance length to allow for particle migration to take place and investigate the effect of trans-membrane pressure,

flow velocity and volume fraction. We evaluate the results and eventually show that shear-induced diffusion can be used to design much more efficient, albeit rather unconventional membrane fractionation processes.

4.4. Materials and Methods

Emulsions of silicone oil (density of 1.01 g/cm^3; silicone oil AR 20, Sigma Aldrich, Germany) in water were prepared at oil volume fractions ranging from 0.10 to 0.47. Depending on the oil volume fraction, the silicone oil, demineralized water and span80 (Sigma-Aldrich, Germany) as well as Tween80 (Sigma-Aldrich, USA) were mixed in different ratios. The Span80 concentration was always 1% (w/w) as was the Tween80 concentration. A pressure vessel was filled with the mixture, which was then passed six times through a 5 micron filter (PVDF Durapore, Millipore Corporation, Bedford USA) at 0.5 bar, which resulted in a droplet size of around 5.2 micron and a span of 0.84 (emulsion 1). This emulsion was taken as the starting point for emulsion 2, and further refined by passing six times through a 2.7 micron filter under 2 bars (Glass microfiber GD/X, Whatman, GE, USA). The typical size of this emulsion was 2.4 micron and had a span of 0.36 (emulsion 2). Alternatively, an emulsion containing droplets of 2 and 5.5 micron could be prepared with Ultra-Turrax (IKA, T18, Germany; 20000 rpm for 10 minutes), resulting in a set ratio of large particles of 0.2 compared to the total, allowing no variation in particle size ratio.

Membrane microfiltration experiments were performed with the two emulsions that were mixed in a pre-determined ratio. A round nickel sieve (1.39 cm^2) with uniform spherical pores of 20 μm (Veconic sieve, Stork Veco BV, The Netherlands) was placed in a module with length of 40.5 cm. The first 34.5 cm was a closed channel to establish a fully developed velocity profile and allow for migratory effects due to hydrodynamic inter-particle interaction, after which the membrane was positioned. The emulsion was fed to the system with a positive displacement pump (VG1000digit, Verdergear, Germany). Pressure sensors (EL-PRESS P-502C, Bronkhorst High-Tech B.V., the Netherlands) were installed at the beginning and the end of the module, and after the sieve. The pressure data were recorded with Bronkhorst High-Tech software. The trans-membrane flux was measured with a balance (CP4202S, Sartorius, Germany) connected to a computer (Memfill-Lite

Chapter

4

software, Wageningen University, the Netherlands). The cross flow velocities were between 0.3 and 0.59 m/s, and the channel height was 0.2 mm. The permeate flow was set at a specific value with a peristaltic pump (series 205U, Watson Marlow, England) (see Figure 4.1). The experiments were chosen such that a positive trans-membrane pressure was applied over the whole length of the membrane. In some exceptional cases (4 out of 27) we measured a small negative trans-membrane pressure at the exit of the module (see Figure 4.1). We found that these measurements coincided well with the trends found in the other experiments and expect that the actual pressure difference inside the module was always positive over the entire length of the module. Particle sizes of the initial emulsions, the mixtures and the permeate were measured in the Malvern Mastersizer (Malvern Instruments Ltd, UK). The total volume fraction of oil was determined by a dry weight measurement, for which the samples were stored overnight in an oven at 80 degrees Celsius (Memmert, Germany). The ratio between large and small droplets was determined by analysis of the Malvern Mastersizer data. Additionally a massbalance of small and large droplets was made, to verify that the size of the emulsion droplets was not affected by the set-up. Only results from experiments with constant trans-membrane flux and trans-membrane pressure during operation time, indicating deposition-free operation, were used for analysis and are presented in this article.
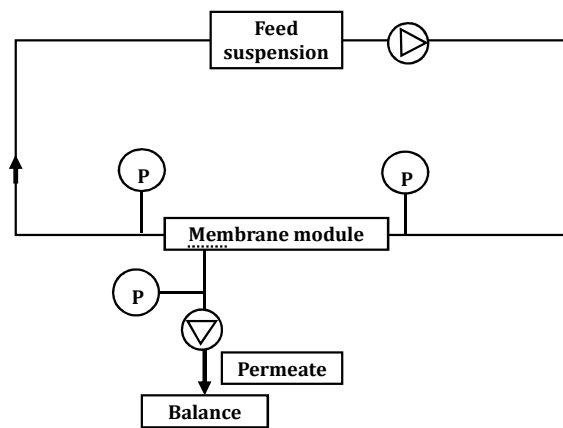

Figure 4.1. Experimental set-up for fractionation experiment.

The transmission of large or small droplets is defined as in equation 4.10:

$$Transmission = \frac{\phi_p}{\phi_b}$$
<div align="right">(4.10)</div>

where ϕ_p is the oil volume fraction of specific droplets in the permeate (-) and ϕ_b is the oil volume fractions of these droplets in the bulk (-). A transmission of 1 indicates full permeation; a transmission of 0 implies full retention. The selectivity between large and small droplets is defined in equation 4.11:

$$\alpha = \frac{\phi_{S,p}}{\phi_{L,p}} \frac{\phi_{L,b}}{\phi_{S,b}}$$
<div align="right">(4.11)</div>

Where $\phi_{S,p}$, $\phi_{L,p}$ are the oil volume fractions of the small droplets in the permeate (-) and the large ones respectively, and $\phi_{L,b}$, $\phi_{S,b}$ are the oil volume fractions of the large droplets in the bulk (-) and of the small ones respectively.

Chapter

4

4.5.   Results and Discussion

As mentioned in the theory section, shear-induced diffusion is a function of volume fraction, and particle volume ratio. Additionally, the ratio between cross-flow velocity and permeate flow determines the transmission of particles of various sizes. We now present these effects individually, and compare them in the respective sections.

4.5.1.   Volume fraction

In Figure 4.2a the transmission of large and small droplets is shown for different oil volume fractions, but always for a relative oil volume fraction of large droplets ($\phi_L/(\phi_L+\phi_S)$) of 0.21 (specifics of other process conditions are given in the Figure caption). At low concentrations, the transmission of both small and large droplets is relatively close to one, even though the large droplets are slightly retained (transmission around 0.6) and the small droplets are completely transmitted (transmission around 1). This is evident in Figure 4.2b, which shows that the droplet size distributions of bulk and permeate are rather similar for an oil volume fraction of 0.28. At low oil volume fraction, most probably fluid skimming (as described in chapter 6) causes a small difference in retention between large and small droplets. At a volume fraction of around 0.35, the transmission of the large

droplets decreases sharply and becomes zero. One can see in Figure 4.2c that large droplets are absent at an oil volume fraction of 0.47, indicating complete retention of larger droplets. Since the membrane pores are much larger than these large droplets, this indicates that the large droplets migrated away from the membrane and towards the middle of the channel. Additionally, the concentration of the small droplets in the permeate has increased as is reflected in a transmission of almost 1.2. Regarding the size distributions shown in Figures 4.2b and c, one should note that the grey and black curves cannot be compared quantitatively, because the area under the graph is by definition always 100% volume.

For the calculation of the transmission of both droplets, we have used the total concentration of the droplets in the permeate (determined by dry weight) and the ratio between small and large droplets in the permeate (derived from the distribution).

Chapter
4

(a)

(b)

(c)
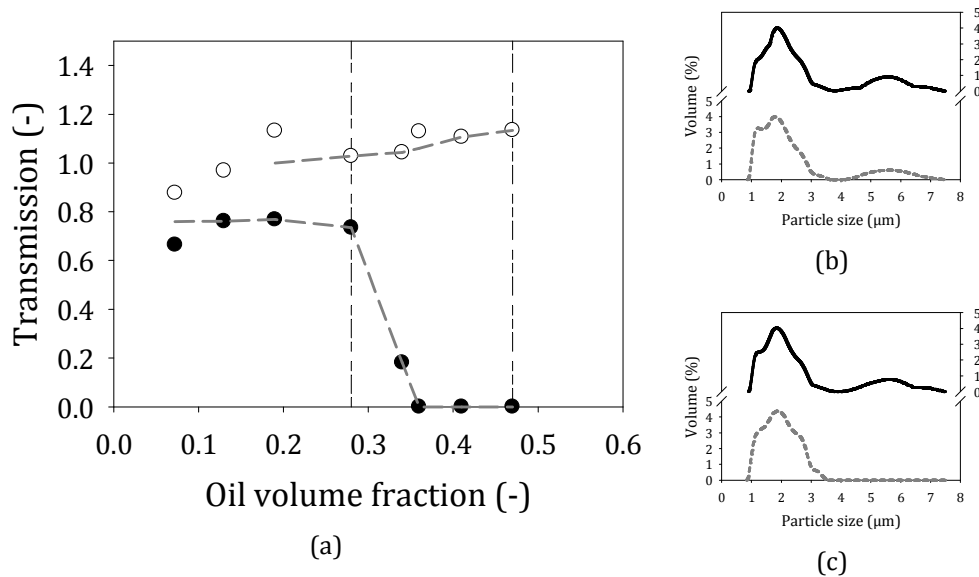
Figure 4.2a. Transmission of large (●) and small (○) droplets as a function of oil volume fraction. The dashed line is there to guide the eye through the experimental data. h is $2·10^{-4}$ m, J is $5·10^{-6}$ m/s, v is 0.3 m/s, ϕ_L/ϕ_{tot} is 0.21 and d_L/d_S is 2.81; Figure 4.2b and 4.2c represent the volume percentage of droplets present in the feed (black line) and in the permeate (dashed grey line), at total volume fractions of 0.28 (top image) and 0.47 (bottom image) as indicated by the dashed lines in Figure 4.2a.

The general behaviour is in line with the mechanism of shear-induced migration. As the shear-induced diffusion coefficient is strongly dependent on the particle size, the larger particles will migrate much more quickly than the small ones. This shows up in the experiments as the permeate having only small emulsion droplets, and retention of the large droplets. The fact that the volume fraction of small droplets in the permeate is actually larger than in the feed emulsion, indicates that the large droplets influence the small droplets in their migration behaviour, even though the oil volume fraction of the large particles is only 0.07 at a total concentration of 0.37.

There might be an additional effect. At the entrance of the module, the larger droplets start to migrate towards the centre of the channel. Since the shear rate is highest near the walls, the larger droplets are first depleted there, resulting in a higher local volume fraction just above the depleted layer. Such a higher concentration could then induce expulsion of the smaller droplets, for example towards the walls and thus lead to a transmission higher than 1.

Chapter

4

In Figure 4.3, concentration profiles of 1.53 μm and 2.65 μm particles are shown, as previously measured by CSLM in a 100 micron closed channel in chapter 3. The height in the channel is made dimensionless and expressed as *z/2H*. The total concentration is 38%, ϕ_L/ϕ_{tot} is 0.5 and the velocity is 20.8 μm/s. Even though it was not possible to match the conditions in the CSLM experiment completely to those in the filtration experiments, one can see that particles of different size segregate close to the walls and in the middle of the channel. This phenomenon is also expected to happen in our membrane experiments, and here we used the CSLM results only to visualise this effect. Shear-induced diffusion is expected to play a key role; for the membrane experiments this effect may even have been enhanced by the higher particle concentration near the membrane.

One can see that not only the larger particles accumulate somewhat in the centre, the smaller particles are expelled towards the walls. The theory indicates that the only force that counter-acts this segregation effect is Brownian diffusion. Therefore the profile can probably develop further and we expect that the migration can continue towards much stronger segregation in longer channels.
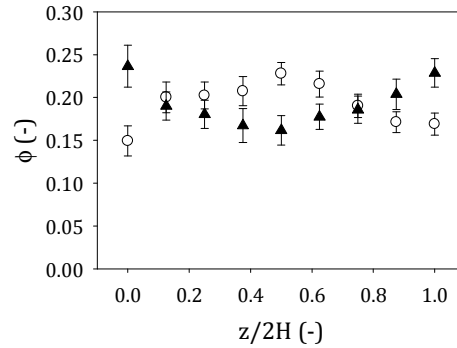
Figure 4.3. Concentration profiles for 2.65 μm (○) and 1.53 μm (▲) particles. ϕ_{tot} is 0.38, H is 50 μm, x is 24 cm, v is 20.8 μm/s and ϕ_L/ϕ_{tot} is 0.50.

In Figure 4.4, the overall transmission of large and small oil droplets together is shown. At low concentrations the transmission is somewhat below one, most probably due to fluid skimming as mentioned before. At high oil volume fractions > 0.35, fluid skimming is hindered by inter-particle interactions. The permeate still has a transmission slightly below 1, indicating that the migration of large droplets away from the membrane is not completely counteracted by migration of small ones towards the membrane. Above a concentration of 35%, fluid skimming is not likely to occur, because the concentration of particles is thus high that the particles that are closest to the pore may not be able to exit the pore anymore due to the presence of other particles. The observed effects are probably related to migration of small and large particles away from the walls as a result of particle interactions.
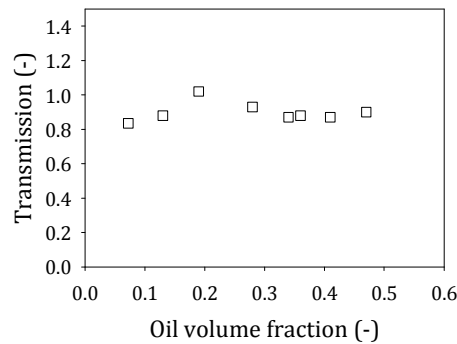

Figure 4.4. Transmission (□) as a function of oil volume fraction. h is 2·10^{-4} m, v is 0.3 m/s, J is 5·10^{-6} m/s, ϕ_L/ϕ_{tot} is 0.21, ϕ is 0.42 and d_L/d_S is 2.81.

The *selectivity* of the same process as function of volume concentration, as is done in Figure 4.5, indicates that some separation occurs at low concentration. However, the selectivity increases dramatically at volume fractions > 0.35 leading to an infinitely high selectivity above 0.37, since the volume fraction of large droplets in the permeate becomes zero.
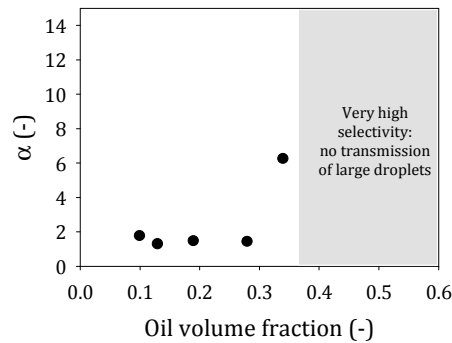

Figure 4.5. Selectivity (●) as a function of oil volume fraction. h is 2·10^{-4} m, v is 0.3 m/s, J is 5·10^{-6} m/s, ϕ_L/ϕ_{tot} is 0.21, ϕ is 0.42 and d_L/d_S is 2.81.

4.5.2.   Particle volume ratio and size ratio

In Figure 4.6 the influence of the *relative* oil volume fraction of large droplets (ϕ_L/(ϕ_L+ϕ_S) is shown; the total absolute oil volume fraction is 0.37. The transmission of the large droplets is zero with a relative fraction of large droplets below about 0.3, when using a flux of 4.7·10^{-6} m/s (round symbols). Large droplets do permeate in higher amounts, at slightly higher flux and velocity (triangular symbols). For both situations, the transmission of small droplets is high and increases when ϕ_L/ϕ_{tot} becomes larger, most probably as a result of an increased concentration of larger droplets occupying the centre of the channel and pushing the small droplets aside. For a larger size difference between large and small particles, the separation is more pronounced. This is expected since the diffusivity of droplets depends on the square of their size; although it should be noted that the droplets used here are less than a factor of 3 different in size.

The selectivity is infinitely high as long as the large droplets are absent in the permeate, while it decreases with increasing relative oil volume fraction of the large droplets. Figure 4.7 shows this trend for the experiments carried out with

Chapter

4

emulsions that are closest in size (see also Figures 4.5 and 4.6). The chance that large droplets end up in the permeate increases at higher concentration of large droplets when operated at constant permeate flux. There are simply too many particles, and some of them are sterically hindered to move to the centre. One may expect that at lower permeate flux the selectivity will be higher (see also section 4.5.3.). However, it is in fact surprising that particles that are so close in size, can be separated while being present at such high concentrations.
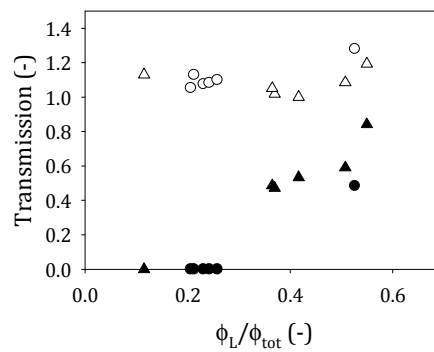
Figure 4.6. Transmission of large (●, ▲) and small (○,Δ) droplets as a function of ϕ_L/ϕ_{tot}. h is $2 \cdot 10^{-4}$ m and ϕ is 0.37. J is $4.7 \cdot 10^{-6}$ m/s, v is 0.3 m/s and d_L/d_S is 2.66 for circles; J is $1 \cdot 10^{-5}$ m/s, v is 0.59 m/s and d_L/d_S is 1.98 for triangles.
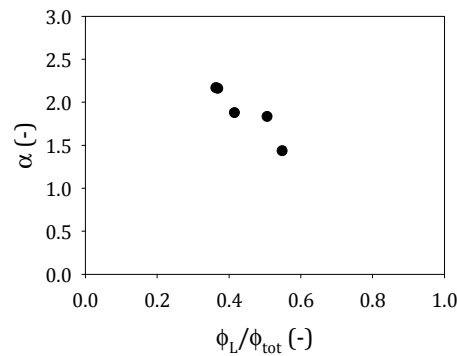
Figure 4.7. Selectivity (●) as a function of ϕ_L/ϕ_{tot}. h is $2 \cdot 10^{-4}$ m, J is $1 \cdot 10^{-5}$ m/s, v is 0.59 m/s, ϕ is 0.37 and d_L/d_S is 1.98.

4.5.3.   Influence of the stage cut (permeate flow in relation to cross-flow)

At an oil volume fraction of 0.42, and a permeate flux of $5 \cdot 10^{-6}$ m/s (Figure 4.2a) there is total segregation between small and large droplets. The permeate flux is very important for this effect, as is shown in Figure 4.8. At low permeate flux the transmission of large particles is low or even zero, while that of small particles remains high. However, above a flux of $6.5 \cdot 10^{-6}$ m/s, the transmission of large droplets suddenly increases, while the transmission of small droplets decreases. The layer of fluid that will become the permeate increases in size at higher flux, and large particles that may not have migrated far enough will be incorporated in the permeate. Additionally, the concentration of small particles decreases further away from the membrane.
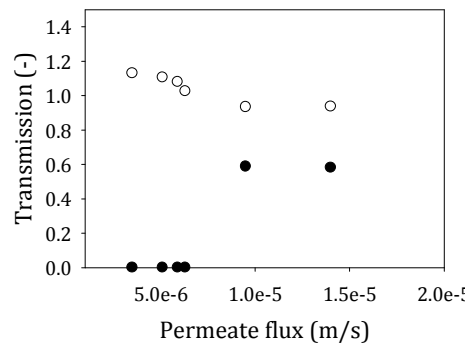
Figure 4.8. Transmission of large (●) and small (○) droplets as a function of permeate flux. h is $2 \cdot 10^{-4}$ m, v is 0.3 m/s, ϕ_L/ϕ_{tot} is 0.21, ϕ is 0.42 and d_L/d_S is 2.80.

4.6.   Comparison

In Figure 4.9a, b and c, we made various results non-dimensionless using the stage cut v_p/v_f, defined as the velocity ratio of permeate and cross-flow. The effects are similar to those reported in Figure 4.8, because the concentration profile does not change when the velocity of the feed is increased. This is also demonstrated in equation 4.9, where the velocity is in the time scale for diffusion as well as convection via the shear rate and therefore does not appear in the Péclet number. However, the stage cut determines the thickness of the fluid layer entering the permeate compartment in membrane filtration processes. At lower stage cuts, large droplets can be well separated from small droplets. At a total oil volume fraction of 0.27 and ϕ_L/ϕ_{tot} below 0.15 this v_p/v_f ratio seems to be $< 0.5 \cdot 10^4$ (Figure

4.9a). At higher concentration (42%) and 0.2 relative fraction of large droplets, this limit seems to have moved to a v_p/v_f ratio of < $0.3 \cdot 10^4$ (Figure 4.9b, based on data from Figure 4.8).

Figure 4.9a. Transmission of large (●) and small (○) droplets as a function of v_p/v_f. h is $2 \cdot 10^{-4}$ m, ϕ_L/ϕ_{tot} is below 0.15, ϕ is 0.27 and d_L/d_S is 2.40.

Figure 4.9b. Transmission of large (●) and small (○) droplets as a function of v_p/v_f. h is $2 \cdot 10^{-4}$ m, ϕ_L/ϕ_{tot} is 0.2, ϕ is 0.42 and d_L/d_S is 2.80.
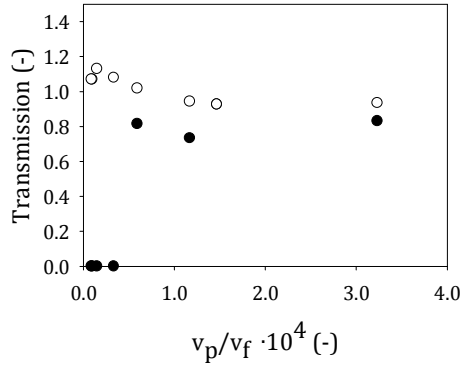

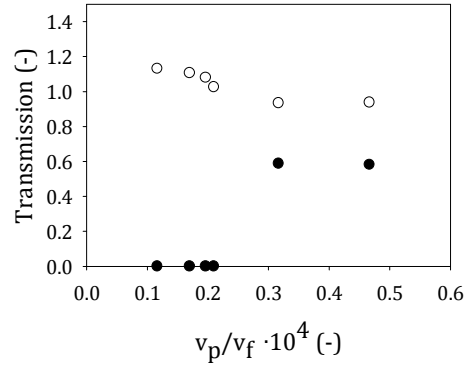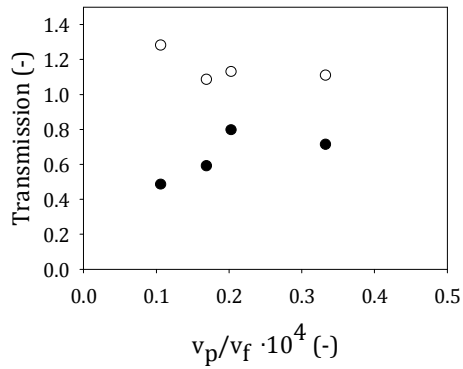
Figure 4.9c. Transmission of large (●) and small (○) droplets as a function of v_p/v_f. h is $2 \cdot 10^{-4}$ m, ϕ_L/ϕ_{tot} is between 0.5 and 0.6, ϕ is 0.37 and d_L/d_S is 2.16.

In Figure 4.9c, where the concentration is 37% and the relative oil volume fraction of large droplets is between 0.5 and 0.6, segregation is less strong, but selective

separation may be possible at lower permeate fluxes that were not covered in this investigation. Besides, it is noteworthy, that under these conditions the transmission of small droplets is very high (1.3 at α of 2.62). There seems to be a critical stage cut which is dependent on the total volume fraction and the relative fraction of large droplets.

This latter effect is investigated in more detail, since it could indicate that during a batch concentration process, the separation would improve because of the effects that were observed. For this we started with 100 mL of emulsion with total oil fraction of 37% containing a relative large droplet oil volume fraction of 0.21. The permeate flux is such that $v_p/v_f < 0.2 \cdot 10^4$), for which we expect that the transmission of small droplets increases, while the transmission of the large droplets is zero. The measured transmission data are in good agreement with our expectations (Figure 4.10a).

Chapter

4
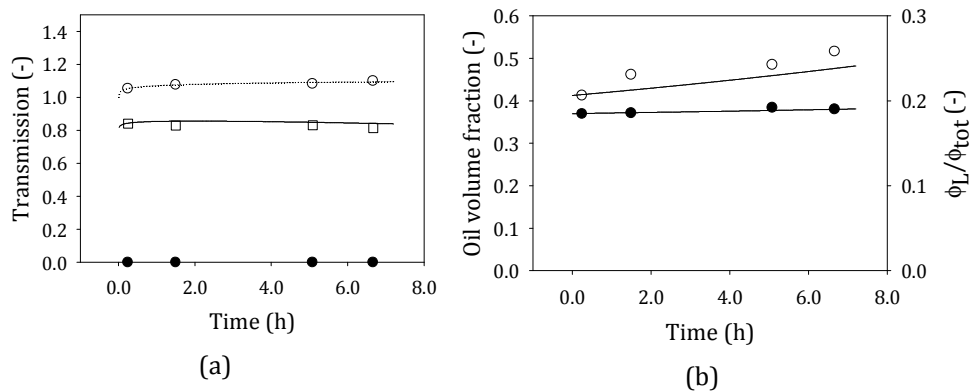
Figure 4.10. Total transmission (□) and transmission of large (●) and small (○) droplets (a) and oil volume fraction (●) and ϕ_L/ϕ_{tot} (○) (b) as a function of time. h is $2 \cdot 10^{-4}$ m, J is $4.7 \cdot 1^{-6}$ m/s, v is 0.3 m/s, d_L/d_S is 2.66. Black lines are calculations of total transmission (a), oil volume fraction and ϕ_L/ϕ_{tot} (b), based on the measured transmission of small particles (dotted line).

During the experiment, the total volume fraction of oil in the feed remained constant. The fraction of large particles in the feed increased steadily, while at the same time the concentration of the small droplets in the feed decreased (not depicted here). Thus in time there is a shift in ϕ_L/ϕ_{tot} ratio towards higher values, leading to an increase of the transmission of small droplets (Figures 4.10a and b).

The measurements are in line with theoretical simulations of total transmission, oil volume fraction and ϕ_L/ϕ_{tot} depicted by the black lines in Figure 4.10a and b and based on transmission data of the small particles (dotted line). This shows that shear-induced diffusion can be used advantageously in many different ways, allowing even concentration of two particles simultaneously.

4.7. Application

From the previous sections it is clear that shear-induced segregation is a new and versatile mechanism that can be used in many different ways to improve processes. In the geometry used here, accumulation or clogging of components is prevented; the need for cleaning is reduced, leading to less waste water, less chemicals and less energy. No dilution is required; in fact the separation requires high concentrations. An additional energy cut is achieved by the possibility to apply low cross-flow velocities and pressures. Besides, the fraction composition can be steered through the trans-membrane pressure.

Size separation of particles in the fluid, requires equipment that should be able to separate the fluid layers consisting of different particle sizes. Membranes can be used as demonstrated in this chapter, but also other options such as concentric pipes of different diameters may be considered for a tube geometry, or dividing walls in a rectangular channel. Regarding membranes, it is essential that there is a non-porous area of which the length depends on the size and concentration of the particles, but in most cases an entrance length of 10 cm is sufficient (for relatively shallow channels). In practice this should not be too difficult to realise through the potting length. Further it is expected that the membrane length would need to become shorter than is usual nowadays, but this is compensated by the much higher and constant flux that can be reached.

If this is not desirable, channels with consecutive non-porous and porous areas can be considered (Figure 4.11a). The non-porous areas are obviously needed to allow segregation to take place and in the porous areas (ultimately only a big hole) the permeate is collected. The length of the non-porous area is determined by the entrance length needed for the particles to segregate, which may repeatedly be applied. Since the selectivity decreases as the ratio ϕ_L/ϕ_{tot} increases further along

the channel through removal of small particles, the non-porous areas may need to become longer, or the local permeate flux lower. When considering larger scale operation, the first option is easier to realise. Alternatively, a tapered channel (Figure 4.11b) can be considered which will enhance separation as a result of a decrease in channel height. At equal entrance length for particle migration, diffusivity increases when the ratio between half the channel height and particle size (H/a) decreases (equation 4.9).

(a)   (b)
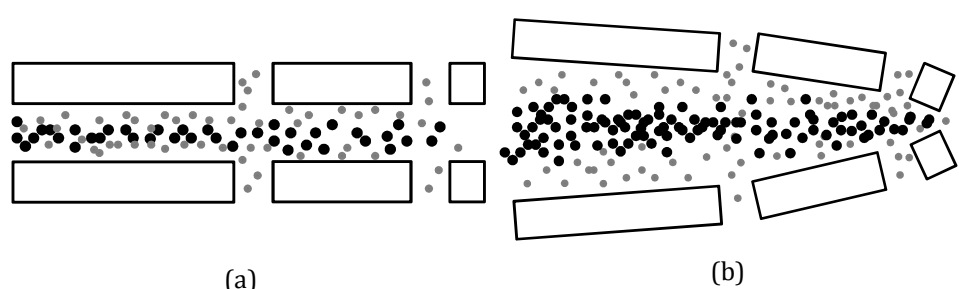
Figure 4.11. Schematic drawing of channels with non-porous and porous areas (here depicted as open area). Particles can segregate in the channel and small particles are removed in the porous areas. Design (a) uses uniform height of the channel, while design (b) is tapered.

Chapter

4

The typical channel heights that need to be used to enhance shear-induced diffusion are below 1 mm, ideally 0.2 mm and lower; and also this is well within reach of current membrane modules. In the systems described in this chapter we used a channel height of 0.2 mm (H/a of around 40) and particles segregated within the first 10 cm of the channel. Alternatively also microfluidic devices can be used since they would allow operation with even shallower channels, and the entrance length will become shorter.

For stable operation, the stage cut is an essential parameter and needs to be controlled accurately. For pores that are generally very densely packed on a small area, this means that they should be homogenous in size and shape. When using one big opening instead of many pores, the shape and size can be tuned according to the local velocities and pressures. Small H/a ratios lead to stronger pressure drops over the channel and this pressure can be used to determine the amount of fluid through a hole. The cross-flow velocity is not in the Péclet number (equation 4.9) and therefore the cross-flow velocity can be chosen such, that the preferred

pressure drops are obtained (for example in a microfluidic microchannel with side-branches acting as holes).

All these strategies can be applied without being worried about accumulation of components, therewith reducing the need for cleaning. The product flux is in fact equal to industrial fluxes, with very constant performance and if needed total fractionation; cross-flow velocities and pressures are much lower than currently used, which is favourable from an energy point of view. The fluxes on a $L/(m^2 \cdot h \cdot bar)$ basis are in the order of $1 \cdot 10^4$ $L/(m^2 \cdot h \cdot bar)$, which is much higher than those with 'classic' operational microfiltration fluxes; typically in the range of 150-2000 $L/(m^2 \cdot h \cdot bar)$. Besides, we found that particles close in size can be segregated with shear-induced diffusion, even at a ratio of 1:1.73 separation is possible, which is not possible with classic membrane filtration. Logically, a higher selectivity may be obtained when particle sizes are further apart.

4.8. Conclusions

In the process demonstrated in this chapter, shear-induced diffusion of emulsion droplets leads to fractionation of different sized droplets in filtration processes. Filters can be used that have pores that are considerably larger than the droplets, without accumulation of droplets on the filter. Different fractions can be obtained by tuning the flow and feed characteristics, which may lead to zero permeation of large droplets and enhanced permeation of small droplets, especially at high concentrations. Complete fractionation can be achieved with differences in size as small as 50%. The process can remove only small particles from the feed at 40 $L/(m^2 \cdot h)$ and can fractionate at even higher flux (2-10 fold higher) depending on the degree of fractionation that is required, and always at constant retention as function of time. The processes presented here operate at very low cross flow velocity and trans-membrane pressure, and show that flow-induced particle migration, i.e. shear-induced diffusion, can successfully be applied to filtration processes to improve selectivity, making pore size a feature that is no longer of importance for the actual separation.

Chapter 5

Separation of Concentrated Emulsions

using Hydrodynamic Interactions

5. Separation of Concentrated Emulsions using Hydrodynamic Interactions

5.1.   Abstract

Separation of concentrated suspensions by centrifugation or membrane separation is currently preceded by dilution to concentrations below five per cent, thereby wasting valuable energy and water. We show that hydrodynamic interactions between particles can induce separation on particle size in Poiseuille flow, through a channel with partly porous walls. The separation becomes more effective at higher concentrations and can be adjusted by changing process conditions. Larger particles are completely retained and smaller particles are exuded, at concentrations higher than in the flow, through pores much larger than the particles. The process is stable over time and not affected by any fouling of the wall or pores. The observations are consistent with the shear-induced migration principle, though effects of fluid skimming can be observed. Since the process works well at low velocities and high concentrations, industrial application could have major benefits by minimizing water, waste and energy use.

Chapter

5

5.2.   Introduction

Fractionation of large and small particles or separation of particles from a suspension with membrane separation is influenced by accumulation and clogging of particles on the membrane (Chavan 1983; Goldsztein 2005) and to prevent this, these processes have to be operated at low concentrations (Leniger and Beverloo 1975; Lisińska and Leszczyński 1989). At these low concentrations, separation is easier to achieve and although many improvements have been made to process concentrated suspensions (Huang, Cox et al. 2004; Di Carlo, Irimia et al. 2007), they usually operate not that well (Rushton, Ward et al. 2008). If separation and fractionation could be carried out with concentrated suspensions this would have clear advantages, and to achieve this we use hydrodynamic particle interactions.

Although migration in concentrated suspensions has been studied by several authors ranging from the most basic observations (Abbott, Tetlow et al. 1991; Graham, Altobelli et al. 1991), to rheology (Chow, Sinton et al. 1994; Mills and

Snabre 1995; McCarthy and Kerr 1998; Cheng, McCoy et al. 2011), modeling (Phillips, Armstrong et al. 1992; Nott and Brady 1994; Chen, Lam et al. 2004; Vollebregt, van der Sman et al. 2010) and the (ir)reversible behavior of sheared suspensions (Pine, Gollub et al. 2005), for separation applications this is not the case. Some authors studied systems that are of relevance to this field; especially bidisperse suspensions were studied by Husband *et al.* (1994), Krishnan *et al.* (1996), Semwogerere and Weeks (2008), and Shauly *et al.* (1998) (Husband, Mondy et al. 1994; Krishnan, Beimfohr et al. 1996; Shauly, Wachs et al. 1998; Semwogerere and Weeks 2008). Lyon and Leal (1998) described the difference in hydrodynamic diffusion coefficients for particles of different sizes, based on the hydrodynamic particle-particle interactions and showed how these particles can influence each other (Lyon and Leal 1998). Hydrodynamic migration occurs when particles disturb the flow field around another particle; either by their rotation in shear flow, or by moving to a slower or faster-moving streamline (Breedveld, van den Ende et al. 2001). When three or more particles are involved simultaneously, the net displacement is random, resulting in diffusion-type behaviour of the particles. These interactions are much more abundant when the concentration increases, so significant hydrodynamic migration takes place especially in concentrated suspensions.

Phillips *et al.* (1992) indicated that this process is driven by a number of forces: not only a gradient in particle volume fraction, but also gradients in shear rate and viscosity lead to net migration (equation 5.1) (Phillips, Armstrong et al. 1992):

$$J_{mig} = -D_{shear} \nabla \ln\left(\dot{\gamma}\phi\eta^{\lambda}\right) \tag{5.1}$$

In which $\dot{\gamma}$ is the shear rate (s^{-1}), ϕ the oil volume fraction (-), η the viscosity (Pa·s) and λ a constant (-).

Since in Poiseuille flow, the shear rate in the centre of the channel is zero, and highest at the wall of the channel, one can immediately see that migration of particles takes place from the wall, towards the centre of the channel. D_{shear} is given in equation 5.2:

$$D_{shear} = K\dot{\gamma} a^2 \phi^2$$

(5.2)

With a the particle radius (m) and K is described by equation 5.3:

$$K = 1 + 0.5 e^{8.8\phi}$$

(5.3)

The average shear rate and the shear rate in Poiseuille flow very close to the wall (γ_{wall}) are described in equation 5.4 and 5.5 respectively.

$$\dot{\gamma} = \frac{6 \cdot \bar{v}}{h} - \frac{12 \cdot \bar{v} \cdot z}{h^2}$$

(5.4)

$$\gamma_{wall} = \frac{8 \cdot \bar{v}}{h}$$

(5.5)

With $\bar{v}$ the average velocity in the channel (m/s), z the distance from the channel wall (m) and h the channel height (m).

Regular membrane separation suffers from strong accumulation of components near and on the membrane and in the membrane pores (Belfort, Davis et al. 1994; Song 1998; Wang and Song 1999; Knutsen and Davis 2006) and prevention of accumulation through adjustment of process conditions or membrane modification is complex (Sandblom 1978; Field, Wu et al. 1995; Howell 1995; Tardieu, Grasmick et al. 1998; Saboya and Maubois 2000), and mostly not complete. To make use of hydrodynamic migration, we combine a closed channel in which hydrodynamic diffusion takes place towards the centre of the channel, followed by a channel with porous walls. A slight overpressure leads to permeation of the suspension closest to the wall, through the pores. We define the transmission (equation 5.6) of particles of a specific size with

$$Transmission = \frac{\phi_p}{\phi_b}$$

(5.6)

Chapter

5

in which ϕ_p is the volume fraction of specific particles in the permeate (-) and ϕ_b is the volume fraction of these particles in the feed solution (-). A transmission of 1 implies that the suspension particles have the same concentration in feed and permeate; a transmission of 0 implies complete retention. The effect of hydrodynamic migration is tested with concentrated emulsions, with different droplet sizes.

5.3. Experimental

Emulsions of silicone oil (density of 1.01 g/cm^3; silicone oil AR 20, Sigma Aldrich, Germany) in water were prepared at oil volume fractions ranging from 0.10 to 0.47. Depending on the oil volume fraction, the silicone oil, demineralized water and span80 (Sigma-Aldrich, Germany) as well as Tween80 (Sigma-Aldrich, USA) were mixed in different ratios. The Span80 concentration was always 1% (w/w) as is the Tween80 concentration. An emulsion containing droplets of 2 (span is 0.66) and 5.5 micron (span is 0.30) could be prepared with an Ultra-Turrax (IKA, T18, Germany; 20000 rpm for 10 minutes), resulting in a set ratio of 20 volume% large particles compared to the total.

Membrane microfiltration experiments were performed with the two emulsions that were mixed in a pre-determined ratio. A round nickel sieve (1.39 cm^2) with uniform spherical pores of 20 μm or rectangular pores of 15 x 390 μm (Veconic sieve, Stork Veco BV, The Netherlands) was placed after 34.5 cm of closed channel. The emulsion was fed to the system with a positive displacement pump (VG1000digit, Verdergear, Germany). Pressure sensors (EL-PRESS P-502C, Bronkhorst High-Tech B.V., the Netherlands) were installed at the beginning and the end of the module, and after the sieve. The pressure data were recorded with Bronkhorst High-Tech software. The pressure over the membrane was measured with a balance (CP4202S, Sartorius, Germany) connected to a computer (Memfill-Lite software, Wageningen University, the Netherlands). The cross flow velocities were 0.3 m/s and the channel height was 0.2 mm. The permeate flow was set at a specific value with a peristaltic pump (series 205U, Watson Marlow, England).

Particle sizes of the initial emulsions, the mixtures and the permeate were measured in the Malvern Mastersizer (Malvern Instruments Ltd, UK). The total

volume fraction of oil was determined by a dry weight measurement, for which the samples were stored overnight in an oven at 80 degrees Celsius (Memmert, Germany). Additionally a mass balance of small and large particles was made, to verify that the size of the emulsion particles is not affected and process conditions are constant during the experiments

5.4. Results

Equation 5.2 indicates that the hydrodynamic diffusion of large particles is much faster than that of smaller ones. Therefore, the suspension near the walls will become depleted of the larger suspension particles. Figure 5.1 shows the predicted particle concentration based on equation 5.1, for 2 and 5.5 micron particles and two concentrations at a dimensionless height in the channel (z/h).
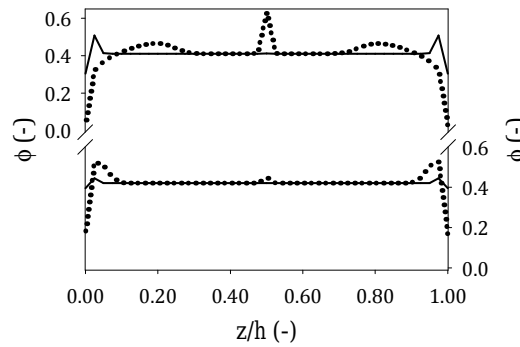
Figure 5.1. Prediction of the concentration profile for 5.5 μm and 2 μm particles according to eq. 1. Upper graph: concentration of 5.5 μm particles. Lower graph: concentration of 2 μm particles. Black lines correspond to an entrance length of 0.345 meter and dotted lines correspond to an entrance length of 27 meter. The total concentration is 42% and the channel height 200 μm.

The lines in Figure 5.1 correspond with the 5.5 micron and 2 micron emulsion droplets which will be used in the experiments. Due to their higher diffusion coefficient, larger particles move faster than smaller particles. The smaller particles are then displaced and pushed closer to the wall. After a certain entrance length, the concentration of large particles in the center of the channel is higher than that of the feed solution; in addition the smaller particles accumulate in the region close to the wall.

An emulsion consisting of 2 and 5.5 micron droplets was first led through a closed entrance channel of 34.5 cm, followed by a membrane with round pores of 20 micron. One would not expect any retention based on size exclusion. The pressures and flows in the channels and across the porous walls were constant in time, which indicates that no particles accumulated in and on the channel walls. Indeed, the separation performance was constant in time. Figure 5.2 shows the experimental transmission of small and large particles, as a function of the total particle volume fraction in the feed suspension.
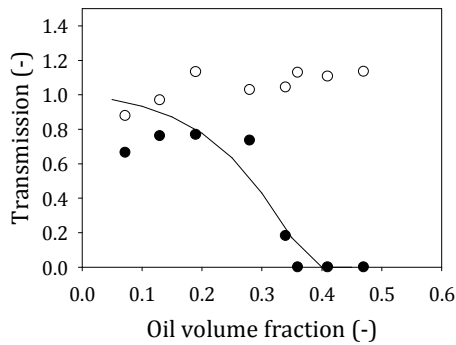
Figure 5.2. Transmission of large (●) and small (○) particles as a function of oil volume fraction. The predicted transmission according to eq. 1 of the 5.5 μm particles is shown by the line. The channel height is $2 \cdot 10^{-4}$ m, the fluid velocity through the membrane is $5 \cdot 10^{-6}$ m/s, the average velocity is 0.3 m/s, 20% of the particle volume consists of large particles and the non-porous channel is 0.345 meter.
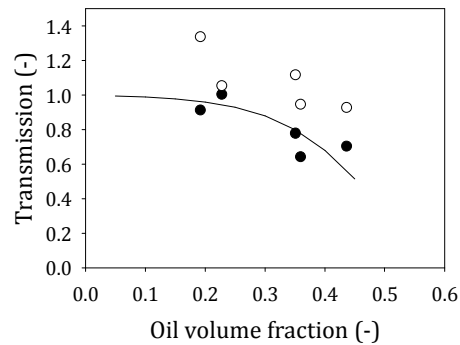
Figure 5.3. Transmission of large (●) and small (○) particles as a function of oil volume fraction. The predicted transmission according to eq. 1 of the 5.5 μm particles is shown by the line. The channel height is $2 \cdot 10^{-4}$ m, the velocity of the fluid through the membrane is $5 \cdot 10^{-6}$ m/s, the average velocity is 0.3 meter per second, 20% of the particle volume consists of large particles and the closed entrance length is 0.06 meter.

At high oil volume fractions, where hydrodynamic diffusion is most pronounced, the transmission of larger particles becomes zero (see Figure 5.2). At the same time, the transmission for the smaller particles becomes even larger than 1, indicating higher concentrations in the permeate than in the feed. Thus, for emulsions with total volume fractions above 35% there is total segregation between 2 and 5.5 micron particles, with higher volume fractions both in the

permeate and the concentrate, relative to their volume fractions in the feed suspension. At lower concentrations, these effects are lost.

When using a non-porous entrance channel of 6 cm instead of 34.5 cm, the separation is very different as illustrated in Figure 5.3; clearly the length of the entrance channel is of essence for the migration to take place. For both situations (Figures 5.2 and 5.3), the transmission of large droplets predicted with equation 5.1, matches the observations closely. Please note that the equation is in fact valid for a monodisperse suspension and that we take into account here that only 20% of the total concentration consists of large particles. This means that 20% of the particles close to the wall have to be removed, to obtain a transmission of zero for the large particles. Further the equation does not contain any fit parameters.

In addition to the effect of hydrodynamic migration, which acts in the bulk of the suspension, there is interaction between individual particles and the wall itself. Single particles close to the wall may be withheld from entering a pore by the fluid skimming effect. As long as the cross-flow dragging the particle over a pore mouth is large enough relative to the flow through a pore, it will be taken up again by the feed, and will not enter the pore. The ratio of cross-flow and transversal flow through the pores is the most important parameter here. It is described here as the time a particle needs to travel over the pore, compared to the time a particle needs to sink into the pore and is called the dimensionless time:

$$\Theta = \frac{l_{pore}J}{\varepsilon_{length}v_x(z)z} \approx \frac{Jh(l_{pore} + l_{closed})}{6\bar{v}a^2} \tag{5.7}$$

In this equation l_{pore} is the pore length in the direction of the cross-flow over the pore (m), J the trans-membrane flux (m/s), ε_{length} is the length porosity (-), $v_x(z)$ the velocity of the particle at a height z (m/s) which corresponds to the height of the particle in the channel (m). The length porosity is given by equation 5.8:

$$\varepsilon_{length} = \frac{l_{pore}}{(l_{pore} + l_{closed})} \tag{5.8}$$

Chapter

5

l_{closed} is the closed part of the membrane between two consecutive pores (m). The velocity in the channel at a particle radius (a) away from the wall is given in equation 5.9.

$$v_x(a) = 6\,\bar{v}\left[\frac{a}{h} - \left(\frac{a}{h}\right)^2\right] \approx \frac{6\,\bar{v}\,a}{h} \quad \text{when } a << h \qquad (5.9)$$

When Θ is large, the particle will be sucked into the pore and end up in the permeate; when it is small, it will be retained. The transmission of particles depends on the design of the pores in the walls.

In Figure 5.4, two tested designs are shown: rectangular pores are placed either perpendicular or parallel to the cross-flow. Figure 5.5 shows the transmissions at a droplet concentration of 42% for different pore geometries at various dimensionless times. As pore geometry is included in the dimensionless time, the onset of transmission increase is equal for the different pores.

In Figure 5.5 the transmission of large particles, at dimensionless times between 0.06 and 0.08, is measured to be around 0.6 for round pores. In equation 5.10, the Ferry-Faxen equation (Ferry 1936) predicts the transmission of particles based on size exclusion as function of the ratio of the particle size to the radius of the pore, $\delta = a/R_{pore}$.

$$\text{Transmission} = (1-\delta)^2 \cdot \left[1 - 0.104\,\delta - 5.21\delta^2 + 4.19\,\delta^3 + 4.18\,\delta^4 - 3.04\,\delta^5\right] \quad (5.10)$$

For the particles with an average size of 5.5 micron, the transmission is expected to be 0.36. However, as particles are dragged towards the pore, local concentrations above the pore may increase, and in steady state again lead to a transmission of 1.

5.5. Practical relevance

As is shown in figure 5.2 the separation works better at high concentrations, and can even lead to absolute separation. Thus, suspensions can be separated in concentrated form, leading to much smaller equipment. Besides, less solvent is needed which then does not need to be removed after separation.

(a)

(b)
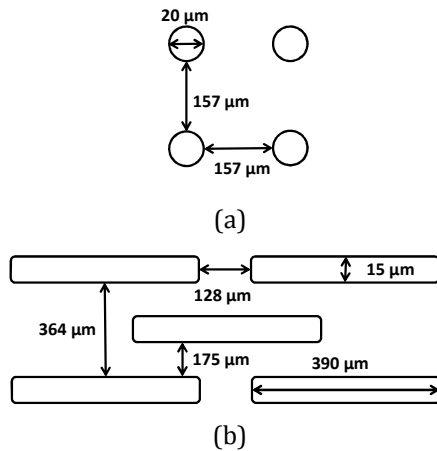
Figure 5.4. Filter design and pore dimensions for 20 micron round pores (a) and 15 by 390 micron rectangular pores (b). Note that the graph is not drawn to scale.
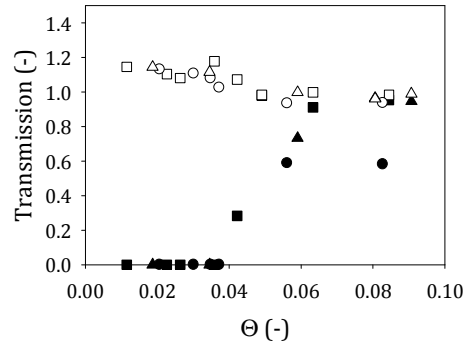
Figure 5.5. Transmission of large (●,■,▲) and small (○,□,Δ) particles as a function of dimensionless time Θ. The channel height is $2·10^{-4}$ m, 20% of the particle volume consists of large particles and the total oil volume fraction is 0.42. The round symbols are for the circular pore; the length porosity is 9%. The square symbols are for the rectangular pore perpendicular to the cross-flow direction; length porosity is 8%. The triangular symbols are for the rectangular pore parallel to the cross-flow direction; length porosity is 75%.

We illustrate the practical relevance of the principles, with an example from the brewing industry. The removal of beer from concentrated yeast suspensions (~45%) after primary removal of yeast from beer can be profitable and sustainable. At this moment, no processes are available to remove the remaining beer from the concentrated yeast stream. This beer consists of roughly 3% of the total beer produced in a factory. Hydrodynamic migration is possible in a narrow channel having pores of 10 μm, and low cross-flow velocities. Processing will consume around $7.7·10^{-3}$ kWh/hL of energy and beer which was regarded as waste before can now be a valuable product. The beer can be sold for 0.13 euro per litre and depending on the costs per membrane area (which is normally between 50

and 500 euro/m^2), the return of investment period is much less than 1 year for a membrane area of 20 m^2 (Figure 5.6) (for additional information, see appendix).
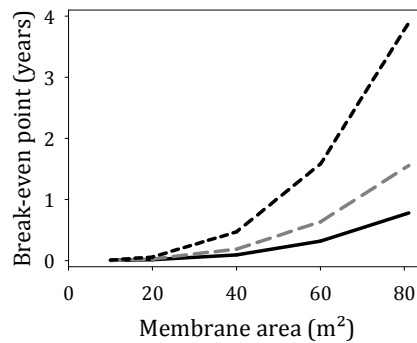
Figure 5.6. Break-even point as function of membrane area for microfiltration of concentrated yeast streams. Lines represent the break-even point in years for different membrane costs, being 100 euro/m² (black line), 200 euro/m² (grey dashed line) and 500 euro/m² (black dashed line). Calculations are based on a channel length of 1.7 cm, with a porous part of 88%. The channel height is 0.1 mm, with a membrane flux of 150 L/(m²·h), a cross-flow velocity of 0.05 m/s and a particle size of 2 micron. The membrane has pores of 10 micron and a length porosity of 91%. For additional information see chapter 7.

It is possible to separate the suspension into several fractions having different average particle size. This could be done by having consecutive porous zones in the channel. In between the porous zones, some channel length with solid walls may be applied to have re-migration of the particles away from the channel walls. The absolute flow rate is not important, as long as the flow is laminar. The migration is determined by the total number of encounters of particles. A flow rate that is twice as high, will result in twice the number of encounters per second, and hence the same displacement per unit of channel length. Finally, the system is quite robust. While membrane processes are severely hindered by fouling on the membrane and in the pores, hydrodynamic diffusion is a bulk process. Even when fouling would take place on the walls and in the pores, their dimensions compared to the particles are so large, that the process is not hindered by it. This, in combination with the very high concentrations possible, makes that the new principle of hydrodynamic separation has great potential for practical application, and allows separations to occur that are otherwise not possible.

5.6. Conclusion

Hydrodynamic interparticle interaction allows fractionation of suspensions on particle size in very concentrated suspensions. The more concentrated the suspension is, the more efficient the effect is. The large particles can be totally segregated from the small particles, while the concentration of the smaller particles in the permeate can be even higher than in the feed solution, leading to a net concentration. This principle is robust against fouling, is independent of (laminar) flow rate, and the separation can be tuned by adapting the ratio of flow rates (cross-flow and permeation). It can be easily developed into an alternative to current separation processes, like membrane filtration, to obtain clear fractions of both small and large particles. Processing of these concentrated systems can be done without dilution, therewith saving energy, water and waste. Further, as the process runs at very low flow rates, it is very efficient in energy use.

Chapter

5

5.7. Appendix – Energy calculations

5.7.1. Process conditions

For hydrodynamic particle interactions to take place and to make optimal use of them, it is necessary to operate in the laminar regime, with a positive flux over the entire length of the membrane. For these aspects, the following equations are used.

A. Negative trans-membrane pressures over the membrane length should be prevented. The trans-membrane pressure, given in equation A5.1, should be at least half the pressure drop over the membrane length.

$$J = \frac{\Delta P}{\eta_0 R_m}$$

(A5.1)

With J the transmembrane flux (m³/m²·s), ΔP the trans-membrane pressure (Pa), η_0 the viscosity of the continuous phase (Pa·s) and R_m the membrane resistance (1/m).

For concentrated suspensions (> 30%), the particles need sufficient time to diffuse and below a mathematical guideline is given. Additionally the dimensionless time, which is the ratio between the time a particle needs to travel over the pore, compared to the time a particle needs to sink into the pore, should be lower than 0.04 for a concentration of around 42% .

A. Phillips *et al.* (1992) indicated that there are various driving forces for particle behaviour, leading to particles having the tendency to move towards regions with lower volume fraction, lower shear rate and lower viscosity (Phillips, Armstrong et al. 1992). The particle flux as a result of these forces is given in equation A5.2.

$$J_{mig} = -D_{shear} \nabla \ln\left(\dot{\gamma}\phi\eta^{\lambda}\right)$$

(A5.2)

In which $\dot{\gamma}$ is the shear rate (s⁻¹), ϕ the oil volume fraction (-), η the viscosity (Pa·s), λ a constant (-) and D_{shear} the shear-induced diffusion coefficient (m²/s).

B. The ratio between the time scale of the convective and the diffusive process is a Péclet number (equation A5.3), described in chapter 3 and should be smaller than 1 to have an effect of shear-induced diffusion.

$$\text{Pe}^* = \frac{\tau_{dif}}{\tau_{con}} = \left(\frac{H}{a}\right)^2 \frac{1}{12\text{D}_\varphi} \frac{H}{L} \tag{A5.3}$$

With τ_{dif} the time scale for diffusion (s), τ_{con} the time scale for convection (s), H the channel half-height, a the particle radius (m), D_ϕ the dimensionless shear-induced siffusion coefficient (-) and L the entrance length (m).

C. The dimensionless time for concentrated suspensions is described by equation A5.4.

$$\Theta = \frac{l_{pore} \cdot J}{\varepsilon_{length} \cdot v_x(z) \cdot z} \approx \frac{J \cdot h \cdot (l_{pore} + l_{closed})}{6 \cdot \bar{v} \cdot a^2} \tag{A5.4}$$

In this equation l_{pore} is the pore length (m), J the trans-membrane flux (m/s), ε_{length} is the length porosity, $v_x(z)$ the velocity of the particle at a height z (m/s) which corresponds to height of the particle radius in the channel (m).

5.7.2.   Module design

A. The length e_L (m) of the closed channel needed to establish a fully developed velocity profile is given in equation A5.5.

$$e_L = 0.06 \text{Re}_c h \tag{A5.5}$$

With Re_c the dimensionless Reynolds number (-) described in equation A5.6.

$$\text{Re}_c = \frac{\rho \bar{v} h}{\eta} \tag{A5.6}$$

With ρ the density of the suspension (kg/m³), $\bar{v}$ the average velocity in the channel (m/s), h the channel height (m) and η the viscosity (Pa·s).

5.7.3.   Pressure drop and energy

A. As a practical limitation we assume that the pressure drop over the membrane channel (Δp) should be as low as possible.

$$\Delta p = \frac{32\rho \bar{v}^2 \left(L_m + e_L + L\right)}{\text{Re}_c \, h} \qquad \text{(A5.7)}$$

With ρ the density of the suspension (kg/m³), Δp the pressure drop (N/m²) and $\bar{v}$ the average velocity in the channel (m/s), L_m the membrane length (m), e_L the length to establish a fully developed velocity profile (m) and L the closed entrance length for hydrodynamic interactions (m), Re_c the Reynolds number (-) and h the channel height (m).

B. The energy consumption for a microfiltration process is mainly determined by the circulation pumps to deliver the relatively high cross-flow velocities (Mulder 1996). The energy consumption to pressurize a liquid is given by equation A5.8 for one channel.

$$E_p = \frac{q_v \Delta p}{\eta_{eff}} \qquad \text{(A5.8)}$$

With q_v the flow rate (m³/s), Δp the pressure drop (N/m²) and η_{eff} the efficiency of the pump, which is generally between 0.5 and 0.8; in the calculations an efficiency of 0.6 is assumed.

Chapter 6

Separation of Dilute Suspensions using Fluid Skimming

6. Separation of Dilute Suspensions using Fluid Skimming

6.1. Abstract

We here report on the separation of yeast cells, with micro-engineered membranes having pores that are typically five times larger than the cells. The separation is due to neither shear-induced diffusion, nor initial lift, but to an effect similar to fluid skimming. The separation performance is linked to the ratio between cross-flow and trans-membrane flux, and could be captured with a dimensionless number relating those. On the basis of this dimensionless number, flux and transmission of the cells could be predicted.

The mechanism rests on having a sufficiently high cross-flow velocity, such that particles are not dragged too deep in the pore, but are dragged with the cross-flow back into the feed stream. The separation factor can simply be changed by changing the ratio between crossflow velocity and trans-membrane flux.

Since the membranes have very large pores, fouling does not play a role. Constant high trans-membrane flux values of 200 to 2200 $L/m^2 \cdot h$ were reached for trans-membrane pressures ranging from 0.02 to 0.4 bar (typical industrial fluxes are 150 $L/m^2 \cdot h \cdot bar$ with a maximum of 2000 $L/m^2 \cdot h \cdot bar$ for short periods of time, comparable to 50 to 400 $L/m^2 \cdot h$ (Rijn 2004; Moraru and Ulrich Schrader 2009)). Although the effect is strongest with monodispersed pores, it will be possible to exploit the mechanism with conventional membranes. As such, it may open up a new route toward non-fouling crossflow microfiltration.

6.2. Introduction

Microfiltration is an energy-efficient and clean process that is used in for example chemical, food and pharmaceutical industries (Daufin, Escudier et al. 2001; Strathmann 2001). It has been successfully applied over several decades, but is still being improved. The main challenge is the deposition and accumulation of particles (fouling) on the membranes, which negatively influences the trans-membrane flux and transmission of (micro- and ultrafiltration) membranes. Many

Chapter

6

studies have been done on trans-membrane flux reduction and fouling mechanisms, and often different feed suspensions and / or process conditions are compared. Actions can be taken to minimize or prevent fouling, for example by surface modification or by applying better hydrodynamic conditions. If the hydrodynamics are optimally used, particles are expected to be kept away from the surface. This might lead to cleaning and surface modification becoming less crucial or even redundant. Geraldes *et al.* (2002) stressed the importance of 'flow management' and well before him, Belfort (1988, 1989) highlighted the importance of fluid mechanics as a way to control mass transfer towards the membrane (Belfort 1988; Belfort 1989; Geraldes, Semião et al. 2002).

Most of the developments in fluid dynamics in relation to membrane separation have focused on increased mass transfer through surface shear with e.g. turbulence promoters (addition of spacers), back-flushing / -pulsing, generation of Dean vortices (curved fluid streamlines), Taylor vortices (rotating membranes), oscillating flow and introduction of for example air bubbles (air sparging) (Shen and Probstein 1979; Kroner and Nissinen 1988; Yong Chung, Bates et al. 1993; Blanpain-Avet, Doubrovine et al. 1999; Cui, Chang et al. 2003). All these measures are effective in increasing mass transfer and thereby increasing trans-membrane flux. However, the total energy consumption of the membrane process increases as well, as are the capital and operational costs. In some cases, a decrease in energy consumption was noted, when the amount of energy is expressed per m^3 permeate (Arroyo and Fonade 1993; Blanpain-Avet, Doubrovine et al. 1999), but this is usually because flow with regular vortices (Dean, Taylor) was compared to truly turbulent flow. Although no specific attention will be paid to operational and capital costs in this article, the improvement of hydrodynamics in a membrane module without the need of complex module design or complex process operation is expected to result in a decrease in these costs.

Fouling leads to narrowing of pores due to adsorption of foulants onto the pore walls, pore blockage and the development of a cake layer on top of the membrane. The detrimental effects of fouling are mostly due to the necessarily small dimensions of the pores, coupled to the separation that is required. A process that would permit separation with much larger pores than the size of the particles to be

retained, or transmitted, would thus strongly reduce the fouling issues. A large pore may still become internally fouled by adsorption but it would still be large; thus, the effect of the fouling would not be severe. The same is true for pore blockage: a large pore would not easily be blocked by much smaller particles.

In this chapter, we report on a mode of cross-flow operation based on improved hydrodynamics by fluid skimming or flow lane sieving, which permits the use of membranes with larger pore sizes than the particles retained. Experimental evidence of the mechanism will be combined with an analysis of the pathways of particles. The overall performance is compared with the rates predicted with the theory of shear-induced diffusion and inertial lift; finally a window of operation for the mechanism is formulated.

6.2.1.   Theory

Several studies have investigated hydrodynamics in combination with particle deposition for back-transport of particles away from the membrane (surface) (Altena and Belfort 1984; Otis, Altena et al. 1986; Romero and Davis 1991; Tardieu, Grasmick et al. 1998; Jiang, Kennedy et al. 2007; Boissier, Lutin et al. 2008), or on convective fluid behaviour above a well-defined membrane pore (Schmitz, Houi et al. 1992). Feed suspensions with particles between 0.1 and 10 μm have been studied and therefore shear-induced diffusion is the main back-transport mechanism. Inertial lift will be evaluated as an alternative explanation, but is typically only significant for particles larger than 10 μm. Brownian motion can be neglected, since only particles smaller than 0.1 μm are influenced significantly by this mechanism. The trans-membrane flux as a result of shear-induced diffusion J_{shear} (m/s) can be described by equation 6.1, according to Davis and Sherwood (1990) (Davis and Sherwood 1990).

$$J_{shear} = 0.072 \gamma_{w,0} \left(\frac{\phi_w a^4}{\phi_b L_m} \right)^{\frac{1}{3}} \qquad (6.1)$$

In equation 6.1, $\gamma_{w,0}$ is the nominal shear rate at the membrane surface (1/s), ϕ_w the solid volume fraction at the membrane surface (-), a the particle radius (m), ϕ_b the solid volume fraction of the bulk liquid (-), and L_m the membrane length (m).

This equation is valid for $\phi_b < 0.1$, and describes the limiting trans-membrane flux, imposed by the maximum back-transport rate of particles from membrane surface towards the feed bulk phase. The particle-free layer at the beginning of the membrane is neglected.

For the trans-membrane flux as a result of inertial lift J_{lift} (m/s), equation 6.2 can be used (Drew, Schonberg et al. 1991; Belfort, Davis et al. 1994):

$$J_{lift} = 0.036 \rho a^3 \left(\frac{\gamma_{w,0}^{2}}{\eta(\phi)} \right) \hspace{3cm} (6.2)$$

In which, ρ is the density of the fluid (kg/m^3) and $\eta(\phi)$ the viscosity of the suspension as a function of the solid volume fraction (Pa·s).

Besides back-transport of particles, convective flow above a pore (or branch) can also significantly influence particle behaviour, as was observed for flow of blood cells. It was found that capillaries positioned after a side branch of a blood vessel had low concentrations of blood cells. This effect was called fluid skimming and is actually based on the convective fluid behaviour above and in the side pore. Fluid skimming was for the first time simulated by Yan *et al.* (1991). They found that concentrations of particles in a small circular side tube were lower than in the large main tube, because of a particle-free layer near the wall in the large main tube and the hydrodynamic interactions with the pore entrance. Similar effects have been reported for fluidization technology, axial filters and blood circulation (Yan, Acrivos et al. 1991). In blood circulation this effect was called plasma skimming and discovered by Krogh (1922). All studies show the flow of particles in a side branch, both theoretical (Yan, Acrivos et al. 1991; Wu, Weinbaum et al. 1992) and experimental (Krogh 1922). However, application of this theory to separation and fractionation on larger scale than microsystems has not been considered yet.

6.3.   Experimental

Instant, dehydrated yeast cells (*Saccharomyces cerevisiae*) (Algist Bruggeman N.V., Belgium) were used to make different suspension concentrations ranging from 0.001 to 0.1 solid volume fraction. Dried cells were re-suspended in demineralised

water until the desired concentration was reached. The suspensions were put on ice in order to prevent growth of the yeast cells. Glycerol was added to a mol fraction of 0.07, to make the yeast (close to) naturally buoyant, therewith preventing sedimentation of the cells.
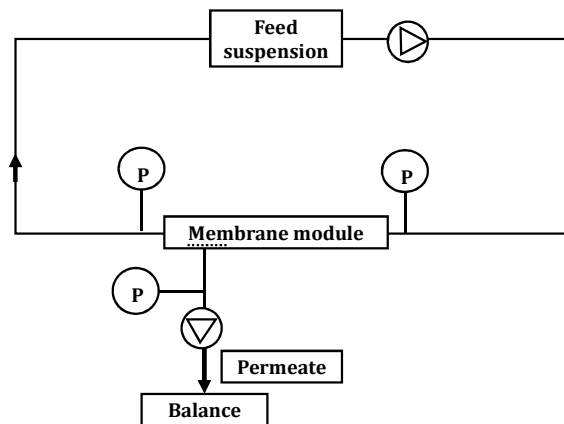
Figure 6.1. Experimental set-up for fractionation experiment.

A nickel microsieve with spherical pores of 20 micron was used to fractionate the suspensions (Veconic sieve, Stork Veco BV, the Netherlands). The microsieve was placed in a module with length of 40.5 cm, of which the first 34.5 cm was a closed channel to establish a fully developed velocity profile. The microsieve was placed after 34.5 cm and had an area of 1.39 cm^2. The suspension was fed to the system with a positive displacement pump (VG1000digit, Verdergear, Germany).

Pressure sensors (EL-PRESS P-502C, Bronkhorst High-Tech B.V., the Netherlands) were installed at the beginning and the end of the module, and after the membrane. The pressure data were recorded with Bronkhorst High-Tech software. The trans-membrane flux was measured with a balance (CP4202S, Sartorius, Germany) connected to a computer (Memfill-Lite software, Wageningen University, the Netherlands). The permeate flow was set at a specific value with a peristaltic pump (series 205U, Watson Marlow, England). A schematic drawing of the set-up can be found in Figure 6.1. Typical values used in the experiments are trans-membrane fluxes between 4.5·10^{-5} and 45·10^{-5} m/s, yeast volume fractions from 0.001 to 0.1,

Chapter

6

cross-flow velocities between 0.25 and 1 m/s, and channel heights between 0.25 and 1 mm.

The particle size and concentration of the permeate were determined with the aid of the Coulter Counter (Multisizer 3, Beckman Coulter, US). Samples were, when needed, diluted and mixed with a vortex mixer. The size distribution is shown in Figure 6.9a. Only results from experiments with constant trans-membrane flux and trans-membrane pressure during operation time were used for analysis and are presented in this article.

6.4. Results and Discussion

6.4.1. Theoretical window of operation

In order to investigate particle behaviour in the fluid, the experimental window of operation for particle deposition free fractionation needs to be determined. The excess particle flux is indicative whether cake layer formation occurs or not (Davis and Leighton 1987; Romero and Davis 1988). This excess particle flux Q' (-), which is the excess amount of particles transported in the concentration polarisation layer, relative to the bulk concentration, obeys the following relation:

$$Q' = \frac{J^3 \phi_b L_m}{\dot{\gamma}^3 a^4} \qquad (6.3)$$

In which J is the trans-membrane flux (m³/m²·s).

The trans-membrane flux J (m³/m²·s) and shear rate γ (1/s) are defined in equations 6.4 and 6.5, respectively (the dimensions in our system do not allow turbulent flow).

$$J = \frac{\Delta P}{\eta_0 R_m} \qquad (6.4)$$

$$\dot{\gamma} = \frac{6\bar{v}}{h} \qquad (6.5)$$

With, ΔP the trans-membrane pressure (Pa), η_0 the viscosity of the continuous phase (Pa·s), R_m the membrane resistance (1/m), $\bar{v}$ the averaged velocity of the fluid (m/s), and h the channel height (m).

The maximum value of Q' is restricted by the maximum solid volume fraction of particles at the wall, which is mostly assumed to be around 0.64. For dilute suspensions this leads to a maximum Q' value of 10^{-4} by making use of equation 6.6 and 6.7 (Davis and Leighton 1987; Romero and Davis 1988):

$$Q' = \int_{\phi_b}^{\phi_w} \left(\int_{\phi}^{\phi_w} \frac{D'(\phi')}{\phi \eta'(\phi')^2} d\phi' \right) \frac{(\phi - \phi_b)D'(\phi)}{\phi \eta(\phi)} d\phi \tag{6.6}$$

Here ϕ is the solid volume fraction (-). D'(ϕ) is the dimensionless hydrodynamic diffusion coefficient (-) described by equation 6.7:

$$D'(\phi) = \frac{1}{3} \phi^2 \left(1 + 0.5 e^{8.8\phi} \right) \tag{6.7}$$

The viscosity of the suspension $\eta(\phi)$ (Pa·s) follows from equation 6.8 (Krieger and Dougherty 1959).

$$\frac{\eta(\phi)}{\eta_0} = \left(1 - \frac{\phi}{\phi_{max}} \right)^{-m} \tag{6.8}$$

Here η_0 is the viscosity of the particle-free liquid (Pa·s), ϕ_{max} is the maximum random packing density for the suspension (-), which is assumed to be 0.64 for monodisperse suspensions of hard spheres and m = 2.

Below a Q'-value of 10^{-4} the concentration of particles at the membrane surface will remain below ϕ_{max}, and no stagnant layer of particles will form on the porous membrane and from this and equations 6.3-6.5 follows that the maximal trans-membrane flux J_{max} (m/s) that can be applied is:

Chapter

6

$$J_{\max} = 0.0464 \left(\frac{6\bar{v}}{h} \right) \left(\frac{a^4}{\phi_b L_m} \right)^{\frac{1}{3}}$$

(6.9)

Second, the permeate flow should remain positive over the entire length of the membrane. When trans-membrane pressures are low, the trans-membrane flux will be positive at the beginning of the membrane, but may be negative at the end of the membrane. This situation needs to be prevented if we want to focus on net particle behaviour. The pressure drop in a channel, Δp (Pa), is described in equation 6.10.

$$\Delta p = f L_m \left(\frac{w+h}{wh} \right) \rho \bar{v}^2$$

(6.10)

In equation 6.10, f is the fanning friction factor (see equation 6.11) and w the width of the membrane module (m). The fanning friction factor for laminar flow is shown in equation 6.11, with Re_c the dimensionless Reynolds number (-) as defined in equation 6.12, with η the fluid viscosity (Pa·s) and $\bar{v}$ the fluid velocity (m/s).

$$f = \frac{16}{\mathrm{Re}}$$

(6.11)

$$\mathrm{Re}_c = \left(\frac{2wh}{w+h} \right) \frac{\bar{v}\rho}{\eta}$$

(6.12)

The trans-membrane pressure should be higher than the pressure drop in the channel above the membrane in order to prevent reverse flow. From this, the minimal trans-membrane flux J_{min} (m/s) that may be applied can be derived.

$$J_{\min} = \frac{16\bar{v}L_m}{R_m} \left(\frac{w+h}{2wh} \right)^2$$

(6.13)

The minimal trans-membrane flux indicated in equation 6.13 and the maximal trans-membrane flux indicated in equation 6.9, define the theoretical window of

operation for the trans-membrane flux, illustrated in Figure 6.2 for the particles used in this study. The solid black line indicates the minimal trans-membrane flux that has to be applied; other lines show the dependency of the maximum trans-membrane flux that can be applied on the concentration of the suspension, as indicated in the legend. The theoretical window of operation for the whole set of experiments is the white region.
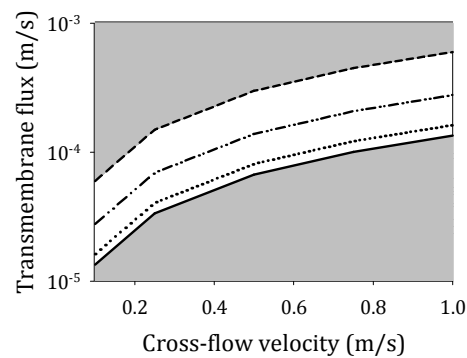
Figure 6.2. Theoretical window of trans-membrane flux operation as a function of cross-flow velocity for experiments with a channel height of 0.5 mm. With trans-membrane fluxes that are too high (upper grey area), a cake layer is formed on the membrane; with trans-membrane fluxes that are too low, the trans-membrane pressure at the end of the membrane becomes negative. The black solid line indicates the minimal trans-membrane flux in m/s (-), the dotted line is the maximal trans-membrane flux for a 5% suspension (···), dotted-dashed line is the maximal trans-membrane flux for a 1% suspension (·-·-·), short dashed line is the maximal trans-membrane flux for a 0.1% suspension (- - -).

6.4.2. Experimental results

Different process conditions were investigated that were targeted at operation below the critical flux criterion (equation 6.9). An illustrative example is shown in Figure 6.3, where the influence of cross-flow velocity on the permeate particle size is given. The experiment started with a relatively high crossflow velocity, at which the particle size in the permeate was considerably smaller than in the feed suspension. When the cross-flow velocity was then decreased, the permeate particle size increased almost up to the level of the feed solution. Upon subsequent increase of the cross-flow velocity to the initial value, the initial value for the permeate particle size was found again. This means that a reversible process is

causing the change in permeate particle size, and that no fouling or accumulation of particles occurs. This mechanism may be shear-induced diffusion or inertial lift, which are both known to act more strongly at higher cross-flow velocities.
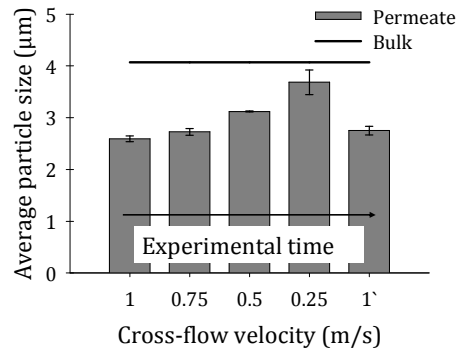
Figure 6.3. Influence of decreasing and increasing cross-flow velocity on average permeate particle size during one experiment. Size of the particles in the feed is indicated with the solid line. Solid volume fraction 0.01, channel height 0.5 mm, and trans-membrane flux 9·10^{-5} m/s.

Chapter

6

In the next discussion two dimensionless numbers are introduced; the transmission, which is the concentration ratio of particles in permeate (ϕ_p) and bulk (ϕ_b) (equation 6.14), and the ratio between the average particle size in the permeate (d_p) and in the bulk (d_b), called d_{ratio} (equation 6.15).

$$\text{Transmission} = \frac{\phi_p}{\phi_b} \qquad\qquad (6.14)$$

$$d_{ratio} = \frac{d_p}{d_b} \qquad\qquad (6.15)$$

Figure 6.4 shows the influence of the trans-membrane flux on both parameters for a low solid fraction (ϕ_b) of 0.001, while Figure 6.5 is a compilation of many solid volume fractions.

From Figure 6.4, one can see that with increasing trans-membrane flux, both particle size ratio and transmission in the permeate increase to almost the value of the feed, while they both decrease strongly at low trans-membrane fluxes. This is

only logical if particles can move away from the membrane, or are excluded from the pores; otherwise, the concentrations in permeate and feed should be the same, as is the case for the particle size.
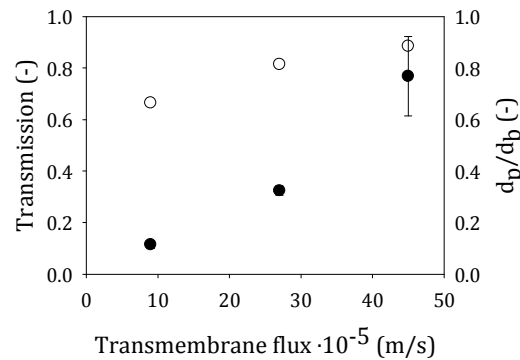
Figure 6.4. (a) Influence of trans-membrane flux on particle size ratio (○) and transmission (●). Cross-flow velocity 1 m/s, 0.001 solid volume fraction, channel height 0.5 mm.

At low permeate trans-membrane flux, the force transporting the particles away from the membrane is stronger than the drag force towards the membrane. At high trans-membrane flux, the transmission shows a larger experimental variation, probably indicating that the system is less stable due to some particle deposition. We investigated whether the crossflow velocity, or channel height had a consistent influence on transmission and $d_{ratio,}$ and found that this was not the case. Only particles close to the membrane are influenced by the presence of the pore, and those further away are not, but may be brought to that position by the overall flow conditions (e.g. crossflow velocity and channel height do indeed have influence on this position). However, the relations describing the position (and as a result the velocity) of particles are complex; therefore, it only seems logical that no straightforward link with cross-flow velocity or channel height can be detected in the experiments presented here.

Figure 6.5 shows that the separation is strongly dependent on the particle concentration. At low particle concentrations, the difference in size and concentration between permeate and feed is much more pronounced than at higher concentration. This is in contrast to what we expect for shear-induced

Chapter

6

133

diffusion: equation 6.7 shows that this mechanism should lead to stronger segregation at higher concentrations.
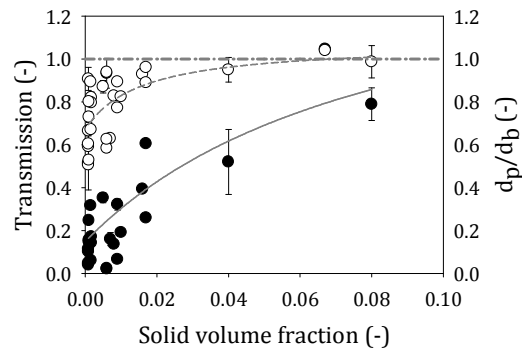
Figure 6.5. Influence of the feed particle concentration ϕ_b on the particle size ratio (○) and transmission (●). Cross-flow velocities and trans-membrane pressure varied. Grey curves are drawn to guide the eye through experimental data.

Inertial lift is in principle not directly dependent on the particle concentration, but is dependent on the viscosity of the suspension. One would also expect that at higher concentrations, particle collisions (i.e., shear-induced diffusion) would disturb the inertial lift effect. Thus one would expect a lowering of the inertial lift effect at higher concentrations, but not to the extent as shown here experimentally. This will be put on a more solid basis in the next section.

6.4.3.   Comparison to theory

When theoretical trans-membrane fluxes for shear-induced diffusion and inertial lift (equation 6.1 and 6.2 respectively) are compared with the experimental fluxes (Figure 6.6), one can see that fluxes expected for inertial lift are orders of magnitude lower than those measured (e.g. 10^{-7} m/s compared to 10^{-4} m/s); therefore, this mechanism cannot explain the observed effects. Inertial lift only takes place when the Reynolds number of the particle Re_p (-) defined in equation 6.16 (Altena and Belfort 1984), is larger than 0.1, while the maximum Re_p for the experimental conditions investigated is $2 \cdot 10^{-3}$. Therefore inertial lift does not seem to play a role in the experiments.

Chapter

6

$$\mathrm{Re}_p = \frac{\dot{\gamma}\rho a^2}{3\eta(\phi)}$$ (6.16)

The trans-membrane flux as a result of shear-induced diffusion is described by equation 6.1. The concentration of the particles at the membrane surface, ϕ_w, is somewhere in between ϕ_b and ϕ_{max}, and therefore it is useful to determine the minimum and maximum flux for shear-induced diffusion.

In Figure 6.6, the theoretical fluxes described in equation 6.1 and 6.2, are compared to the experimental fluxes. The flux for shear-induced diffusion is similar in size to the experimental flux. Shear-induced diffusion may thus play a significant role here, albeit that it cannot explain all observations, especially not those at high concentration. It was shown that the dependence on the particle concentration is opposite to what one would expect for shear-induced diffusion. Our conclusion is therefore that shear-induced diffusion cannot explain our experimental results.

Chapter

6
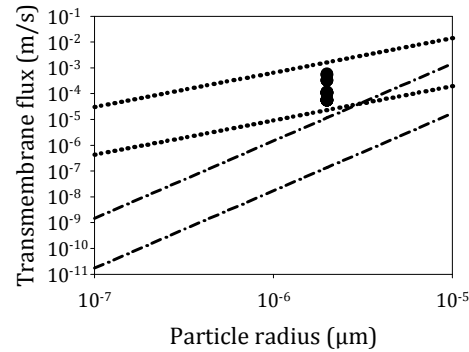
Figure 6.6. Trans-membrane flux as a result of particle radius. Black solid dots indicate experimental trans-membrane fluxes (●), dotted line depicts minimal and maximal theoretical trans-membrane flux as a result of shear-induced diffusion for the experimental conditions (···), dash-dot line depicts minimal and maximal theoretical trans-membrane flux as a result of inertial lift for the experimental conditions (- · -).

6.4.4. Particle passage across a pore

As shear-induced diffusion and inertial lift do not seem to be of major importance to our findings, the influence of particles following fluid flow lines is theoretically

investigated. A particle near the membrane will be subject to two translations, one perpendicular, and one parallel to the membrane. The particle will be dragged towards the membrane due to the permeating fluid, while at the same time it will be moving across the membrane with the cross-flow. If the translation perpendicular to the membrane surface is not large enough, the particle will pass the pore (Figure 6.7). Since all pores are circles with a diameter of 20 micron placed at equal distances (157 micron) from each other, at each pore the same effect will take place (Kim and Zydney 2006).
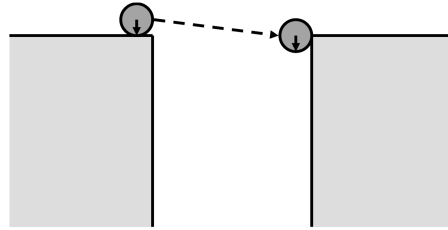
Figure 6.7. Schematic drawing of particle trajectory when the dimensionless time is 1.

In the following section, a relation will be established on the basis of a simplified particle trajectory above a pore. This equation is related to experimental results and used to describe separation performance.

The time a particle needs to cross the diameter of the pore $t_\parallel$(s) is given in equation 6.17. The pore diameter is reduced by two times the particle diameter to correct for Ferry retention.

$$t_\parallel = \frac{d_{pore} - 2a}{u_a} \tag{6.17}$$

With d_{pore} the diameter of the membrane pore (m) and u_a the velocity at a height of one average particle radius (a) from the membrane (m/s), which can be calculated from a Poiseuille profile (Kim and Zydney 2006):

$$u_a = 6\bar{v}\left[\left(\frac{a}{h}\right) - \left(\frac{a}{h}\right)^2\right] \approx \frac{6\bar{v}a}{h} \text{ for a<<h} \tag{6.18}$$

During the crossing of the particle over the pore, it is simultaneously sucked towards the pore, by the flow through the pore (u_{pore}). The time needed for a particle to travel half of the particle diameter into the pore $t_\perp$ (s) is given in equation 6.19.

$$t_\perp = \frac{a}{u_{pore}} = \frac{a\varepsilon}{J}$$ (6.19)

In which, ε is the membrane porosity (-), u_{pore} the fluid velocity through one pore (m/s) and J the superficial trans-membrane flux (m³/m²·s). If the first (parallel) time is shorter than the second (perpendicular) time, the particle will skim off the rim of the pore, and be retained. If the first time is longer, the particle will end up in the permeate. Thus, the ratio of these two times (defined in equations 6.17 and 6.19), is the dimensionless time Θ (-) as shown in equation 6.20.

$$\Theta = \frac{t_\parallel}{t_\perp} = \frac{u_{pore}(d_{pore} - 2a)}{au_a} = \frac{Jh(d_{pore} - 2a)}{6\varepsilon\bar{v}a^2}$$ (6.20)

At $\Theta = 1$, particles are expected to exactly end up at the edge of the pore with their centre of mass (see Figure 6.7). In Figure 6.8, this dimensionless time is plotted on the x-axis. Low Θ values can be interpreted as such that the time needed to be dragged into the pore is larger than the time needed to cross the pore. Particles will skim over the rim of the pore and be retained, resulting in a low transmission and small particle size. At high Θ, the particles are expected to easily enter the pore, thereby increasing transmission and particle size. The trends that were observed are as expected based on the model, although the transition from low transmission to higher values is at a slightly unexpected Θ value, which is not equal to 1.

It should be noted that these effects were observed for dilute suspensions. As shown in Figure 6.5, at higher concentrations the separation is notably more difficult, and we expect that particle interactions above the pore hinder the particles from being released back to the cross-flowing liquid upon passage of the pore and are even pushed through the pore. Fluid skimming only works when the concentration of particles above the membrane is low, which means that the fluid

Chapter

6

skimming should be more pronounced than the particle-particle interactions (shear-induced diffusion). As we have seen in chapter 5, shear-induced diffusion can result in a low concentration of particles above the membrane and as a result a fluid skimming mechanism can take place.
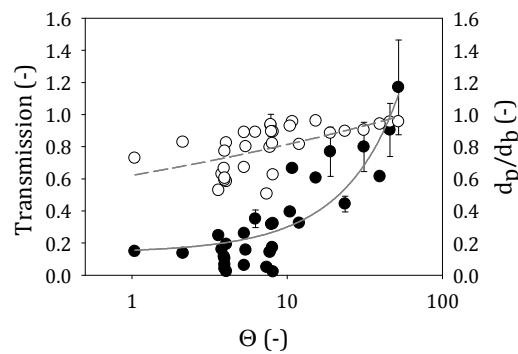
Figure 6.8. Influence of dimensionless time Θ on particle transmission (●) and particle size ratio (○). Dimensionless time was varied by changing crossflow velocity, channel height and trans-membrane flux for suspension concentrations up to 5%. Curves are drawn to guide the eye through the experimental data.

Chapter

6

When considering the particle size ratio and transmission, one might expect a transmission and particle size ratio of 1 at Θ = 1. The transition seems to be taking place at a higher value, which imposes that particles are retained more readily than would be expected on the basis of the simple reasoning before.

One complicating factor is that the suspension is slightly polydisperse; Θ is calculated for the average particle size. Larger particles in the polydisperse sample are still retained at higher Θ, as their own *a* is larger than the average *a*. Additionally, the membrane has round pores: the trajectory over the pore therefore has different lengths, depending on whether the particle will cross over the middle of the pore, or towards either side. Both effects lead to a decrease in transmission and particle size ratio.

To further illustrate the effect of polydispersity of the suspension and the round-shaped pores, a simulation is made of the influence of both factors on transmission and particle size ratio. The particle size distribution of the yeast is shown in Figure

6.9a. An estimation is made for the transmission and of each particle size ratio in the size distribution, based on the expected thickness of the fluid layer entering the pore. All particles having a radius smaller than a can enter the pore; the percentage of particles and the average particle radius of the particles entering the pore can be calculated. With fluid skimming a particle-free fluid layer of around 1 micron (radius of smallest particle present) is diluting the fluid stream entering the pore and therefore added in the simulation. Additionally, round-shaped pores cause a distribution of pore lengths to travel for the particle; an averaged dimensionless time illustrating the different pore distances to travel is described in equation 6.21.

$$\Theta_{corr} = \frac{u_{pore}}{au_a}\left(\frac{1}{2i}\int_{-i}^{i}\left(\frac{1}{2}d_{pore}^{2} - i^{2} \right)di - 2a \right) \tag{6.21}$$

In equation 6.21, i indicates the length over which integration has to be done, in this case the pore radius (m).
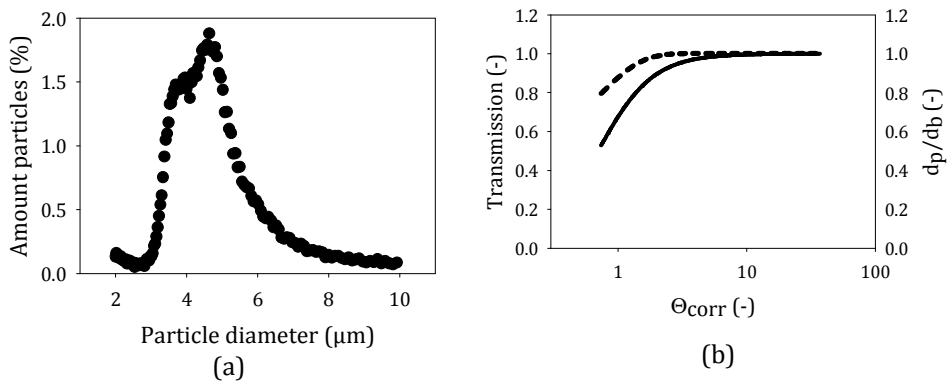
Figure 6.9. (a) Particle size distribution of yeast suspension; (b) Theoretical simulation of the influence of the particle size distribution on transmission (–) and particle size ratio (···) for a round-pore corrected dimensionless time Θ.

The simulation in Figure 6.9b shows that the transition should indeed take place around 1 when fluid skimming is the main mechanism playing a role, even when taking into account both complicating factors. We can therefore conclude that the experimental observed effect in Figure 6.8 is stronger than theory predicts (Figure 6.9b) based on fluid skimming alone. It is possible that there is a thicker fluid layer

near the membrane that is depleted of particles, consisting of a particle-free fluid layer of around 1 micron (radius of smallest particle present), due to fluid skimming and an additional particle-free fluid thickness due to wall interactions.

Even though for experimental values the transition does not occur at Θ = 1, the fact that transmission and particle size ratio do follow the dependency of Θ, supports the mechanism of fluid skimming. To confirm this, the pore geometry is varied. Other membranes were applied, with slit-shaped pores with a dimension of 15 x 390 micron. They were operated parallel and perpendicular to the cross-flow direction, therewith varying the cross-pore time systematically. Figure 6.10 shows that also these results coincide with the previous results, therewith strengthening our belief in an explanation based on the dimensionless time, although the experimental results are stronger than would be expected from the first theoretical considerations. This diagram can therefore be used to link pore design and process conditions, in order to predict transmission and particle size for dilute suspensions.
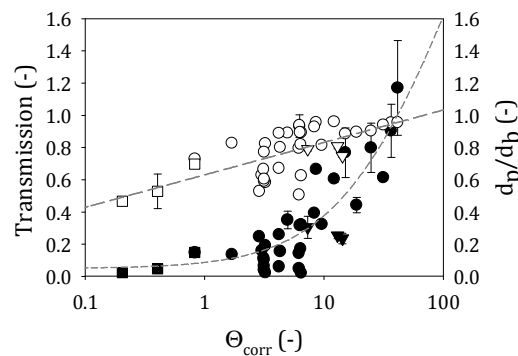
Figure 6.10. Influence of dimensionless time Θ_{corr} (only round pores corrected) on particle transmission (closed symbols) and particle size ratio (open symbols). Round pores with 20 micron diameter ($\circ,\bullet$), slit-shaped pores with pore width 15 micron ($\square,\blacksquare$) and slit-shaped pores with pore width 390 micron ($\nabla,\blacktriangledown$). Curves are drawn to guide the eye through experimental data.

As mentioned in the introduction, some investigations were done by Yan *et al.* (1991) on cells and their distribution over smaller side branches (Yan, Acrivos et al. 1991; Yan, Acrivos et al. 1991). In their work also a so-called dimensionless Q-value was used (equation 6.22), describing the ratio between volumetric flow rates, similar to the description of our dimensionless time (equation 6.20). The

description for dimensionless time however, includes the ratio between particle radius and pore diameter; as a result, a simulation of the size of the particles entering the pore and therewith the transmission and particle size ratio, can be easily made.

$$Q = \frac{q_p}{\dot{\gamma}\, 2R_p \pi R_p^{\,2}} = \frac{Jh}{6\,\bar{v}\,d_{pore}\varepsilon}$$ (6.22)

In which R_p is the radius of the pore (m), and q_p the volumetric flow rate through the pore (m³/s)

6.5.   Conclusion

It was shown that with well-defined metal microsieves, one can obtain retention of particles that are several times smaller than the pore size. The effect could for a large part be explained by a skimming mechanism. Particles flowing over the membrane will experience a translation towards the permeate (due to the trans-membrane flux) and a translation parallel to the membrane. When the cross-flow velocity has a minimum value relative to the trans-membrane flux, the particle skims over the pore and is retained. When the trans-membrane flux is increased, the particle will be transmitted once more. Experimental results are in qualitative agreement with this theory, even though the effect seems stronger than could be expected based on theory. The mechanism was confirmed for different membrane pore geometries, trans-membrane flux and crossflow combinations.

The effect may indicate a way of avoiding the negative effects of fouling: a membrane may be used with much larger pores than the size of the components that are retained. In addition, one could envisage that a system with one pore size may lead to different separation characteristics, simply by changing the ratio between cross-flow and trans-membrane flux.

Especially systems with relatively low concentrations (up to 4%) of particles will benefit from the described mechanism, if process conditions are chosen appropriately. By imposing the right trans-membrane flux versus cross-flow, the process can be operated at constant flux, generally around four times higher than

Chapter

6

industrial applied trans-membrane fluxes (200 to 2200 L/m²·h for pressures between 0.02 and 0.4 bar, while industrial fluxes are around 50 to 400 L/m²·h) without membrane fouling occuring. Please note that the conditions used are normally outside the scope of regular membrane processes; i.e. use membranes with large pores to separate particles, which are considerably smaller than the pores.

Chapter

6

Discussion 7

Energy Reduction in Industrial Food

Separation Processes

7. Energy Reduction in Industrial Food Separation Processes

7.1. Discussion thesis

In this section of the thesis, the findings from previous chapters are evaluated and assembled into a general conclusion. In addition, the newly gained insights are combined with the current state of the field, and future developments. An overview is given of aspects for processing food suspensions, that would benefit from further extension of our insights.

In the second chapter, techniques to measure concentration and velocity profiles in microchannels were presented. From the evaluation of the techniques it was concluded that CSLM and NMR are the most promising techniques to measure the migration of particles in concentrated suspensions flowing in microchannels. However, while CSLM at this moment offers the best resolution, it is an invasive method, since it requires the presence of fluorescent labels. NMR has the potential advantage that it is completely non-invasive.

In the third chapter, these measurements were performed with CSLM. NMR was also used but not reported yet because it could only practically be used in a 1 millimetre tube with a magnet of 1 Tesla; for smaller channels stronger magnets are needed which were not yet available. The presence of fat globules leads to suppression of the T_1 signal of water (Figure 7.1). The T_1 signal decreases tenfold when increasing the fat concentration from 22% to 33%, which allowed visualization of the concentration of the fat globules. Measuring fat globule size under flowing conditions as a function of the location is a different challenge. The droplet size of emulsions can be measured with the hindered diffusion inside a droplet (Packer and Rees 1972). This has been successfully applied to o/w emulsions (Lee, McCarthy et al. 1998), for which very strong magnet fields of around 5 Tesla were necessary. Goudappel *et al.* (2001) showed that bench-top pulsed-field gradient NMR spectrometry can also be used (Goudappel, van Duynhoven et al. 2001). Voda and van Duynhoven (2009) also showed in their review that diffusion in the continuous phase can be measured, but the challenge

Chapter

7

how to measure droplet size and concentration in microchannels under flow still remains (Voda and Van Duynhoven 2009).
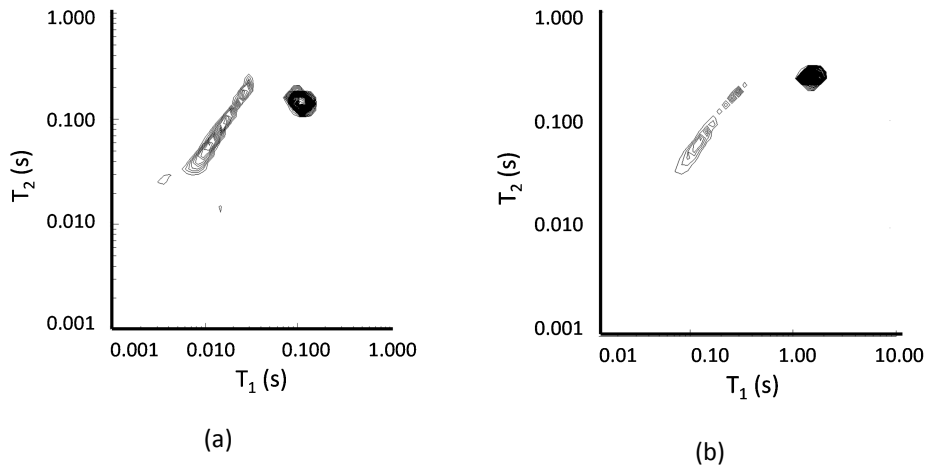
Figure 7.1. T_1T_2 spectrum water with 33% (v/v) fat (a) and 22 (v/v) fat (b). The right dotted area is the signal of water. The left stretched area is the signal of fat.

In the third chapter the concentration profiles of bidisperse suspensions are visualized with CSLM. The concentration profile development was very fast (within 10 cm) for the large particles while the profile development of the small particles was expected to take much longer than 10 cm. However, in the experiments, higher concentrations of small particles were observed near the walls within 10 cm, probably as a result of the rapid migration of large particles to the middle which exudes the smaller ones to positions near the wall. This implies that the segregation takes place more quickly than expected based on the interaction between the different types of particles. This effect may be lost further down the channel, where smaller particles may migrate again into the central areas of the channel after equilibrium is reached for the larger particles. Consequently, for fractionation with membrane microfiltration it is advantageous to use shorter membranes.

In the fourth chapter, the insight gained in chapter three regarding particle behaviour and entrance length is applied to membrane microfiltration, using a combination of a closed channel and a porous area. It is confirmed that expulsion of small particles towards the membrane as a result of shear-induced diffusion can

be used for separation. Transmission of small particles can take place at concentrations that are even higher than their concentration in the feed, implying a net concentration of the small particles in the permeate. The large particles at the same moment are completely retained in the concentrate, even though membranes were used that have pores that are at least four times larger than the largest particle, at high fluxes and without fouling occurring. Thus, this chapter gives the proof of the principle of separation based on shear-induced fractionation.

The fifth chapter builds on chapter 4, and uses the results for the design of a separation process based on the hydrodynamic particle-particle interactions combined with membrane design at pore level. By allowing for particle migration in concentrated systems before the membrane, separation above the pore becomes feasible. While conventional separation processes all work optimal at dilute conditions, and do not work above a certain concentration (microfiltration, centrifugation, sedimentation or creaming, etc.), the current mechanism is much more effective at higher concentrations, and thus promises to deliver separation in intensified processes.

As said in the previous paragraph, the mechanism of shear-induced migration works much better at higher volume fractions of the dispersed phase(s). However, we found that even dilute suspensions may be separated with membranes having very large pores, by adjusting the permeate and cross-flow velocities. The sixth chapter therefore discusses the separation of dilute suspensions, using fluid skimming and inertial lift as mechanisms. Also here a closed channel was used in combination with a porous area, and the entrance length did influence separation performance (Figure 7.2). At shorter entrance length particles have less time to be lifted away from the membrane and the transmission of the yeast cells increases as does the size of the particles as function of dimensionless time. Therefore it seems that an entrance length is needed for inertial lift to take place.

The conclusions from all chapters indicate that there are various options to make better use of microfiltration and transform microfiltration into a more robust range of processes. For this, non-standard process conditions are needed compared to what is currently common practice. The following section makes this

Chapter

7

more concrete by demonstrating the use of flow-induced particle migration for the design of microfiltration processes of food suspensions such as beer and milk. These processes are compared with the currently available (membrane) processes, on the basis of energy use.
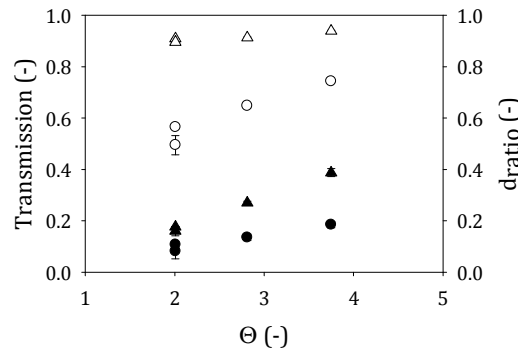
Figure 7.2. Transmission (black symbols) and d$_{ratio}$ (white symbols) for different dimensionless times and a closed entrance length of 0.345 cm (round symbols) and 0.06 cm (triangles). h is 0.5 mm, φ is 0.001 and J is 8.5·10^{-5} m/s.

7.2.   Application of findings to food processes

7.2.1.   Process conditions

We will assume a hollow fibre or tubular membrane module. To make optimal use of the findings presented in this thesis, it is necessary to operate in the laminar regime, without particle deposition, and with a positive flux (i.e., generation of permeate) over the entire length of the membrane. For these aspects, the following relations are valid.

    A.   To prevent negative trans-membrane pressures over the membrane length, when UTP is not used, the average permeate flux needs to be at least (for more information see chapter 6);

$$J_{\min} = \frac{16\,\bar{v}\,L_m}{R_m h^2} \tag{7.1}$$

With J_{min} the minimal permeate flux (m/s), h de feed channel height (m), $\bar{v}$ the average velocity in the feed channel (m/s), L_m the membrane length (m) and R_m the membrane resistance (1/m).

B. Further, the maximum excess particle flux as defined by Romero and Davis is used as upper flux boundary (Romero and Davis 1988), also described in chapter 6;

$$J_{max} = 0.0464 \left(\frac{6\bar{v}}{h} \right) \left(\frac{a^4}{\phi_b L_m} \right)^{\frac{1}{3}}$$

(7.2)

With J_{max} the maximum membrane permeate flux (m/s), a the particle radius (m), and ϕ_b the solid volume fraction of the bulk (-).

C. For ensuring a laminar flow regime, the Reynolds number should be smaller than 2300.

$$\mathrm{Re}_c = \frac{\bar{v}\rho h}{\eta}$$

(7.3)

With Re_c the dimensionless Reynolds number (-), ρ the density (kg/m³) and η the viscosity (Pa·s).

7.2.2.   Suspension conditions

For dilute suspensions, the dimensionless time as presented in chapter 6 is used:

A. The dimensionless time is chosen to be smaller than 1, when no closed entrance length is installed;

$$\Theta = \frac{Jh(d_{pore} - 2a)}{6\varepsilon\bar{v}a^2}$$

(7.4)

With J the permeate flux (m/s), d_{pore} the diameter of the pore (m) and ε the membrane porosity (-).

For concentrated suspensions (> 30%), the particles need sufficient time to diffuse and a mathematical guideline is given, as presented in chapter 5. Additionally the dimensionless time, which is the ratio between the time a particle needs to travel over the pore, compared to the time a particle needs to sink into the pore, should

be lower than 0.04 for a concentration of around 42%, which is the actual concentration used later.

A. Phillips *et al.* (1992) indicated that there are various driving forces for particle behaviour, leading to particles having the tendency to move towards regions with lower volume fraction, lower shear rate and lower viscosity (Phillips, Armstrong et al. 1992). The particle flux as a result of these forces is given in equation 7.5.

$$J_{mig} = -D_{shear}\nabla\ln\left(\dot{\gamma}\phi\eta^{\lambda}\right) \tag{7.5}$$

In which $\dot{\gamma}$ is the shear rate (s^{-1}), ϕ the oil volume fraction (-), η the viscosity (Pa·s) and λ a constant (-) and the shear-induced diffusion coefficient D_{shear} (m^2/s).

B. The ratio between the time scale of the convective and the diffusive process is a Péclet number (equation 7.6), described in chapter 3 and should be smaller than 1 for shear-induced diffusion to dominate.

$$\text{Pe}^* = \frac{\tau_{dif}}{\tau_{con}} = \left(\frac{H}{a}\right)^2 \frac{1}{12\text{D}_\phi}\frac{H}{L} \tag{7.6}$$

With τ_{dif} the time scale for diffusion (s), τ_{con} the time scale for convection (s), H the channel half-height, a the particle radius (m), D$_\phi$ the dimensionless shear-induced diffusion coefficient (-) and L the entrance length (m).

C. The dimensionless time for concentrated suspensions is described by equation 7.7.

$$\Theta = \frac{l_{pore}\cdot J}{\varepsilon_{length}\cdot v_x(z)\cdot z} \approx \frac{J\cdot h\cdot(l_{pore}+l_{closed})}{6\cdot\bar{v}\cdot a^2} \tag{7.7}$$

In this equation l_{pore} is the pore length (m), J the trans-membrane flux (m/s), ε_{length} the length porosity, $v_x(z)$ the velocity of the particle at a height of z (m/s) which corresponds to the height of the particle radius in the channel (m).

7.2.3. Module design

A. The length e_L (m) of the closed channel needed to establish a fully developed velocity profile is given in equation 7.8.

$$e_L = 0.06 \, \mathrm{Re}_c \, h \qquad (7.8)$$

7.2.4. Pressure drop and energy

A. As a practical limitation we assume that the pressure drop over the membrane channel (Δp) should be as low as possible.

$$\Delta p = \frac{32 \rho \bar{v}^2 \left(L_m + e_L + L \right)}{\mathrm{Re}_c \, h} \qquad (7.9)$$

B. The energy consumption for a microfiltration process is mainly determined by the circulation pumps to deliver the relatively high cross-flow velocities (Mulder 1996). The energy consumption to pressurize a liquid is given by equation 7.10 for one channel.

$$E_p = \frac{q_v \Delta p}{\eta_{eff}} \qquad (7.10)$$

With q_v the flow rate (m³/s), ΔP the pressure drop (N/m²) and η_{eff} the efficiency of the pump, which is generally between 0.5 and 0.8; in the calculations an efficiency of 0.6 is assumed.

Next we focus on two examples from the food field, namely beer and milk production and compare standard microfiltration and processes based on the findings from this thesis.

7.3. Beer

Various steps carried out during beer production could benefit from the findings in this thesis. Here we limit ourselves to removal of yeast, both from dilute and concentrated streams, and discuss them in terms of energy usage.

Chapter

7

- Malting
- Milling
- Mashing
- Brewing
- Clarification
- Cooling
- Fermentation
- Removal yeast
- Pasteurization
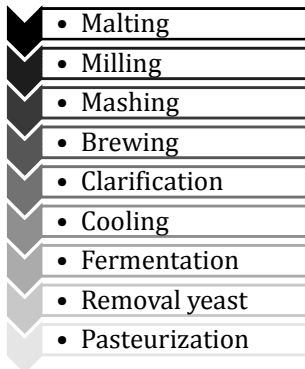
Fluid skimming effects can be used up to a percentage of 5%, while shear-induced diffusion is beneficial at much higher concentration. Here we propose an alternative process to traditional microfiltration. Fluid skimming is used to reach 5% concentration, followed by standard microfiltration and some conventional processes and finally a step that removes relatively small amounts of liquid from an already concentrated yeast suspension, as depicted in Figure 7.3.
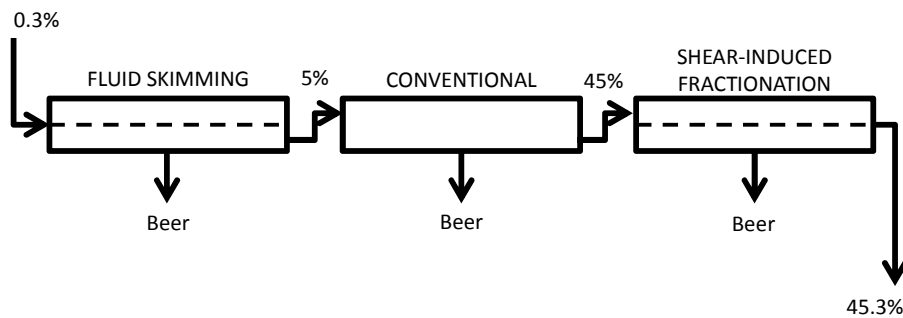
Figure 7.3. Process design of the concentration of yeast suspensions and the removal of beer.

7.3.1. Dilute yeast streams

'Traditional' cross-flow microfiltration is currently used as an alternative for dead-end filtration with diatomaceous earth. It retains yeast cells and colloidal particles that are responsible for haze formation and transmits soluble proteins and carbohydrates (Gan, Howell et al. 2001). It is a challenge to keep fluxes at constant high levels, because of accumulation of components on the membrane. Carbohydrates (Gan, Field et al. 1997) are related to in-depth pore fouling, β-glucans form a gel on the membrane, while yeast cells and proteins contribute to surface fouling.

Data from industrial practice show that beer is treated with membranes having pores of 0.45 micron, a membrane length of 1 m, with an internal diameter of 1.5 mm and a module area of 9.3 m². The cross-flow velocity is 2 m/s, with trans-membrane pressures up to 1.6 bar, giving fluxes of 100 L/(m²·h) for 7 up to 10

hours (Noordman, Berghuis et al. 1999). In general, membranes having pore sizes between 0.2 and 1.3 micron and average fluxes between 10 and 100 L/(m²·h) are used. To remove yeast cells, their size and concentration are important. The size of yeast cells is 2 to 10 micron and their concentration is around 5-11·10⁶ cells/mL (Blanpain-Avet, Doubrovine et al. 1999; Gan, Howell et al. 2001), which corresponds to a concentration of 0.03 to 0.7% in the beer before clarification. Fluid skimming and inertial lift are most relevant for removal of yeast cells and the permeate is then regarded as a clear liquid. Additionally, fluid skimming and inertial lift can be used to concentrate the retentate up to 5%.

According to the standards of the European Brewing Convention, the critical size of particles entering the permeate is 0.8 micron (Daufin, Escudier et al. 2001), which is taken as the cut-off value for our process. The process is designed such that the 0.8 micron particles have a dimensionless time of 1 (equation 7.4). The membrane has a surface porosity of 0.15 to assure sufficient space between the pores, which are 20 micron, and as flux, a value of 50 L/(m²·h) is chosen. The channel height is 100 micron (10 times the largest yeast cells) and a cross-flow velocity of 0.19 m/s is applied. In order to prevent negative trans-membrane pressures, the membrane length was chosen at 4.6 cm at a membrane resistance of $1·10^{12}$ m^{-1} (alternatively a cross-flow can be applied in the permeate side, albeit at the expense of additional energy costs). Only a very short entrance length is needed of 0.2% of the total length, because fluid skimming is a separation process mainly acting on the pore. In the new microfiltration system the energy is reduced with 72% (see table 7.1). Since we chose to work at half the flux of the traditional process, the membrane area that needs to be installed is twice as large; but the cross flow velocity is much lower and that is the reason for the energy costs saving, which may legitimise the installation of more membrane area as will be discussed later.

Chapter

7

In industry a kWh costs around 0.12 euro (Chavan 1983) and every hour 0.1 kWh is saved per m² membrane area. Normally, 15 hours of filtration are combined with eight back-flushes of 0.5 hour and one intensive cleaning of 3 hours (Lisińska and Leszczyński 1989). In the fluid skimming process, fouling is drastically reduced if relevant at all: the fouling caused by proteins and carbohydrates is mainly related to pore size and here we use a pore size of 20 micron and expect

that e.g. pore blocking is not an issue as was also experimentally observed. Therefore it seems reasonable to assume that the process does not need back-flushes and 4 hours of cleaning are saved (~25% of the running time).

Table 7.1. Overview of membrane properties, process conditions and decrease in energy consumption for the conventional and fluid skimming removal of yeast cells.

		Conventional microfiltration process	Fluid skimming
Membrane	*Pore size*	0.45 μm	20 μm
	Length	1 m	0.05 m
	Porous part	1 m	4.6 cm
	Area	10 m²	20 m²
	Porosity	0.6	0.15
	Diameter	1.5 mm	100 μm
Process conditions	*Cross-flow velocity*	2 m/s	0.19 m/s
	Flux	100 L/(m²·h)	50 L/(m²·h)
	Concentration	0.03 – 0.7 %	0.03 – 0.7 %
	Viscosity	3.5 mPa·s	3.5 mPa·s
	Pressure drop channel length	0.9 bar	0.8 bar
Energy compared to conventional			28% of conventional process (i.e., 72 % less)

Assuming that the process will run for 20 hours after which a cleaning cycle is applied for hygiene purposes, we can calculate the break-even point for the installed membrane area in relation to energy savings, and the price of membranes per m². In Figure 7.4, the break-even point is calculated for different membrane prices based on literature values. Mueller and Witte say the average costs of organic membranes are 50 euro/m² and of ceramic membranes 500 euro/m² (Mueller and Witte 2008). The membrane life time is around 7 years for organic

membranes and around 20 years for ceramic membranes (Xi and Shapley 2008). On average membranes with well-defined pores as used in this study cost more than 500 euro per m², but are produced in small quantities and large scale production should decrease the price. Given the membrane area of 20 m² the average break-even point will be at 4 years, which is shorter than the average life time of 7 years, and is clearly beneficial for production costs. Even at 500 euro per m² the break-even point will be below the life-time of the membrane, although obviously the benefits will be less pronounced.

Figure 7.4. Break-even point as function of membrane area for microfiltration of dilute yeast streams. Lines represent the break-even point in years for membrane costs of 100 euro/m² (black line), 200 euro/m² (grey dashed line) and 500 euro/m² (black dashed line). Production is 1 m³/h.

7.3.2.   Concentrated yeast streams

Currently, after primary removal of yeast, one of the by-products is a concentrated suspension (~45% w/w) of yeast cells, of which we assume the average size to be 4 micron. Note that this concentrated suspension cannot be obtained by the fluid skimming process: the fluid skimming process works until a concentration of 5% and as is shown in Figure 7.3, we propose a series of filtration and other processing steps as a replacement. This concentrated yeast stream consists of roughly 3% of the total beer produced, which is around 10 hL/h in a brewing plant. The removal of the beer will only concentrate the yeast suspension with an additional 0.3%, up to a concentration of 45.3%, and can be processed at the conditions mentioned in table 7.2, at $7.7 \cdot 10^{-3}$ kWh/hL. This is approximately one third of the energy needed for processing of dilute yeast streams, due to the much lower cross-flow velocity.

Chapter

7

Table 7.2. Overview of membrane properties and process conditions for microfiltration after fermentation and removal of beer from a concentrated yeast cell suspension.

		Removal beer from concentrated yeast
Membrane	*Pore size*	10 µm
	Length	1.7 cm
	Porous part	1.5 cm
	Area	20 m²
	Closed area	12%
	Length porosity	0.91
	Diameter	0.1 mm
Process conditions	*Cross-flow velocity*	0.05 m/s
	Flux	150 L/(m²·h)
	Concentration	45 %
	Viscosity	34 mPa·s
	Pressure drop length channel	0.9 bar

When sold at 0.13 euro per litre, depending on the costs per membrane area, the break-even point is even less than 4 years, as illustrated in Figure 7.5.
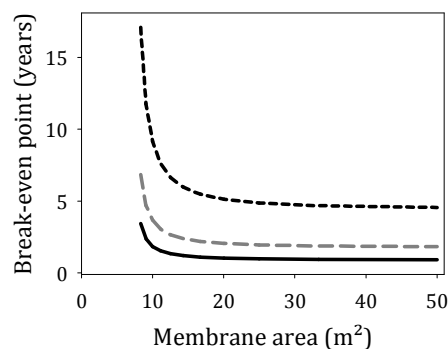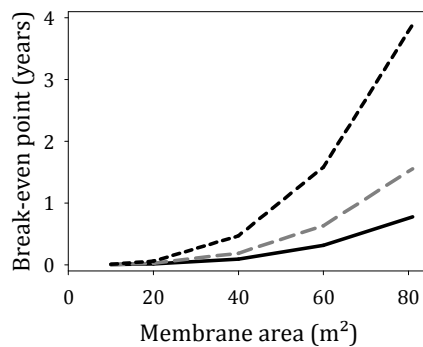
Figure 7.5. Break-even point as function of membrane area for microfiltration of concentrated yeast streams. Lines represent the break-even point in years for membrane costs of 100 euro/m² (black line), 200 euro/m² (grey dashed line) and 500 euro/m² (black dashed line). Production is 3 m³/h.

As membrane area decreases, the flux through the membrane needs to increase. To prevent particles entering the pore, as illustrated by the dimensionless number in equation 7.7, the cross-flow velocity will need to be increased and as a consequence the pressure drop over channel length will increase. Further it is important to use a membrane design that minimizes the dimensionless time and in this design a length porosity of 0.91 is chosen by using pores of 10 micron with closed spaces of 1 micron in between. The membrane area is chosen to be 20 m², to keep pressure drop over the length of the channel below 1 bar. The return of investment will be 21 days for a membrane which will cost 500 euro/m².

Table 7.3. Comparison of processes for yeast separation on the basis of energy consumption per hectolitre (www.vlb-berlin.org).

Process	**Energy consumption (kWh/hL)**	**Principle**
Kieselguhr filtration (electric power + steam)	0.13	Dead-end filtration with filter aid
Conventional microfiltration	0.11	Cross-flow microfiltration in constant flux regime
Microfiltration based on fluid skimming	0.03	Fluid skimming / inertial lift
Concentrated yeast cell microfiltration	$7.7 \cdot 10^{-3}$	Shear-induced migration

A summary of the processes for beer and their energy consumption is shown in table 7.3. Conventional microfiltration of dilute yeast streams can be improved when the module channel height and the velocity can be reduced drastically, resulting in an energy consumption reduction of at least 70%. These energy savings will start paying off after ~2 years and will reduce production costs. For concentrated processes, the removal of beer that remained in the stream can be profitable, and is expected to give a return of investment in less than one year.

Chapter

7

7.4. Milk

- Standardization

- Pasteurization

- Homogenization
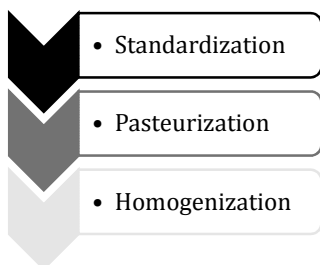
In dairy processing, different membranes are applied to separate various components, such as milk fat globules, casein, proteins, lactose and smaller components (Mohanty and Purkait 2009). Here we describe how the findings in this thesis may contribute to alternatives for current processes.

The composition of milk is shown in table 7.4, the sizes of the various dispersed components are given in table 7.5. When considering the findings in this thesis and the sizes of the components, the fat globules and the bacteria are logical targets for process improvement.

Table 7.4. Composition of bovine milk (Jenness 1974).

Source	Water (%)	Fat (%)	Casein (%)	Whey protein (%)	Lactose (%)	Ash (%)
Cow (Bos taurus)	87.3	3.7	2.8	0.6	4.8	0.7

.

Table 7.5. Average size of particles in milk (Saboya and Maubois 2000)

Component	Size (micron)
Casein micelles	0.03-0.3
Bacteria	0.2-15
Fat globules	0.2-6
Somatic cells	6-15

7.4.1. Fractionation of fat globules

Currently, fat globules are separated irrespective of their size by centrifugation, for which the energy consumption is around 0.02 kWh/L. Membrane microfiltration can also be used for this purpose and besides that, fat globules can be segregated in large and small fat globules, the latter ones giving better textural characteristics. A patent by Goudédranche *et al.* (2000) showed that fat globules smaller than 2

micron significantly contribute to smoother and finer textural characteristics of dairy products (Goudédranche, Fauquant et al. 2000). In table 7.6, three scenarios are shown, conventional microfiltration, fractionation of fat globules using cream as starting material, and fractionation starting from whole milk.

When fractionating milk fat globules from whole milk, in which the fat percentage is 4%, fluid skimming can be used to fractionate globules smaller than 2 micron. The installed membrane area should be 0.12 m² for fractionation of milk. To keep the break-even point of the membranes as low as possible (Figure 7.6) and within a feasible range the membrane costs should be below 500 euro/m². Application of these process conditions will result in an energy reduction of almost 55% compared to the conventional microfiltration process described earlier, mainly because the cross-flow is reduced and there is no need for a cross-flow at the permeate side. Additionally, even the membrane area is reduced with 50% compared to conventional microfiltration.

When considering cream as a starting point, the concentration will be around 35% and shear-induced diffusion could be used for fractionation. We have shown in chapter 3, 4 and 5 that this is very well possible, because the size of the fat globules in milk is comparable to the size of the emulsion droplets we have used in the experiments. For a permeate flux of 190 L/(h·m²), the energy consumption is 72% lower than with the standard membrane process. Low cross-flow velocities are used and no cross-flow in the permeate is needed. However, compared on an energy basis it seems advantageous to fractionate fat globules from whole milk as illustrated in Table 7.7; the membrane processes are expected to be more energy friendly than centrifugation and will also allow for fractionation which is otherwise not possible.

Chapter

7

Table 7.6. Overview of membrane properties, process conditions and decrease in energy consumption for the conventional microfiltration and fractionation of fat globules based on findings from this thesis using milk or cream as starting material.

		Conventional microfiltration	**Fractionation from cream (shear-induced)**	**Fractionation from whole milk (skimming**
Membrane	*Pore size*	5 µm	10 µm	20 µm
	Length	1 m	2.1 cm	0.02 m
	Porous part	1 m	1.5 cm	0.015 m
	Area	0.24 m²	0.06 m²	0.12 m²
	Closed area		29 %	98 %
	Porosity	0.6	0.91 (length porosity)	0.15
	Diameter	4 mm	0.1 mm	100 µm
	Permeate cross-flow	present		
Process conditions	*Cross-flow velocity*	4.6 m/s	0.07 m/s	0.70 m/s
	Flux	420 L/(m²·h)	190 L/(m²·h)	840 L/(m²·h)
	Conc.	4 %	35 %	4 %
	Viscosity	1 mPa·s	20 mPa·s	1 mPa·s
	Pressure drop channel length	0.5 bar	0.9 bar	0.4 bar
Energy compared to conventional			28% of conventional process (i.e., 72 % less)	14% of conventional process (i.e., 86 % less)
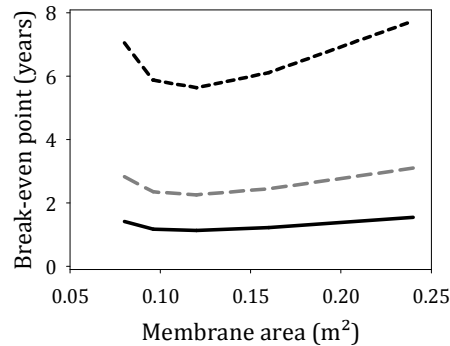
Figure 7.6. Break-even point as function of membrane area for microfiltration of whole milk. Lines represent the break-even point in years for different membrane costs of 100 euro/m² (black line), 200 euro/m² (grey dashed line) and 500 euro/m² (black dashed line). Production is 0.1 m³/h.

Table 7.7. Comparison of processes for fat globule separation/fractionation on the basis of energy consumption per litre.

Process	Energy consumption (kWh/L)
Conventional centrifugation	0.02
Conventional microfiltration	$6.6 \cdot 10^{-4}$
Fractionation in cream	$1.8 \cdot 10^{-4}$
Fractionation in whole milk	$9.2 \cdot 10^{-5}$

7.4.2. Removal of micro-organisms

Membranes can also be used to separate bacteria from skim milk, so-called cold sterilisation. To remove bacteria from skim milk, the cross-flow circulation is at 7.2 m/s along a membrane with an average pore size of 1.4 micron operated at a uniform trans-membrane pressure (UTP) of around 0.5 bar with no appreciable retention of proteins and total solids. Fluxes obtained industrially are in the order of 500 to 700 L/(h·m²) during 6 to 9 hours (Saboyainsta and Maubois 2000).

When considering fluid skimming as an alternative, we take a dimensionless time of 1 for bacteria with a size of 0.1 micron as a worst-case scenario; in general bacteria are one order of magnitude larger and the process will be even more profitable than described here. However, in cold pasteurization it is important that there as an absolute retention of bacteria. To obtain fluxes of 500 L/(h·m²), the

Chapter

7

cross-flow velocity can be 0.86 m/s. The porosity of the membrane is chosen equal to 0.6, with uniform 1.4 micron spherical pores, which can nowadays be manufactured easily. The channel height is chosen at 150 µm (10 times the largest particle present) (see table 7.8). In our system we do not have to use the UTP concept, and membrane length is short to keep positive trans-membrane pressure over the entire length of the membrane. In our design 10 short membranes will be placed after each other, with short closed areas in between to allow for particle re-orientation. For a permeate flow of 10 m³/h, the membrane area is ideally 20 m² with a break-even point of less than three years (Figure 7.7). Comparison on the basis of energy consumption shows an energy reduction of 51% when applying fluid skimming (Table 7.8).
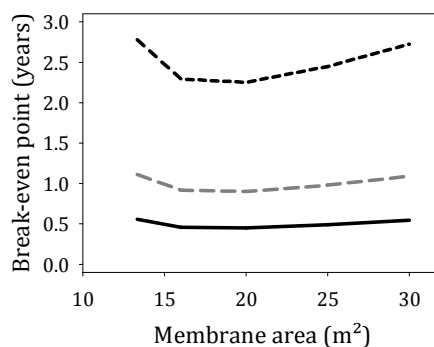
Figure 7.7. Break-even point as function of membrane area for removal of micro-organisms from milk in microfiltration. Lines represent the break-even point in years for different membrane costs of 100 euro/m² (black line), 200 euro/m² (grey dashed line) and 500 euro/m² (black dashed line). Production is 10 m³/h.

Chapter

7

Table 7.9 shows that microfiltration can be a very energy efficient way to remove micro-organisms from milk. Above all, the application of fluid skimming in membrane microfiltration can even reduce the energy from 0.4 to $2.3 \cdot 10^{-4}$ kWh/L.

Table 7.8. Overview of membrane properties, process conditions and decrease in energy consumption for the conventional and fluid skimming removal of micro-organisms from skim milk.

		Conventional microfiltration	Fluid skimming
Membrane	*Pore size*	1.4 μm	1.4 μm
	Length	16 m	0.03 m
	Porous part	16 m	10·1.5 mm
	Area	20 m^2	20 m^2
	Closed area		1.5 %
	Porosity	0.6	0.6
	Diameter	4 mm	150 μm
Process conditions	*Cross-flow velocity*	7.2 m/s	0.86 m/s
	Flux	500 L/(m^2·h)	500 L/(m^2·h)
	Concentration	4.6·10^{-4} % (20000 CFU/mL)	4.6·10^{-4} % (20000 CFU/mL)
	Pressure drop channel length	3.3 bar	0.4 bar
Change energy consumption			49% of conventional process (i.e., 51 % less)

Table 7.9. Comparison of processes for removal of micro-organisms on the basis of energy consumption per litre (Cheng, McCoy et al. 2011).

Process	Energy consumption (kWh/m^3)
Conventional pasteurization (electric power + heating)	400
Conventional microfiltration (electric power)	0.66
Fluid skimming (electric power)	0.23

7.5. Concluding remarks

In all the suggested processes from the previous sections, it is of great importance to understand the dynamics of the dispersions near the membrane and the pores in the membrane. If the system is correctly designed to operate in the right flow regime, either with fluid skimming or with shear-induced migration, separation will take place, even with a membrane that has much larger pores than any particle present in the feed. For this, the membrane properties, and the flow conditions have to be controlled well, and the properties of the feed have to be known very well. Generally, for the new type of processes described in this thesis, we need membranes with an unconventional set of design parameters. Membranes with uniform large pores are required, which combine low fouling with precise pore size and shape. Large pores usually lead to very low hydrodynamic resistance in a membrane, which means that the flux needs to be maintained by controlling a very small trans-membrane pressure, which is often impractical. Thus, these new membranes need to be relatively thick, to induce some hydrodynamic resistance for permeation. This will prevent negative trans-membrane pressures and will make the use of cross-flow at the permeate side redundant.

Current developments in membrane design bring membranes with this combination of properties within reach. This is of great importance, since the effects described here were exclusively found for membranes with uniform pores. Further, the use of large pores, which is rather uncommon in membrane applications, allows for operation at constant fluxes that are comparable or better than those currently used in practice but now without any noticeable flux reduction by fouling; therewith potentially reducing the cleaning costs to levels that are currently unheard of, and making back-pulsing unnecessary. It needs to be mentioned, that the entrance channel should be an integral design of the membrane module and for some membranes such as the Stork Veco sieves used here this is possible since the pores and pore fields in these membranes are explicitly designed. The membrane design could then be such that a closed entrance length is followed by a short area with pores, and these units can be repeated after each other as long as pressure drops over the channel are still within the limit. When using more standard membranes, this would imply that the potting area would need to be extended. In fact this is not more than a change in awareness while allowing for usual module design.

It was shown that various effects occur and can be used to improve membrane processes in terms of constant flux, energy consumption and prevention of fouling. In some cases even the membrane area can be reduced for a given production capacity. We are confident that the research in this thesis has only shown the proverbial top of the iceberg regarding the potential that flow-induced particle migration may have to improve membrane microfiltration, if studied in sufficient detail. Thus, this topic deserves much more attention to come to more sustainable processes and better starting materials for better (food) products.

Chapter

7

Chapter 8

References

8. References

Abbasi, M., M. R. Sebzari, et al. (2011). "Modeling of membraane fouling and flux decline in microfiltration of oily wastewater using ceramic membranes." Chemical Engineering Communications **199**(1): 78-93.

Abbott, J. R., N. Tetlow, et al. (1991). "Experimental-observations of particle migration in concentrated suspensions - Couette-flow." Journal of Rheology **35**(5): 773-795.

Ackerson, B. J. (1991). "Shear induced order in equilibrium colloidal liquids." Physica A **174**(1): 15-30.

Acrivos, A., R. Mauri, et al. (1993). "Shear-induced resuspension in a couette device." International Journal of Multiphase Flow **19**(5): 797-802.

Adamczyk, A. A. (1988). "2-Dimensional particle tracking velocimetry (PTV): Technique and image processing algorithms." Experiments in fluids **6**(6): 373-380.

Aguilera, J. M. (2005). "Why food microstructure?" Journal of Food Engineering **67**(1-2): 3-11.

Al-Akoum, O., L. Ding, et al. (2002). "Casein micelles separation from skimmed milk using a VSEP dynamic filtration module." Desalination **144**(1-3): 325-330.

Al Quddus, N., W. A. Moussa, et al. (2008). "Motion of a spherical particle in a cylindrical channel using arbitrary Lagrangian–Eulerian method." Journal of Colloid and Interface Science **317**(2): 620-630.

Altena, F. W. and G. Belfort (1984). "Lateral migration of spherical-particles in porous flow channels - application to membrane filtration." Chemical Engineering Science **39**(2): 343-355.

Altobelli, S. A., R. C. Givler, et al. (1991). "Velocity and concentration measurements of suspensions by nuclear-magnetic-resonance imaging." Journal of Rheology **35**(5): 721-734.

Andersson, S. R. and A. Rasmuson (2000). "Flow measurements on a turbulent fiber suspension by laser Doppler anemometry." Aiche Journal **46**(6): 1106-1119.

Arroyo, G. and C. Fonade (1993). "Use of intermittent jets to enhance flux in crossflow filtration." Journal of Membrane Science **80**(1): 117-129.

Asmolov, E. S. (1999). "The inertial lift on a spherical particle in a plane Poiseuille flow at large channel Reynolds number." Journal of Fluid Mechanics **381**: 63-87.

Aubin, J., M. Ferrando, et al. (2010). "Current methods for characterising mixing and flow in microchannels." Chemical Engineering Science **65**(6): 2065-2093.

Ayliffe, H. E., A. B. Frazier, et al. (1999). "Electric impedance spectroscopy using microchannels with integrated metal electrodes." Microelectromechanical Systems, Journal of **8**(1): 50-57.

Ayranci, I., G. Pinguet, et al. (2007). "Effect of particle polydispersity on particle concentration measurement by using laser Doppler anemometry." Experimental Thermal and Fluid Science **31**(8): 839-847.

Chapter

8

Bachalo, W. D. (1994). "Experimental methods in multiphase flows." <u>International Journal of Multiphase Flow</u> **20**: 261-295.

Bao, N., J. Wang, et al. (2008). "Recent advances in electric analysis of cells in microfluidic systems." <u>Analytical and Bioanalytical Chemistry</u> **391**(3): 933-942.

Barigou, M., P. G. Fairhurst, et al. (2003). "Concentric flow regime of solid-liquid food suspensions: theory and experiment." <u>Chemical Engineering Science</u> **58**(9): 1671-1686.

Belfort, G. (1988). "Membrane modules: comparison of different configurations using fluid mechanics." <u>Journal of Membrane Science</u> **35**(3): 245-270.

Belfort, G. (1989). "Fluid mechanics in membrane filtration: Recent developments." <u>Journal of Membrane Science</u> **40**(2): 123-147.

Belfort, G., R. H. Davis, et al. (1994). "The behavior of suspensions and macromolecular solutions in cross-flow microfiltration." <u>Journal of Membrane Science</u> **96**(1-2): 1-58.

Belfort, G., J. M. Pimbley, et al. (1993). "Diagnosis of membrane fouling using a rotating annular filter. 1. Cell culture media." <u>Journal of Membrane Science</u> **77**(1): 1-22.

Berland, K. M., P. T. C. So, et al. (1995). "2-Photon fluorescence correlation spectroscopy - Method and application to the intracellular environment." <u>Biophysical Journal</u> **68**(2): 694-701.

Besseling, R., L. Isa, et al. (2009). "Quantitative imaging of colloidal flows." <u>Advances in Colloid and Interface Science</u> **146**(1-2): 1-17.

Bhagat, A. A. S., S. S. Kuntaegowdanahalli, et al. (2009). "Inertial microfluidics for continuous particle filtration and extraction." <u>Microfluidics and Nanofluidics</u> **7**(2): 217-226.

Blanpain-Avet, P., N. Doubrovine, et al. (1999). "The effect of oscillatory flow on crossflow microfiltration of beer in a tubular mineral membrane system - Membrane fouling resistance decrease and energetic considerations." <u>Journal of Membrane Science</u> **152**(2): 151-174.

Boissier, B., F. Lutin, et al. (2008). "Particles deposition during the cross-flow microfiltration of red wines--incidence of the hydrodynamic conditions and of the yeast to fines ratio." <u>Chemical Engineering and Processing: Process Intensification</u> **47**(3): 276-286.

Bonn, D., S. Rodts, et al. (2008). "Some applications of magnetic resonance imaging in fluid mechanics: Complex flows and complex fluids." <u>Annual Review of Fluid Mechanics</u> **40**(1): 209-233.

Bosma, G., C. Pathmamanoharan, et al. (2002). "Preparation of Monodisperse, Fluorescent PMMA–Latex Colloids by Dispersion Polymerization." <u>Journal of Colloid and Interface Science</u> **245**(2): 292-300.

Bowen, W. R., T. A. Doneva, et al. (2003). "Protein deposition during cross-flow membrane filtration: AFM studies and flux loss." <u>Colloids and Surfaces B: Biointerfaces</u> **27**(2-3): 103-113.

Bowen, W. R. and F. Jenner (1995). "Theoretical descriptions of membrane filtration of colloids and fine particles - An assessment and review." <u>Advances in Colloid and Interface Science</u> **56**: 141-200.

Brans, G., J. Kromkamp, et al. (2006). "Evaluation of microsieve membrane design." Journal of Membrane Science **278**(1-2): 344-348.

Brans, G., C. G. P. H. Schroën, et al. (2004). "Membrane fractionation of milk: state of the art and challenges." Journal of Membrane Science **243**(1-2): 263-272.

Breedveld, V., D. van den Ende, et al. (2001). "Shear-induced diffusion and rheology of noncolloidal suspensions: Time scales and particle displacements." Journal of Chemical Physics **114**(13): 5923-5936.

Brister, P. C., K. K. Kuricheti, et al. (2005). "Fluorescence correlation spectroscopy for flow rate imaging and monitoring - Optimization, limitations and artifacts." Lab on a Chip **5**(7): 785-791.

Brown, J. R., E. O. Fridjonsson, et al. (2009). "Nuclear magnetic resonance measurement of shear-induced particle migration in Brownian suspensions." Physics of Fluids **21**(9): 0933011-0933019.

Butler, J. E. and R. T. Bonnecaze (1999). "Imaging of particle shear migration with electrical impedance tomography." Physics of Fluids **11**(8): 1982-1994.

Chaouki, J., F. Larachi, et al. (1997). "Noninvasive tomographic and velocimetric monitoring of multiphase flows." Industrial & Engineering Chemistry Research **36**(11): 4476-4503.

Chavan, V. V. (1983). "Processing Fundamentals for Suspensions/Emulsions." Journal of Dispersion Science and Technology **4**(1): 47-104.

Chen, X., Y. C. Lam, et al. (2004). "Determination of phenomenological constants of shear-induced particle migration model." Computational Materials Science **30**(3-4): 223-229.

Cheney, M., D. Isaacson, et al. (1999). "Electrical impedance tomography." Siam Review **41**(1): 85-101.

Cheng, X., J. H. McCoy, et al. (2011). "Imaging the Microscopic Structure of Shear Thinning and Thickening Colloidal Suspensions " Science **333**: 1276-1279.

Cheung, K. C. and P. Renaud (2006). "BioMEMS for medicine: On-chip cell characterization and implantable microelectrodes." Solid-State Electronics **50**(4): 551-557.

Chow, A. W., S. W. Sinton, et al. (1994). "Shear-induced particle migration in couette and parallel-plate viscometers - Nmr imaging and stress measurements." Physics of Fluids **6**(8): 2561-2576.

Christopher, D. A., P. N. Burns, et al. (1997). "A high-frequency pulsed-wave doppler ultrasound system for the detection and imaging of blood flow in the microcirculation." Ultrasound in Medicine and Biology **23**(7): 997-1015.

Cimbala, J. M. and D. Sathianathan (1988). "Streakline flow visualization with neutron radiography." Experiments in Fluids **6**(8): 547-552.

Cleveland Iv, T. E., D. S. Hussey, et al. (2008). "The use of neutron tomography for the structural analysis of corn kernels." Journal of Cereal Science **48**(2): 517-525.

Conrad, J. C. and J. A. Lewis (2008). "Structure of colloidal gels during microchannel flow." Langmuir **24**(15): 7628-7634.

Cui, Z. F., S. Chang, et al. (2003). "The use of gas bubbling to enhance membrane processes." Journal of Membrane Science **221**(1-2): 1-35.

Chapter

8

Cui, Z. F. and K. I. T. Wright (1996). "Flux enhancements with gas sparging in downwards crossflow ultrafiltration: performance and mechanism." Journal of Membrane Science **117**(1-2): 109-116.

Curcio, S., V. Calabrò, et al. (2002). "Monitoring and control of TMP and feed flow rate pulsatile operations during ultrafiltration in a membrane module." Desalination **145**(1-3): 217-222.

d'Avila, M. A., R. L. Powell, et al. (2005). "Magnetic resonance imaging (MRI): A technique to study flow an microstructure of concentrated emulsions." Brazilian Journal of Chemical Engineering **22**(1): 49-60.

Daufin, G., J. P. Escudier, et al. (2001). "Recent and emerging applications of membrane processes in the food and dairy industry." Food and Bioproducts Processing **79**(2): 89-102.

David, C., F. Pignon, et al. (2008). "Spatial and Temporal in Situ Evolution of the Concentration Profile during Casein Micelle Ultrafiltration Probed by Small-Angle X-ray Scattering." Langmuir **24**(9): 4523-4529.

Davis, R. H. (1992). "Modeling of fouling of crossflow microfiltration membranes." Separation and purification reviews **21**(2): 75.

Davis, R. H. and D. T. Leighton (1987). "Shear-induced transport of a particle layer along a porous wall." Chemical Engineering Science **42**(2): 275-281.

Davis, R. H. and J. D. Sherwood (1990). "A similarity solution for steady-state cross-flow microfiltration." Chemical Engineering Science **45**(11): 3203-3209.

Davit, Y., G. Iltis, et al. (2011). "Imaging biofilm in porous media using X-ray computed microtomography." Journal of Microscopy **242**(1): 15-25.

Derks, D., H. Wisman, et al. (2004). "Confocal microscopy of colloidal dispersions in shear flow using a counter-rotating cone-plate shear cell." Journal of Physics-Condensed Matter **16**(38): S3917-S3927.

Di Carlo, D. (2009). "Inertial microfluidics." Lab on a Chip **9**(21): 3038-3046.

Di Carlo, D., D. Irimia, et al. (2007). "Continuous inertial focusing, ordering, and separation of particles in microchannels." Proceedings of the National Academy of Sciences **104**(48): 18892-18897.

Di Leonardo, R., J. Leach, et al. (2006). "Multipoint holographic optical velocimetry in microfluidic systems." Physical Review Letters **96**(13): 134502.

Ding, L., O. Al-Akoum, et al. (2002). "Milk protein concentration by ultrafiltration with rotating disk modules." Desalination **144**(1-3): 307-311.

Dinsmore, A. D., E. R. Weeks, et al. (2001). "Three-dimensional confocal microscopy of colloids." Applied Optics **40**(24): 4152-4159.

Drew, D. A., J. A. Schonberg, et al. (1991). "Lateral inertial migration of a small sphere in fast laminar flow through a membrane duct." Chemical Engineering Science **46**(12): 3219-3224.

Dukhin, A. S., P. J. Goetz, et al. (1996). "Acoustic Spectroscopy for Concentrated Polydisperse Colloids with Low Density Contrast." Langmuir **12**(21): 4998-5003.

Duriyabunleng, H., J. Petmunee, et al. (2001). "Effects of the Ultrasonic Waves on Microfiltration in Plate and Frame Module." Journal of Chemical Engineering of Japan **34**(8): 985-989.

Durst, F. (1980). Principles and practice of laser doppler anemometry academic.

Chapter

8

Durst, F., A. Melling, et al. (1981). Principles and practice of laser-Doppler anemometry. London, Academic Press.

Eckstein, E. C., D. G. Bailey, et al. (1977). "Self-diffusion of particles in shear-flow of a suspension." Journal of Fluid Mechanics **79**(1): 191-208.

El Rayess, Y., C. Albasi, et al. (2011). "Cross-flow microfiltration applied to oenology: A review." Journal of Membrane Science **382**(1-2): 1-19.

Eloot, S., F. De Bisschop, et al. (2004). "Experimental evaluation of the migration of spherical particles in three-dimensional Poiseuille flow." Physics of Fluids **16**(7): 2282-2293.

Engler, J. and M. R. Wiesner (2000). "Particle fouling of a rotating membrane disk." Water Research **34**(2): 557-565.

Erickson, D. (2005). "Towards numerical prototyping of labs-on-chip: modeling for integrated microfluidic devices." Microfluidics and Nanofluidics **1**(4): 301-318.

Faivre, M., M. Abkarian, et al. (2006). "Geometrical focusing of cells in a microfluidic device: An approach to separate blood plasma." Biorheology **43**(2): 147-159.

Fan, X., D. J. Parker, et al. (2006). "Labelling a single particle for positron emission particle tracking using direct activation and ion-exchange techniques." Nuclear Instruments and Methods in Physics Research Section A: Accelerators, Spectrometers, Detectors and Associated Equipment **562**(1): 345-350.

Fane, A. G. (1997). Conference Proceedings: Characterization of Polymers with Surface, Lappeenranta, Finland: 51-59.

Ferry, J. D. (1936). "Statistical evaluation of sieve constants in ultrafiltration." The Journal of General Physiology **20**(1): 95-104.

Field, R. W., D. Wu, et al. (1995). "Critical flux concept for microfiltration fouling." Journal of Membrane Science **100**(3): 259-272.

Fillaudeau, L. and H. Carrere (2002). "Yeast cells, beer composition and mean pore diameter impacts on fouling and retention during cross-flow filtration of beer with ceramic membranes." Journal of Membrane Science **196**(1): 39-57.

Frank, M., D. Anderson, et al. (2003). "Particle migration in pressure-driven flow of a Brownian suspension." Journal of Fluid Mechanics **493**: 363-378.

Fryer, P. J., P. G. Fairhurst, et al. (2000). Food & Drink 2000: processing solutions for innovative products : a two-day conference held at the University of Birmingham, 'Using positron emission particle tracking (PEPT) to study food flows'. Rugby, UK, IChemE.

Fukushima, E. (1999). "Nuclear magnetic resonance as a tool to study flow." Annual Review of Fluid Mechanics **31**(1): 95-123.

Gan, Q., R. W. Field, et al. (1997). "Beer Clarification by Cross-Flow Microfiltration: Fouling Mechanisms and Flux Enhancement." Chemical Engineering Research and Design **75**(1): 3-8.

Gan, Q., J. A. Howell, et al. (2001). "Beer clarification by microfiltration — product quality control and fractionation of particles and macromolecules." Journal of Membrane Science **194**(2): 185-196.

Chapter

8

Gao, C., B. Xu, et al. (2009). "Mixing and segregation of microspheres in microchannel flows of mono- and bidispersed suspensions." Physical Review E **79**(3): 036311.

Garroway, A. N. (1974). "Velocity measurements in flowing fluids by MNR." Journal of physics **7**(14): L159.

Gauthier, F., H. L. Goldsmit, et al. (1971). "Particle Motions in Non-Newtonian Media. II. Poiseuille Flow." Journal of Rheology **15**(2): 297-330.

Geraldes, V., V. Semião, et al. (2002). "Flow management in nanofiltration spiral wound modules with ladder-type spacers." Journal of Membrane Science **203**(1-2): 87-102.

Gironès, M. and Girones (2006). "Protein aggregate deposition and fouling reduction strategies with high-flux silicon nitride microsieves." Journal of membrane science **273**(1-2): 68.

Goldsztein, G. H. (2005). "Volume of suspension that flows through a small orifice before it clogs." SIAM Journal on Applied Mathematics **66**(1): 228-236.

Goudappel, G. J. W., J. P. M. van Duynhoven, et al. (2001). "Measurement of oil droplet size distributions in food oil/water emulsions by time domain pulsed field gradient NMR." Journal of Colloid and Interface Science **239**(2): 535-542.

Goudédranche, H., J. Fauquant, et al. (2000). "Fractionation of globular milk fat by membrane microfiltration." Lait **80**(1): 93-98.

Graham, A. L., S. A. Altobelli, et al. (1991). "Nmr imaging of shear-induced diffusion and structure in concentrated suspensions undergoing couette-flow." Journal of Rheology **35**(1): 191-201.

Guerra, A., G. Jonsson, et al. (1997). "Low cross-flow velocity microfiltration of skim milk for removal of bacterial spores." International Dairy Journal **7**(12): 849-861.

Hampton, R. E., A. A. Mammoli, et al. (1997). "Migration of particles undergoing pressure-driven flow in a circular conduit." Journal of Rheology **41**(3): 621-640.

Hashmi, S. M., M. Loewenberg, et al. (2007). "Spatially extended FCS for visualizing and quantifying high-speed multiphase flows in microchannels." Optics Express **15**(10): 6528-6533.

Havelock, D. (1996). "Signal processing in acoustics." Journal of the Acoustical Society of America **100**(3): 1263-1263.

Hong, Q. A., M. P. Sheetz, et al. (1991). "Single-particle tracking - Analysis of diffusion and flow in 2-dimensional systems." Biophysical Journal **60**(4): 910-921.

Hoult, D. I., C. N. Chen, et al. (1986). "The field-dependence of nmr imaging .2. Arguments concerning an optimal field-strength." Magnetic Resonance in Medicine **3**(5): 730-746.

Howell, J. A. (1995). "Sub-critical flux operation of microfiltration." Journal of Membrane Science **107**(1-2): 165-171.

Huang, L. R., E. C. Cox, et al. (2004). "Continuous particle separation through deterministic lateral displacement." Science **304**(5673): 987-990.

Hur, S. C., H. T. K. Tse, et al. (2010). "Sheathless inertial cell ordering for extreme throughput flow cytometry." Lab on a Chip **10**(3): 274-280.

Chapter

8

Husband, D. M., L. A. Mondy, et al. (1994). "Direct measurements of shear-induced particle migration in suspensions of bimodal spheres." Rheologica Acta **33**(3): 185-192.

Isa, L., R. Besseling, et al. (2006). "Experimental studies of the flow of concentrated hard sphere suspensions into a constriction." Journal of Physics: Conference Series **40**: 124-132.

Jaffrin, M. Y. (2008). "Dynamic shear-enhanced membrane filtration: A review of rotating disks, rotating membranes and vibrating systems." Journal of Membrane Science **324**(1-2): 7-25.

Jaffrin, M. Y. (2012). "Hydrodynamic techniques to enhance membrane filtration." Annual Review of Fluid Mechanics **44**(1): 77-96.

Jaffrin, M. Y., B. B. Gupta, et al. (1994). "Energy saving pulsatile mode cross flow filtration." Journal of Membrane Science **86**(3): 281-290.

James, B. J., Y. Jing, et al. (2003). "Membrane fouling during filtration of milk––a microstructural study." Journal of Food Engineering **60**(4): 431-437.

Jenness, R. (1974). "Biosynthesis and Composition of Milk." J Investig Dermatol **63**(1): 109-118.

Jiang, T., M. D. Kennedy, et al. (2007). "Controlling submicron particle deposition in a side-stream membrane bioreactor: A theoretical hydrodynamic modelling approach incorporating energy consumption." Journal of Membrane Science **297**(1-2): 141-151.

Karnis, A., H. l. Goldsmit, et al. (1966). "Kinetics of flowing dispersions .I. Concentrated suspensions of rigid particles." Journal of Colloid and Interface Science **22**(6): 531-553.

Karnis, A., H. L. Goldsmith, et al. (1966). "The flow of suspensions through tubes: V. Inertial effects." The Canadian Journal of Chemical Engineering **44**(4): 181-193.

Keane, R. D. (1995). "Super-resolution particle imaging velocimetry." Measurement science & technology **6**(6): 754.

Kikura, H., J. Matsushita, et al. (2004). "Thermal behaviour and particle size evaluation of primary clusters in a water-based magnetic fluid." Science and Technology of Advanced Materials **5**(5-6): 703-707.

Kim, M. C., K. Y. Kim, et al. (2004). "Reconstruction algorithm of electrical impedance tomography for particle concentration distribution in suspension." Korean Journal of Chemical Engineering **21**(2): 352-357.

Kim, M. M. and A. L. Zydney (2006). "Theoretical analysis of particle trajectories and sieving in a two-dimensional cross-flow filtration system." Journal of Membrane Science **281**(1-2): 666-675.

Knutsen, J. S. and R. H. Davis (2006). "Deposition of foulant particles during tangential flow filtration." Journal of Membrane Science **271**(1-2): 101-113.

Koh, C. J., P. Hookham, et al. (1994). "An experimental investigation of concentrated suspension flows in a rectangular channel." Journal of Fluid Mechanics **266**: 1-32.

Kose, K. (1992). "A real-time NMR image-reconstruction system using echo-planar imaging and a digital signal processor." Measurement science & technology **3**(12): 1161-1165.

Chapter

8

Krieger, I. M. and T. J. Dougherty (1959). "A mechanism for non-Newtonian flow in suspensions of rigid spheres." Transactions of the Society of Rheology **3**: 137-152.

Krishnan, G. P., S. Beimfohr, et al. (1996). "Shear-induced radial segregation in bidisperse suspensions." Journal of Fluid Mechanics **321**: 371-393.

Krishnan, G. P. and J. David T. Leighton (1995). "Inertial lift on a moving sphere in contact with a plane wall in a shear flow." Physics of Fluids **7**(11): 2538-2545.

Krogh, A. (1922). The anatomy and physiology of capillaries. New Haven.

Kromkamp, J. (2005). Particle separation and fractionation by microfiltration, Wageningen Netherlands: Wageningen Universiteit (Wageningen University).

Kromkamp, J., F. Faber, et al. (2006). "Effects of particle size segregation on crossflow microfiltration performance: Control mechanism for concentration polarisation and particle fractionation." Journal of Membrane Science **268**(2): 189-197.

Kroner, K. H. and V. Nissinen (1988). "Dynamic filtration of microbial suspensions using an axially rotating filter." Journal of Membrane Science **36**: 85-100.

Krstić, D. M., M. N. Tekić, et al. (2002). "The effect of turbulence promoter on cross-flow microfiltration of skim milk." Journal of Membrane Science **208**(1-2): 303-314.

Kuiper, S., C. van Rijn, et al. (2002). "Filtration of lager beer with microsieves: flux, permeate haze and in-line microscope observations." Journal of Membrane Science **196**(2): 159-170.

Kulrattanarak, T., R. G. M. van der Sman, et al. (2008). "Classification and evaluation of microfluidic devices for continuous suspension fractionation." Advances in Colloid and Interface Science **142**(1-2): 53-66.

Kunst, B. H., A. Schots, et al. (2004). "Design of a confocal microfluidic particle sorter using fluorescent photon burst detection." Review of Scientific Instruments **75**(9): 2892-2898.

Kuruzovich, J. N. and P. R. Piergiovanni (1996). "Yeast cell microfiltration: optimization of backwashing for delicate membranes." Journal of Membrane Science **112**(2): 241-247.

Kytömaa, H. K. (1995). "Theory of sound propagation in suspensions: a guide to particle size and concentration characterization." Powder Technology **82**(1): 115-121.

Lagasse, R. R. and K. R. Thompson (2002). "Spatial gradients in particle reinforced polymers characterized by X-ray attenuation and laser confocal microscopy." Polymer **43**(3): 803-812.

Lareo, C., P. J. Fryer, et al. (1997). "The Fluid Mechanics of Two-Phase Solid-Liquid Food Flows: A Review." Food and Bioproducts Processing **75**(2): 73-105.

Lee, H., T.-J. Yoon, et al. (2009). "Rapid detection and profiling of cancer cells in fine-needle aspirates." Proceedings of the National Academy of Sciences **106**(30): 12459-12464.

Lee, H. Y., M. J. McCarthy, et al. (1998). "Experimental characterization of emulsion formation and coalescence by nuclear magnetic resonance restricted

diffusion techniques." <u>Journal of the American Oil Chemists Society</u> **75**(4): 463-475.

Lee, Y. and M. M. Clark (1998). "Modeling of flux decline during crossflow ultrafiltration of colloidal suspensions." <u>Journal of Membrane Science</u> **149**(2): 181-202.

Leighton, D. and A. Acrivos (1987). "Measurement of shear-induced self-diffusion in concentrated suspensions of spheres." <u>Journal of Fluid Mechanics</u> **177**: 109-131.

Leighton, D. and A. Acrivos (1987). "The shear-induced migration of particles in concentrated suspensions." <u>Journal of Fluid Mechanics</u> **181**: 415-439.

Leniger, H. A. and W. A. Beverloo (1975). <u>Food Process Engineering</u>, D. Reidel Publishing Company.

Lens, P. N. L., R. Gastesi, et al. (2003). "Diffusional properties of methanogenic granular sludge: H-1 NMR characterization." <u>Applied and Environmental Microbiology</u> **69**(11): 6644-6649.

Li, N. N., A. G. Fane, et al. (2008). <u>Advanced Membrane Technology and Applications</u>, John Wiley & Sons.

Lima, R., T. Ishikawa, et al. (2009). "Measurement of Individual Red Blood Cell Motions Under High Hematocrit Conditions Using a Confocal Micro-PTV System." <u>Annals of Biomedical Engineering</u> **37**(8): 1546-1559.

Lindken, R., J. Westerweel, et al. (2006). "Stereoscopic micro particle image velocimetry." <u>Experiments in Fluids</u> **41**(2): 161-171.

Lisińska, G. and W. Leszczyński (1989). <u>Potato Science and Technology</u>, Elsevier Applied Science.

Longest, P. W., C. Kleinstreuer, et al. (2004). "Efficient computation of micro-particle dynamics including wall effects." <u>Computers & Fluids</u> **33**(4): 577-601.

Lopez, M. (2008). <u>Enhancement of mixing and transport in microfluidic devices by chaotic dynamics and shear-induced diffusion</u>, The University of Wisconsin - Madison.

Lumma, D., A. Best, et al. (2003). "Flow profile near a wall measured by double-focus fluorescence cross-correlation." <u>Physical review. E, Statistical, nonlinear, and soft matter physics</u> **67**: 0563131-05631310.

Lyon, M. K. and L. G. Leal (1998). "An experimental study of the motion of concentrated suspensions in two-dimensional channel flow. Part 1. Monodisperse systems." <u>Journal of Fluid Mechanics</u> **363**: 25-56.

Lyon, M. K. and L. G. Leal (1998). "An experimental study of the motion of concentrated suspensions in two-dimensional channel flow. Part 2. Bidisperse systems." <u>Journal of Fluid Mechanics</u> **363**: 57-77.

Maas, H. G. (1993). "Particle tracking velocimetry in three-dimensional flows." <u>Experiments in fluids</u> **15**(2): 133-146.

Mabrook, M. F. and M. C. Petty (2003). "Effect of composition on the electrical conductance of milk." <u>Journal of Food Engineering</u> **60**(3): 321-325.

Magde, D., W. W. Webb, et al. (1972). "Thermodynamic fluctuations in a reacting system - Measurement by fluorescence correlation spectroscopy." <u>Physical Review Letters</u> **29**(11): 705-708.

Chapter

8

Majors, P. D., R. C. Givler, et al. (1989). "Velocity and concentration measurements in multiphase flows by nmr." Journal of Magnetic Resonance **85**(2): 235-243.

Makardij, A., X. D. Chen, et al. (1999). "Microfiltration and ultrafiltration of milk: some aspects of fouling and cleaning." Food and Bioproducts Processing **77**(2): 107-113.

Manneville, S. (2008). "Recent experimental probes of shear banding." Rheologica Acta **47**(3): 301-318.

Manneville, S., L. Becu, et al. (2004). "High-frequency ultrasonic speckle velocimetry in sheared complex fluids." European Physical Journal-Applied Physics **28**(3): 361-373.

Maru, K. and Y. Fujii (2010). "Differential Laser Doppler Velocimeter With Enhanced Range for Small Wavelength Sensitivity by Using Cascaded Mach-Zehnder Interferometers." J. Lightwave Technol. **28**(11): 1631-1637.

McCarthy, K. L. and W. L. Kerr (1998). "Rheological characterization of a model suspension during pipe flow using MRI." Journal of Food Engineering **37**(1): 11-23.

McLaughlin, J. B. (1993). "The lift on a small sphere in wall-bounded linear shear flows." Journal of Fluid Mechanics **246**: 249-265.

Meinhart, C. D., S. T. Wereley, et al. (1999). "PIV measurements of a microchannel flow." Experiments in Fluids **27**(5): 414-419.

Merlin, A., J. Angly, et al. (2011). "Time-resolved microfocused small-angle X-ray scattering investigation of the microfluidic concentration of charged nanoparticles." The European Physical Journal E: Soft Matter and Biological Physics **34**(6): 1-7.

Mills, P. and P. Snabre (1995). "Rheology and structure of concentrated suspensions of hard-spheres - Shear-induced particle migration." Journal De Physique Ii **5**(10): 1597-1608.

Mishima, K. and T. Hibiki (1998). "Development of high-frame-rate neutron radiography and quantitative measurement method for multiphase flow research." Nuclear Engineering and Design **184**(2-3): 183-201.

Mohanty, K. and M. K. Purkait (2009). Membrane Technologies and Applications, Taylor and Francis.

Mondy, L. A., A. L. Graham, et al. (1986). "Techniques of measuring particle motions in concentrated suspensions." International Journal of Multiphase Flow **12**(3): 497-502.

Mondy, L. A., C. Retallack, et al. (2008). "On bubbles rising through suspensions of solid particles." AICHE Journal **54**(4): 862-871.

Moraru, C. and E. Ulrich Schrader (2009). Applications of membrane separation in the brewing industry. Handbook of Membrane Separations, CRC Press**:** 553-579.

Mores, W. D. and R. H. Davis (2002). "Yeast-fouling effects in cross-flow microfiltration with periodic reverse filtration." Industrial & Engineering Chemistry Research **42**(1): 130-139.

Mueller, U. and M. Witte (2008). "Ceramic membrane applications for spent filter backwash water treatment." Techneau.

Chapter

8

Mulder, M. (1996). <u>Basic principles of membrane technology</u>, Kluwer Academic Publishers.

Nandi, B. K., R. Uppaluri, et al. (2011). "Identification of optimal membrane morphological parameters during microfiltration of mosambi juice using low cost ceramic membranes." <u>LWT - Food Science and Technology</u> **44**(1): 214-223.

Noordman, T. R., O. A. E. Berghuis, et al. (1999). "Membrane filtration for bright beer, an alternative to Kieselguhr filtration." <u>Proceedings of 27th EBC Congress (Cannes, France)</u>: 815-822.

Noordman, T. R., A. de Jonge, et al. (2002). "Application of fluidised particles as turbulence promoters in ultrafiltration: Improvement of flux and rejection." <u>Journal of Membrane Science</u> **208**(1-2): 157-169.

Nott, P. R. and J. F. Brady (1994). "Pressure-driven flow of suspensions - Simulation and theory." <u>Journal of Fluid Mechanics</u> **275**: 157-199.

Novelline, R. A. (1997). <u>Squire's fundamentals of radiology</u>. Cambridge, Mass., Harvard University Press.

Nyquist, H. (2002). "Certain topics in telegraph transmission theory (Reprinted from Transactions of the A. I. E. E., February, pg 617-644, 1928)." <u>Proceedings of the Ieee</u> **90**(2): 280-305.

Otis, J. R., F. W. Altena, et al. (1986). "Measurements of single spherical particle trajectories with lateral migration in a slit with one porous wall under laminar flow conditions." <u>Experiments in Fluids</u> **4**(1): 1-10.

Packer, K. J. and C. Rees (1972). "Pulsed nmr studies of restricted diffusion .1. Droplet size distributions in emulsions." <u>Journal of Colloid and Interface Science</u> **40**(2): 206-218.

Pal, R. (1994). "Techniques for measuring the composition (oil and water content) of emulsions - a state of the art review." <u>Colloids and Surfaces A: Physicochemical and Engineering Aspects</u> **84**(2-3): 141-193.

Park, J.-S., S.-H. Song, et al. (2009). "Continuous focusing of microparticles using inertial lift force and vorticity via multi-orifice microfluidic channels." <u>Lab on a Chip</u> **9**(7): 939-948.

Park, J. S. (2004). "Optically sliced micro-PIV using confocal laser scanning microscopy (CLSM)." <u>Experiments in fluids</u> **37**(1).

Peinemann, K. V., S. P. Nunes, et al. (2010). <u>Membrane Technology: Volume 3: Membranes for Food Applications</u>, Wiley-VCH.

Peters, F., L. Lobry, et al. (2010). "Pressure-driven flow of a micro-polar fluid: Measurement of the velocity profile." <u>Journal of Rheology</u> **54**(2): 311-325.

Phillips, R. J., R. C. Armstrong, et al. (1992). "A constitutive equation for concentrated suspensions that accounts for shear-induced particle migration." <u>Physics of Fluids a-Fluid Dynamics</u> **4**(1): 30-40.

Pilutti, A. M., Nemeth, J. E. , and Nemeth, P. J. E., (2003). "Technical and cost review of commercially available MF/UF membrane products." <u>Desalination</u>: 1-15.

Pine, D. J., J. P. Gollub, et al. (2005). "Chaos and threshold for irreversibility in sheared suspensions." <u>Nature</u> **438**(7070): 997-1000.

Piron, E., F. Rene, et al. (1995). "A cross-flow microfiltration model-based on integration of the mass-transport equation." <u>Journal of Membrane Science</u> **108**(1-2): 57-70.

Chapter

8

Plett, E. (1989). "The constant pressure difference method of microfiltration." Proceedings of the 3rd International Conference on Fouling and Cleaning in Food Processing, Prien, FRG: 283-293.

Pollice, A., A. Brookes, et al. (2005). "Sub-critical flux fouling in membrane bioreactors — a review of recent literature." Desalination **174**(3): 221-230.

Powell, R. L. (2008). "Experimental techniques for multiphase flows." Physics of Fluids **20**(4): 0406051-04060522.

Powell, R. L., J. E. Maneval, et al. (1994). "Nuclear-magnetic-resonance imaging for viscosity measurements." Journal of Rheology **38**(5): 1465-1470.

Prasad, V., D. Semwogerere, et al. (2007). "Confocal microscopy of colloids." Journal of Physics-Condensed Matter **19**(11): 1131021-11310225.

Prince, E. (1999). "Neutron scattering instrumentation: A tutorial review." Applied Spectroscopy Reviews **34**(3): 159 - 172.

Raguin, L. G. and L. Ciobanu (2007). "Multiple echo NMR velocimetry: Fast and localized measurements of steady and pulsatile flows in small channels." Journal of Magnetic Resonance **184**(2): 337-343.

Rausch, K. D. (2002). "Front End to Backpipe: Membrane Technology in the Starch Processing Industry." Starch - Stärke **54**(7): 273-284.

Redkar, S., V. Kuberkar, et al. (1996). "Modeling of concentration polarization and depolarization with high-frequency backpulsing." Journal of Membrane Science **121**(2): 229-242.

Reinecke, N., G. Petritsch, et al. (1998). "Tomographic imaging of the phase distribution in two-phase slug flow." International Journal of Multiphase Flow **24**(4): 617-634.

Rezaei, H., F. Z. Ashtiani, et al. (2011). "Effects of operating parameters on fouling mechanism and membrane flux in cross-flow microfiltration of whey." Desalination **274**(1-3): 262-271.

Rideal, G. (2005). "Filtration: the marketplace." Filtration & Separation **42**(7): 30-33.

Rijn, C. J. M. v. (2004). Nano and micro engineered membrane technology. Amsterdam ; Boston, Elsevier.

Roberto G, P. (2000). "Additional effects on internal flow of non-Newtonian fluids in the presence of a particle." Journal of Non-Newtonian Fluid Mechanics **95**(2–3): 85-100.

Roda, B., A. Zattoni, et al. (2009). "Field-flow fractionation in bioanalysis: A review of recent trends." Analytica Chimica Acta **635**(2): 132-143.

Rodgers, V. G. J. and R. E. Sparks (1992). "Effect of transmembrane pressure pulsing on concentration polarization." Journal of Membrane Science **68**(1-2): 149-168.

Romero, C. A. and R. H. Davis (1988). "Global-model of cross-flow microfiltration based on hydrodynamic particle diffusion." Journal of Membrane Science **39**(2): 157-185.

Romero, C. A. and R. H. Davis (1991). "Experimental verification of the shear-induced hydrodynamic diffusion model of crossflow microfiltration." Journal of Membrane Science **62**(3): 249-273.

Ros, A., W. Hellmich, et al. (2006). "Bioanalysis in structured microfluidic systems." Electrophoresis **27**(13): 2651-2658.

Rousseau, M., L. Di Pietro, et al. (2004). "Preferential Transport of Soil Colloidal Particles: Physicochemical Effects on Particle Mobilization." Vadose Zone Journal **3**(1): 247-261.

Rusconi, R. and H. A. Stone (2008). "Shear-Induced Diffusion of Platelike Particles in Microchannels." Physical Review Letters **101**(25): 254502.

Rushton, A., A. S. Ward, et al. (2008). Solid-Liquid Filtration and Separation Technology, John Wiley & Sons.

Saboya, L. V. and J.-L. Maubois (2000). "Current developments of microfiltration technology in the dairy industry." Lait **80**(6): 541-553.

Saboyainsta, L. V. and J. Maubois (2000). "Current developments of microfiltration technology in the dairy industry." Lait **80**(6): 541-553.

Saito, Y., K. Mishima, et al. (2005). "Measurements of liquid-metal two-phase flow by using neutron radiography and electrical conductivity probe." Experimental Thermal and Fluid Science **29**(3): 323-330.

Sakai, Y., S. Wada, et al. (2003). "Nondestructive evaluation of blood flow in a dialyzer using X-ray computed tomography." Journal of Artificial Organs **6**(3): 197-204.

Samuelsson, G., I. H. Huisman, et al. (1997). "Predicting limiting flux of skim milk in crossflow microfiltration." Journal of Membrane Science **129**(2): 277-281.

Sandblom, R. M. (1978). Filtering Process. US Patent. **4105547**.

Sandison, D. R. and W. W. Webb (1994). "Background rejection and signal-to-noise optimization in confocal and alternative fluorescence microscopes." Applied Optics **33**(4): 603-615.

Santiago, J. G., S. T. Wereley, et al. (1998). "A particle image velocimetry system for microfluidics." Experiments in Fluids **25**(4): 316-319.

Sastry, S. K. and C. A. Zuritz (1987). "A review of particle behavior in tube flow: applications to aseptic processing 1." Journal of Food Process Engineering **10**(1): 27-52.

Schimpf, M. E., K. Caldwell, et al. (2000). Field flow fractionation handbook, Wiley-Interscience.

Schmitz, P., D. Houi, et al. (1992). "Hydrodynamic aspects of crossflow microfiltration. Analysis of particle deposition at the membrane surface." Journal of Membrane Science **71**(1-2): 29-40.

Schneider, K. and W. Klein (1982). "The concentration of suspensions by means of crossflow-microfiltration." Desalination **41**(3): 263-275.

Semwogerere, D., J. F. Morris, et al. (2007). "Development of particle migration in pressure-driven flow of a Brownian suspension." Journal of Fluid Mechanics **581**: 437-451.

Semwogerere, D. and E. R. Weeks (2008). "Shear-induced particle migration in binary colloidal suspensions." Physics of Fluids **20**(4): 0433061-0433067.

Shah, R. K. and A. L. London (1979). Laminar Flow Forced Convection in Ducts, Academic Press.

Shakib-Manesh, A., P. Raiskinmaki, et al. (2002). "Shear stress in a Couette flow of liquid-particle suspensions." Journal of Statistical Physics **107**(1-2): 67-84.

Chapter

8

Shauly, A., A. Wachs, et al. (1998). "Shear-induced particle migration in a polydisperse concentrated suspension." Journal of Rheology **42**(6): 1329-1348.

Shen, J. J. S. and R. F. Probstein (1979). "Turbulence Promotion and Hydrodynamic Optimization in an Ultrafiltration Process." Ind. Eng. Chem. Process Des. Dev. **18**(3): 547-554.

Sherwood, T. K., P. L. T. Brian, et al. (1965). "Salt Concentration at Phase Boundaries in Desalination by Reverse Osmosis." Industrial & Engineering Chemistry Fundamentals **4**(2): 113-118.

Skurtys, O. and J. M. Aguilera (2008). "Applications of microfluidic devices in food engineering." Food Biophysics **3**(1): 1-15.

Song, L. (1998). "Flux decline in crossflow microfiltration and ultrafiltration: mechanisms and modeling of membrane fouling." Journal of Membrane Science **139**(2): 183-200.

Squires, T. M. and S. R. Quake (2005). "Microfluidics: Fluid physics at the nanoliter scale." Reviews of Modern Physics **77**(3): 977-1026.

Stitou, A. and M. L. Riethmuller (2001). "Extension of PIV to super resolution using PTV." Measurement Science & Technology **12**(9): 1398-1403.

Strathmann, H. (1981). "Membrane separation processes." Journal of Membrane Science **9**(1-2): 121-189.

Strathmann, H. (2001). "Membrane separation processes: Current relevance and future opportunities." AIChE Journal **47**(5): 1077-1087.

Sutherland, K. (2006). "Defining the filtration market." Filtration Industry Analyst **2006**(3): 9.

Tan, K. W. (2003). "Experimental investigation of shear-induced particle migration in steady-state isothermic extrusion." Journal of the Society of Rheology **31**(3): 165.

Tardieu, E., A. Grasmick, et al. (1998). "Hydrodynamic control of bioparticle deposition in a MBR applied to wastewater treatment." Journal of Membrane Science **147**(1): 1-12.

Teh, S.-Y., R. Lin, et al. (2008). "Droplet microfluidics." Lab on a Chip **8**(2): 198-220.

Tetlow, N., A. L. Graham, et al. (1998). "Particle migration in a couette apparatus: Experiment and modeling." Journal of Rheology **42**(2): 307-327.

Theberge, A. B., F. Courtois, et al. (2010). "Microdroplets in Microfluidics: An Evolving Platform for Discoveries in Chemistry and Biology." Angewandte Chemie International Edition **49**(34): 5846-5868.

Thompson, N. (2002). "Recent advances in fluorescence correlation spectroscopy." Current opinion in structural biology **12**(5): 634-641.

Toner, M. and D. Irimia (2005). "Blood-on-a-chip." Annual Review of Biomedical Engineering **7**: 77-103.

Vadi, P. K. and S. S. H. Rizvi (2001). "Experimental evaluation of a uniform transmembrane pressure crossflow microfiltration unit for the concentration of micellar casein from skim milk." Journal of Membrane Science **189**(1): 69-82.

van Dinther, A. M. C., C. G. P. H. Schroën, et al. (2009). Design of Microsieves and Microsieve Processes for Suspension Fractionation. New Membranes and

Chapter

8

Advanced Materials for Wastewater Treatment, American Chemical Society. **1022:** 137-149.

van Dinther, A. M. C., C. G. P. H. Schroën, et al. (2011). "High-flux membrane separation using fluid skimming dominated convective fluid flow." Journal of Membrane Science **371**(1-2): 20-27.

van Dinther, A. M. C., C. G. P. H. Schroën, et al. (2012). "Flow induced particle migration for improved membrane microfiltration and fractionation processes." Unpublished manuscript.

Villamiel, M. and P. de Jong (2000). "Influence of High-Intensity Ultrasound and Heat Treatment in Continuous Flow on Fat, Proteins, and Native Enzymes of Milk." Journal of Agricultural and Food Chemistry **48**(2): 472-478.

Visvanathan, C. and R. B. Aim (1989). "Application of an Electric Field for the Reduction of Particle and Colloidal Membrane Fouling in Crossflow Microfiltration." Separation Science and Technology **24**(5-6): 383-398.

Voda, M. A. and J. Van Duynhoven (2009). "Characterization of food emulsions by PFG NMR." Trends in Food Science & Technology **20**: 533-543.

Voigt, A., C. Bayer, et al. (2008). "Laser Doppler field sensor for high resolution flow velocity imaging without camera." Applied Optics **47**(27): 5028-5040.

Vollebregt, H. M., R. G. M. van der Sman, et al. (2010). "Suspension flow modelling in particle migration and microfiltration." Soft Matter **6**(24): 6052-6064.

Wakeman, R. J. (1998). "Electrically Enhanced Microfiltration of Albumin Suspensions." Food and Bioproducts Processing **76**(1): 53-59.

Wakeman, R. J. and E. S. Tarleton (1986). "Experiments using electricity to prevent fouling in membrane filtration." Filtration and Separation **23**(3): 174-176.

Wakeman, R. J. and E. S. Tarleton (1991). "An experimental study of electroacoustic crossflow microfiltration." Chemical Engineering Research and Design **69a**: 386-397.

Wallhäußer, E., W. B. Hussein, et al. (2011). "On the usage of acoustic properties combined with an artificial neural network - A new approach of determining presence of dairy fouling." Journal of Food Engineering **103**(4): 449-456.

Wang, L. and L. Song (1999). "Flux decline in crossflow microfiltration and ultrafiltration: experimental verification of fouling dynamics." Journal of Membrane Science **160**(1): 41-50.

Wang, T., J. Wang, et al. (2003). "Application of Doppler ultrasound velocimetry in multiphase flow." Chemical Engineering Journal **92**(1-3): 111-122.

Wenten, I. G., D. M. Koenhen, et al. (1994). The backshock Process: A nocel backflush technique in microfiltration. Proceedings of the 2nd International Conference on Engineering of Membrane Processes, Italy, Elsevier.

Westerweel, J. (1997). "Fundamentals of digital particle image velocimetry." Measurement science & technology **8**(12): 1379.

Whitesides, G. M. (2006). "The origins and the future of microfluidics." Nature **442**(7101): 368-373.

Willert, C. E. (1991). "Digital particle image velocimetry." Experiments in fluids **10**(4): 181-193.

Chapter

8

Williams, R. A. (2003). "Tomographic imaging of particulate systems." <u>Advanced Powder Technology</u> **14**(1): 1.

Williams, S., C. Park, et al. (2010). "Advances and applications on microfluidic velocimetry techniques." <u>Microfluidics and Nanofluidics</u> **8**(6): 709-726.

Windt, C. W. (2007). <u>Nuclear magnetic response imaging of sap flow in plants</u> Thesis, Wageningen University.

Winzeler, H. B. and G. Belfort (1993). "Enhanced performance for pressure-driven membrane processes: the argument for fluid instabilities." <u>Journal of Membrane Science</u> **80**(1): 35-47.

Wolters, A. M., D. A. Jayawickrama, et al. (2002). "Microscale nmr." <u>Current Opinion in Chemical Biology</u> **6**(5): 711-716.

Wu, W. Y., S. Weinbaum, et al. (1992). "Shear-flow over a wall with suction and its application to particle screening." <u>Journal of Fluid Mechanics</u> **243**: 489-518.

Wu, Y. L., J. H. J. Brand, et al. (2007). "A new parallel plate shear cell for in situ real-space measurements of complex fluids under shear flow." <u>Review of Scientific Instruments</u> **78**(10): 1039021-10390211.

Xi, C. and N. C. Shapley (2008). "Flows of concentrated suspensions through an asymmetric bifurcation." <u>Journal of Rheology</u> **52**(2): 625-647.

Yaffe, M. J. and J. A. Rowlands (1997). "X-ray detectors for digital radiography." <u>Physics in Medicine and Biology</u> **42**(1): 1-39.

Yamada, M., M. Nakashima, et al. (2004). "Pinched flow fractionation: Continuous size separation of particles utilizing a laminar flow profile in a pinched microchannel." <u>Analytical Chemistry</u> **76**(18): 5465-5471.

Yamanaka, G., H. Kikura, et al. (2003). "Flow measurement on oscillating pipe flow near the entrance using the UVP method." <u>Experiments in Fluids</u> **34**(3): 307-315.

Yan, Z. Y., A. Acrivos, et al. (1991). "A 3-dimensional analysis of plasma skimming at microvascular bifurcations." <u>Microvascular Research</u> **42**(1): 17-38.

Yan, Z. Y., A. Acrivos, et al. (1991). "Fluid skimming and particle entrainment into a small circular side pore." <u>Journal of Fluid Mechanics</u> **229**: 1-27.

Yong Chung, K., R. Bates, et al. (1993). "Dean vortices with wall flux in a curved channel membrane system: 4. Effect of vortices on permeation fluxes of suspensions in microporous membrane." <u>Journal of Membrane Science</u> **81**(1-2): 139-150.

Yoo, J. Y. and Y. W. Kim (2008). "Recent experimental studies on microscale channel flows." <u>Proceedings of the 12th Asian Congress of Fluid Mechanics</u>.

Yu, Z. S., X. M. Shao, et al. (2007). "Dynamic simulation of shear-induced particle migration in a two-dimensional circular couette device." <u>Chinese Journal of Chemical Engineering</u> **15**(3): 333-338.

Zeng, L., S. Balanchandar, et al. (2005). "Wall-induced forces on a rigid sphere at finite Reynolds number." <u>Journal of Fluid Mechanics</u> **536**: 1-25.

Zhang, J. and B. J. Balcom (2010). "Parallel-plate RF resonator imaging of chemical shift resolved capillary flow." <u>Magnetic Resonance Imaging</u> **28**(6): 826-833.

www.vlb-berlin.org, visited 28 March 2012

Summary

Membrane microfiltration processes are used in e.g. food, biotechnology, chemical and pharmaceutical industry, and more generally in for example wastewater treatment. Microfiltration is mostly used to separate components that are greatly different in size, e.g. micro-organisms from water, but rarely to fractionate components that are of similar size. This latter option would be interesting for many applications, since it would lead to enriched starting materials and possibly new products, but is hampered by accumulation of components in and on the membrane due to size exclusion by the pores. This leads to flux reduction and increased retention of components in time, basically the accumulated layer determines which components can pass the membrane. Although the accumulated components can be removed by e.g. back-pulsing this only gives a short term solution leading to extensive cleaning procedures given the way membranes are currently operated in practice. Clearly it would be beneficial if accumulation could be prevented, and through that, more stable operation could be achieved.

This thesis presents how flow-induced particle migration can be used for stable membrane flux and retention of components in time. The particle migration mechanisms that are considered in this thesis, shear-induced diffusion, inertial lift, and fluid skimming, act on particles that are typically between 0.1 and 10 micron. They induce separation of components in the fluid moving (larger) particles away from the membrane, therewith facilitating separation; basically pore size no longer determines particle permeation. In the various chapters will be shown that these effects improve processing of dilute suspensions and make processing of highly concentrated systems possible, which is beyond the scope of current microfiltration processes.

This thesis consists of seven chapters. **Chapter one** starts with the main challenge of membrane microfiltration, which is accumulation of components in and on the membrane. Accumulation mechanisms (concentration polarization, cake formation and adsorption) are described, followed by concepts from literature targeted at controlling particle accumulation. Membrane design is discussed, as well as back-transport mechanisms that are to be used in the design of the deposition-free filtration processes presented later in the thesis. These mechanisms include shear-

induced diffusion, inertial lift and Brownian diffusion. The chapter concludes with an overview of the various elements of the thesis in which we combine particle migration with process and membrane design to improve membrane microfiltration.

In **chapter two**, methods to measure velocity and concentration profiles in microfluidic devices are described and compared. The small dimensions of these devices will cause particles to migrate; as is used later in the thesis to facilitate segregation and separation. A drawback of the small dimensions is that they make measurement of velocity and concentration gradients difficult. In this chapter, experimental methods for investigation of migration phenomena that can occur in microfluidic devices are compared focussing on concentration and velocity profiles of bidisperse and polydisperse suspensions. Tomography, ultrasound and optical analysis are reviewed and evaluated on general dimensionless numbers related to process conditions and channel dimensions. Besides, eleven practical criteria are used to evaluate the performance of the methods. NMR and CSLM, although expensive, are the most promising techniques to investigate flowing suspensions in microfluidic devices, where one may be preferred over the other depending on the size, concentration and nature of the suspension, the dimensions of the channel, and the information that has to be obtained.

Chapter three shows experimental results on particle level; the behaviour of suspensions between 9 and 38 volume% is studied with Confocal Scanning Laser Microscopy. Under Poiseuille flow in a closed microchannel shear-induced diffusion causes migration in these suspensions. Under all measured process conditions, particles segregate on size within an entrance length of around 1000 times the channel height. Mostly, the larger particles migrate to the middle of the channel, while the small particles have high concentrations near the walls. This also indicates that the small particles could be collected from their position close to the wall. This is proven through microfiltration of emulsions, using pore sizes that are much larger than the larges particle. The small particles can be removed without accumulation of particles in and on the membrane, and as long as the process conditions are chosen appropriately, high fluxes ($4.4 \cdot 10^4$ L·h^{-1}·m^{-2}·bar^{-1}) can be maintained.

In **chapter four**, the use of particle migration in membrane microfiltration is further elaborated using emulsions consisting of small droplets (~2.0 micron) and large droplets (~5.5 micron) with total concentrations between 10 and 47% and $\phi_{large}/\phi_{total}$ ratios between 0.05 and 0.75. The membrane cross-flow module consist of a closed channel to allow particles to migrate due to shear-induced diffusion followed by a membrane with 20 micron pores, where fractions of these emulsions can be removed. Under appropriate process conditions, the permeate consists only of small droplets, and on top of that their concentration is higher than in the original emulsion, leading to very high selectivity. As expected, the size of the emulsion droplets in the permeate is a function of trans-membrane pressure and oil volume fraction. Especially at high droplet concentration (which is known to cause severe fouling in regular membrane filtration), these effects are occurring as a result of shear-induced diffusion. If only small particles are targeted in the permeate, the module can be operated at fluxes of 40 L/(m^2/h); if fractionation is targeted the fluxes can be considerably higher.

The shear-induced particle migration investigated in chapters three and four, is further quantified in **chapter five**. Separation of concentrated suspensions is currently done by dilution and since the process based on hydrodynamic particle-particle interactions works well at low velocities and high concentrations, industrial application could have major benefits. The hydrodynamic migration acts in the bulk of the suspension and allows for a fluid skimming mechanism to act above the pore by decreasing the concentration of large particles in regions close to the membrane. It was concluded that hydrodynamic particle-particle interactions make it possible to fractionate particles on size in a concentrated emulsion based on a dimensionless number, which relates membrane (pore) design and process conditions.

Besides concentrated suspensions, also dilute suspensions benefit from particle migration. The **sixth chapter** shows how migration phenomena can induce fractionation of yeast cells from water in dilute suspensions, using micro-engineered membranes having pores that are typically five times larger than the cells. The observed effects are similar to fluid skimming (in combination with inertial lift), and the separation performance can be linked to the ratio between

cross-flow and trans-membrane flux, which is captured in a dimensionless number that can predict size of transmitted cells. For sufficiently high cross-flow velocity, the particles pass the pore and become part of the retentate; the separation factor can simply be changed by changing the ratio between cross-flow velocity and trans-membrane flux. Since the membranes have very large pores, fouling does not play a role and constant high trans-membrane flux values of 200–2200 L/m^2·h are reached for trans-membrane pressures ranging from 0.02 to 0.4 bar.

Chapter seven consists of two sections. The first section is a general discussion of the subjects described in this thesis. In the second section, an outlook is given on how current industrial processes can be designed and improved in terms of energy consumption by making use of particle migration. It is shown that return of investment of installation of these new membrane modules is short compared to the membrane life time, due to high energy savings, and in order to reach this, it will be necessary to take unconventional process conditions that target particle migration and membrane design as a starting point. In conclusion, particle migration can improve (membrane) separation processes and even has the potential to lead to totally new separation processes. Particle migration can be advantageous in both dilute as well as concentrated systems, leading to reduced fouling, reduced energy and water consumption and a reduction in waste. This can all be achieved at production capacity similar or better than currently available in microfiltration processes.

Samenvatting

Membraan microfiltratie wordt gebruikt in bijvoorbeeld de levensmiddelen, biotechnologische, chemische en farmaceutische industrie en ook voor meer algemene toepassingen zoals bijvoorbeeld de waterzuivering. Microfiltratie wordt het meeste gebruikt voor het scheiden van componenten die sterk verschillen in grootte, zoals micro-organismen uit water, maar vrijwel niet voor het fractioneren van componenten die qua grootte erg op elkaar lijken. Deze laatste optie is erg interessant voor veel toepassingen, omdat het leidt tot verrijking van grondstoffen en mogelijk tot nieuwe producten. Echter, ophoping van componenten in en op het membraan ten gevolge van de grootte van de porie leidt vaak tot problemen, zoals afname in de flux van het membraan en een toename van retentie van de componenten als functie van de tijd. De laag van opgehoopte componenten bepaalt eigenlijk welke componenten er door het membraan gaan. De opgehoopte componenten kunnen verwijderd worden met behulp van bijvoorbeeld het van richting veranderen van de langstromende suspensie, maar dit geeft vaak alleen een effect op de korte termijn, zodat intensieve schoonmaakprocedures alsnog nodig zijn. Het zou erg voordelig zijn om de ophoping van componenten te kunnen voorkomen en daarmee het proces veel robuster te maken.

Deze dissertatie laat zien hoe deeltjesmigratie, welke door stroming wordt opgewekt, gebruikt kan worden om een stabiele membraanflux en retentie als functie van de tijd te hebben. De migratie mechanismen van deeltjes die in deze dissertatie worden meegenomen zijn: migratie ten gevolge van de afschuifsnelheid, migratie ten gevolge van traagheid en het rakelings over de porie scheren van deeltjes, waarbij vloeistof door de porie wordt afgevoerd. Al deze mechanismen werken voor deeltjes tussen de 0.1 en 10 micron en veroorzaken scheiding van componenten in de vloeistof, waarbij grotere deeltjes van het membraan weg migreren en de scheiding vergemakkelijken. Ten gevolge hiervan is de poriegrootte van het membraan niet langer van belang. De verscheidene hoofdstukken laten zien dat deze effecten het verwerken van verdunde suspensies kunnen verbeteren en het verwerken van geconcentreerde suspensies mogelijk maken. Dit laatste ligt momenteel buiten het bereik van bestaande microfiltratie.

Deze dissertatie bestaat uit zeven hoodstukken. **Hoofdstuk een** begint met de omschrijving van de uitdaging van microfiltratieprocessen, welke de ophoping van componenten in en op het membraan omvat. Ophopingsmechanismen, zoals concentratiepolarisatie, koeklaag en adsorptie, worden beschreven, alsmede ook concepten uit de literatuur die als doel hebben deze ophoping in de hand te houden. Daarnaast wordt aan de orde gebracht hoe membraanontwerp, samen met terugtransportmechanismen, gebruikt kunnen worden in het ontwerp van membraan processen waarbij geen deeltjes neerslaan op het membraan. Deze mechanismen omvatten migratie ten gevolge van de afschuifsnelheid, migratie ten gevolge van traagheid van deeltjes en migratie ten gevolge van Brownse beweging. Het hoofdstuk eindigt met een overzicht van de elementen die in deze dissertatie worden besproken, waarin we deeltjesmigratie combineren met membraan- en procesontwerp om membraanmicrofiltratie te verbeteren.

In **hoofdstuk twee** worden experimentele methoden besproken en vergeleken om snelheids- en concentratieprofielen te meten in microsystemen. De kleine dimensies van deze systemen, zorgen ervoor dat de deeltjes migreren en dit kan worden gebruikt ter bevordering van segregatie en scheiding. Een nadeel is dat deze kleine dimensies het meten van de snelheids- en concentratieprofielen bemoeilijkt. In dit hoofdstuk worden experimentele methoden voor het onderzoeken van migratie in microsystemen vergeleken, waarbij zowel snelheids- als concentratieprofielen in bidisperse en polydisperse suspensies moeten kunnen worden gemeten. Tomografie, ultrasone en optische analyse worden geevalueerd op basis van dimensieloze getallen gerelateerd aan procescondities en dimensies van het kanaal. Daarnaast worden er elf criteria gebruikt om de prestaties van de methoden te evalueren. Het blijkt dat NMR en CSLM, ondanks de kosten, de meest belovende technieken zijn om stromende suspensies in microsystemen te onderzoeken. Afhankelijk van de grootte, de concentratie en de herkomst van de suspensie, de dimensies van het kanaal en de benodigde informatie zal een keuze tussen CSLM of NMR gemaakt moeten worden.

Hoofdstuk drie laat de experimentele resultaten op deeltjesniveau zien; het gedrag van suspensies tussen 9 en 38 volume% wordt onderzocht met CSLM. In een gesloten microkanaal waar Poiseuille stroming plaatsvindt, wordt migratie van

deeltjes veroorzaakt door de afschuifsnelheid. Onder alle gemeten procescondities vindt deeltjessegregatie op grootte plaats binnen een aanstroomlengte van ongeveer 1000 keer de hoogte van het kanaal. In de meeste gevallen migreren de grote deeltjes naar het midden van het kanaal, terwijl de kleine deeltjes in hoge concentratie bij de wand aanwezig zijn. Dit geeft ook aan dat de kleine deeltjes verzameld kunnen worden dicht bij de wand. Dit is aangetoond door middel van microfiltratie van emulsies, met poriën die veel groter zijn dan de deeltjes. De kleine deeltjes kunnen verwijderd worden zonder ophoping van deeltjes op en in het membraan als de procescondities goed gekozen worden en waarbij de flux door het membraan hoog ($4.4 \cdot 10^4$ L·h^{-1}·m^{-2}·bar^{-1}) en constant in de tijd is.

In **hoofdstuk vier** gaan we verder in op het gebruik van deeltjesmigratie in membraanmicrofiltratie van emulsies met kleine druppels (~2.0 micron) en grote druppels (~5.5 micron), een totale concentratie tussen de 10 en 47 volume% en $\phi_{groot}/\phi_{totaal}$ verhouding tussen 0.05 en 0.75. De membraanmodule met langsstroom bestaat uit een gesloten kanaal waarin migratie van deeltjes kan plaatsvinden, gevolgd door een membraan met ronde porien van 20 micron, waardoor fracties van de emulsie kunnen worden verwijderd. Onder de juiste procescondities bestaat het permeaat alleen uit kleine deeltjes en bovendien is de concentratie aan kleine deeltjes hoger dan in de oorspronkelijke emulsie, wat leidt tot een zeer hoge selectiviteit. Zoals verwacht is de grootte van de emulsiedruppels in het permeaat een functie van de druk over het membraan en de volumefractie van de olie. Vooral bij een hoge druppelconcentratie (welke zorgt voor aanzienlijke vervuiling in reguliere membraanfiltratie) treden deze effecten op ten gevolge van afschuifsnelheid die tot diffusie leidt. Wanneer alleen de kleine deeltjes in het permeaat aanwezig dienen te zijn, kan de membraanflux 40 L/(m^2/h) zijn; als fractioneren het doel is kan de flux aanzienlijk hoger zijn.

De migratie ten gevolge van de afschuifsnelheid, welke in hoofdstuk drie en vier is behandeld, wordt in **hoofdstuk vijf** verder gekwantificeerd. Scheiding van geconcentreerde suspensies wordt momenteel gedaan door verdunning en aangezien het proces gebasseerd is op hydrodynamische deeltje-deeltje interacties en goed werkt bij lage snelheden en hoge concentraties, zit er veel voordeel aan het gebruik van dit principe in industriele toepassingen. De hydrodynamische

migratie vindt plaats in de bulk van de suspensie en zorgt ervoor dat het deeltjes over de porie kunnen scheren doodrdat de concentratie van grote deeltjes boven het membraan laag is. Hydrodynamische deeltje-deeltje interacties maken het mogelijk om deeltjes op grootte te fractioneren in een geconcentreerde emulsie gebaseerd op een dimensieloos getal, welke membraan (porie) ontwerp en procescondities aan elkaar relateert.

Naast geconcentreerde suspensies kunnen ook verdunde suspensies voordeel hebben van deeltjesmigratie. Het **zesde hoofdstuk** laat zien hoe migratie concentrering van gistcellen kan bewerkstelligen, waarbij gebruik gemaakt wordt van membraanontwerp op microniveau met porien die vijf maal groter zijn dan de gistcellen. De geobserveerde effecten zijn in overeenstemming met het scheren van deeltjes over een porie waarbij vloeistof wordt afgenomen (in combinatie met migratie ten gevolge van traagheid). De mate van scheiding kan in verband worden gebracht met de verhouding tussen de langsstroomsnelheid en de flux, welke worden gevangen in een dimensieloos getal dat voorspellingen kan doen over de grootte van de deeltjes in het permeaat. Bij voldoende hoge langsstroomsnelheid kunnen de deeltjes over de porie heen scheren en vormen daarmee het retentaat; de scheidingsfactor kan eenvoudig veranderd worden door de verhouding tussen de snelheden aan te passen. Aangezien de membranen zeer grote poriën hebben, speelt vervuiling van het membraan geen rol en kunnen constante, hoge fluxen worden gehaald van 200–2200 L/m^2·h voor trans-membraandrukken van 0.02 tot 0.4 bar.

Hoofdstuk zeven bestaat uit twee onderdelen. Het eerste onderdeel bediscussieert de verschillende onderwerpen die in deze dissertatie worden behandeld. In het tweede onderdeel wordt een vooruitblik geworpen op het gebruik van deeltjesmigratie in industriele processen. Het geeft zicht op hoe een process moet worden ontworpen en hoe het kan worden verbeterd met betrekking tot energieconsumptie. Dit hoofdstuk laat zien dat de terugverdientijd van een installatie met deze nieuwe membraanmodules erg kort is vergeleken met de levensduur van het membraan, ten gevolge van de hoge energiebesparing. Om dit te bereiken zullen onconventionele procescondities en membraanontwerpen moeten worden toegepast, die migratie van deeltjes stimuleren.

Samenvattend kunnen we zeggen dat migratie van deeltjes, (membraan)processen kan verbeteren en zelfs potentie heeft om tot geheel nieuwe scheidingsprocessen te leiden. Migratie van deeltjes kan zowel in verdunde als geconcentreerde systemen leiden tot verminderde vervuiling, verminderd energieverbruik en watergebruik en een afname in de hoeveelheid afval. Tevens hoeven er geen concessies gedaan te worden met betrekking tot de productiecapactiteit, welke hetzelfde of soms zelf hoger is dan in de huidige microfiltratie processen.

Nomenclature

a	particle radius (m)
b	fitting parameter (-)
B_0	static magnetic field strength (T)
c	fitting parameter (-)
d_b	average particle diameter in bulk (m)
d_L	diameter large emulsion droplets (m)
d_S	diameter small emulsion droplets (m)
D	Stokes-Einstein diffusivity (m^2/s)
D_ϕ	dimensionless diffusion coefficient (-)
$D(\phi)$	dimensionless diffusion coefficient (-)
$D'(\phi)$	dimensionless hydrodynamic diffusion coefficient (-)
d_f	fringe spacing (m)
d_p	average particle diameter in permeate (m)
d_{pore}	pore diameter (m)
d_{ratio}	ratio between average particle size in permeate and bulk (-)
D_c	dimensionless parameter (-)
D_h	hydraulic diameter (m)
D_{shear}	shear-induced diffusion coefficient (m^2/s)
D_μ	dimensionless parameter (-)
e_L	length of closed channel needed to establish a fully developed velocity profile (m)
E_p	energy consumption to pressurize a liquid (J)
E_p	evolution parameter (-)
E_p^{fit}	fitted evolution parameter (-)
$E_p^{fit}{}_{norm}$	normalized fitted evolution parameter (-)
f	fanning friction factor (-)
F_e	emitting frequency (Hz)
h	channel height (m)
H	half the channel height (m)
I	length over which intergration has to be done (m)
J	trans-membrane flux (m^3/m^2·s)
J_{lift}	trans-membrane flux as a result of inertial lift (m/s)

J_{shear}	trans-membrane flux as a result of shear-induced diffusion (m/s)
J_{max}	maximum trans-membrane flux to have no cake layer formation (m/s)
J_{min}	minimal trans-membrane flux to have no negative trans-membrane pressure (m/s)
J_{mig}	shear-induced migration flux (m/s)
k	Boltzmann constant (J/K)
K	constant related to shear-induced diffusion (-)
L	closed entrance length (m)
L_m	length of membrane (m)
l_{closed}	length between two pores (m)
l_{pore}	pore length (m)
m	factor for monodisperse hard spheres (-)
N	noise (Hz)
p	acoustic pressure (kg/m·s^2)
ΔP	trans-membrane pressure (Pa)
Δp	pressure drop over channel (Pa)
Pe	dimensionless Péclet number relating importance hydrodynamic to Brownian forces (-)
Pe*	dimensionless Péclet number relating diffusive to convective processes (-)
Q'	excess particle flux (-)
Q	dimensionless Q-value (-)
q_p	volumetric flow rate through the pore (m^3/s)
q_v	flow rate (m^3/s)
Re$_c$	dimensionless channel Reynolds number (-)
Re$_p$	dimensionless particle Reynolds number (-)
R_m	membrane resistance (1/m)
R_p	radius of the pore (m)
S	signal (Hz)
t	time (s)
t_{prf}	time between two emissions (s)
t$_\parallel$	time needed for particle to overcome pore (s)
t$_\perp$	time needed for particle to travel half the diameter (s)

T	temperature (K)
Transmission	ratio between concentration in permeate and bulk (-)
u_a	fluid velocity at a height of one average particle radius (m/s)
u_{pore}	fluid velocity through one pore (m/s)
$\bar{v}$	average velocity (m/s)
v_f	average cross-flow velocity (m/s)
v_{max}	maximum velocity (m/s)
v_p	average permeate flux velocity (m/s)
v_{sound}	speed of sound (m/s)
v_{wave}	sound velocity of the ultrasonic wave in the fluid (m/s)
$v_x(z)$	velocity of the particle in the channel at a height z (m/s)
$v_x(a)$	velocity of the particle in the channel at a height of the particle radius a (m/s)
w	channel width (m)
x	distance in the channel parallel to the flow (m)
X	dimensionless distance from the inlet (-)
y	average distance travelled by the particles perpendicular to the flow (m)
z	position of particle relative to reference wall (m)
Z	characteristic impedance (kg/m²·s)

Greek

α	selectivity of membrane process (-)
$\dot{\gamma}$	shear rate (1/s)
γ_{wall}	shear rate at the wall (1/s)
$\gamma_{w,0}$	nominal shear rate at membrane (1/s)
δ	ratio of the particle size to the radius of the pore (-)
ε	membrane porosity (-)
ε_{length}	length porosity (-)
η	viscosity of the solution (Pa·s)
$[\eta]$	intrinsic relative viscosity (-)
η_{eff}	efficiency of the pump (-)
η_0	viscosity particle-free liquid (Pa s)

$\eta(\phi)$	viscosity as a function of the solid volume fraction of the suspension (Pa·s)
θ	angle between two intersecting waves (°)
Θ	dimensionless time (-)
Θ_{corr}	dimensionless time corrected for round pore size (-)
λ	constant related to shear-induced diffusion (-)
λ_{wave}	wavelength (m)
ρ	density of the suspension (kg/m^3)
ρ_{oil}	density of the oil phase (kg/m^3)
τ_{conv}	time scale of convection (s)
τ_{dif}	time scale for migration (s)
ϕ	solid volume fraction of the suspension (-)
ϕ_b	bulk solid volume fraction (-)
ϕ_L	solid volume fraction of large particles (-)
$\phi_{L,b}$	solid volume fraction of the large particles in the bulk (-)
$\phi_{L,p}$	solid volume fraction of the large particles in the permeate (-)
ϕ_{max}	maximum packing density of suspension (-)
ϕ_p	permeate solid volume fraction (-)
ϕ_S	solid volume fraction of small particles (-)
$\phi_{S,b}$	solid volume fraction of the small particles in the bulk (-)
$\phi_{S,p}$	solid volume fraction of the small particles in the permeate (-)
ϕ_{tot}	solid volume fraction of the bidisperse suspension (-)
$\phi(x,z)$	concentration profile of particles at a certain distance in the channel (-)
$\phi_{ref}(z)$	concentration profile at the inlet (-)
$<\phi(x,z)>_z$	cross-sectional average volume fraction (-)
$<\phi_{ref}(z)>_z$	cross-sectional average volume fraction at the inlet (-)
ϕ_w	solid volume fraction at membrane (-)

Dankwoord

In het volgende stuk wil ik graag alle mensen bedanken die mee hebben geholpen dit proefschrift mogelijk te maken. Allereerst natuurlijk mijn promotor Remko. Jouw enthousiasme gaf me vaak weer veel positieve energie en dat is erg belangrijk voor mij geweest. Daarnaast waardeer ik natuurlijk ook zeer sterk je stortvloed aan nieuwe ideeën en de zeer terechte vragen van de advocaat van de duivel, die me weer op een andere manier deden nadenken. Ook Karin wil ik bedanken voor jouw vertrouwen in mij en jouw manier om mij de helikopterview te laten zien. Van de opmerkingen op mijn artikelen heb ik veel geleerd, zeker wat schrijven betreft.

Binnen het ShIFT team van ISPT heb ik ook hulp gehad. Ruud, vooral van jouw kennis van reeds bestaande literatuur en de connecties binnen de wetenschap heb ik veel baat gehad bij het doen van mijn onderzoek, alsmede ook jouw kritische kijk op natuurkundige aspecten van vloeistof en deeltjes gedrag. Martijntje, ik heb veel geleerd van jouw zakelijke en gestructureerde manier van problemen bekijken en bedank je voor je hulp bij vloeistof- en deeltjesgedrag vraagstukken, alsook het gezelschap tijdens de reisjes naar Aken en Kopenhagen. André, ik vond het altijd prettig om dingen met jou te bespreken vanwege je praktische kennis en benadering. Na sjorren en trekken is de module er dan toch gekomen. Albert, jouw altijd oprechte mening (hetzij positief, hetzij negatief) en je persoonlijk reacties op geschreven stukken, heb ik zeer gewaardeerd. Edwin, omdat je wat verder van het project afstond, was het toch goed om jouw vragen te horen, omdat die uit alle details, de hoofdzaak naar voren haalden. Norhan, eventhough you joined later, I admired your perseverance concerning the project and it was nice to get to know your better when we went to Cetraro. Francisco, it was a good feeling to give the membrane module in such experienced hands.

Natuurlijk wil ik ook Astrid, Herry, Frans, Marion, Menno en Kees bedanken voor hun hulp in het project of betreffende financiële, administratieve en ondersteuningszaken. I would also like to thank the other PhD's of ISPT for the nice atmosphere and the talks during the researchers meetings. Dit geldt zeker voor Christine (en Menno) tijdens ons tripje naar Praag.

Buiten het feit dat ik bij ISPT in dienst was, zat ik fulltime in Wageningen en wil daarom verscheidene mensen daar ook graag bedanken. Jos, jouw hulp in het lab en je praktische kijk zorgden ervoor dat mijn opstelling in het lab beetje bij beetje verbeterde. Mijn oprechte dankbaarheid voor de mensen van de werkplaats en dan met name Hans de Rooij. Ik kon altijd langskomen voor praktische zaken of gewoon een gesprek over mijn frustraties betreffende modules, waarbij jij altijd weer zorgde dat ik positief naar de zesde vertrok.

Ook wil ik Frank en Henk bedanken voor de mogelijkheid tot het doen van experimenten bij biofysica. Frank, je bent een erg positieve man, bent goed in het onder woorden brengen van complexe materie en zag altijd wel weer een nieuwe mogelijkheid en dat zijn dingen waar ik veel van geleerd heb. Tevens heb ik experimenten gedaan bij FrieslandCampina en wil daarvoor Yves en Anno bedanken. Jullie hebben ervoor gezorgd dat ik beter in beeld kreeg wat de mogelijkheden en uitdagingen waren. Ook de Soft Condensed Matter groep uit Utrecht heeft mij erg geholpen bij het doen van mijn onderzoek. Arnout, bedankt dat wij experimenten bij jullie konden doen en dat je op een andere manier naar mijn artikel wilde kijken. Ook Stefan, Teun en Peter bedankt voor het maken van de deeltjes, de uitleg betreffende de CSLM en de technische ondersteuning.

Bij Proceskunde in Wageningen wil ik de mensen van de vakgroep bedanken voor hun gezelligheid tijdens AIO-reizen, labuitjes, sinterklaas, kerstdiners en andere borrels. Met name de lunch was altijd een verademing met de frisse lucht en het prachtige gekwaak van de kikkers. Therefore I would like to thank the Process Engineering Lunch Break International Table: The real die-hards (Francisco, Carsten, Petra, Anja) and the acceptable wheather joiners (Nirmal, Thomas, Yvette, Lena, Marta, Nicolas, Ana, Rupali, Jacqueline, Ekaraj and Pascalle). I also want to thank you for the time spent outside of working hours. Tevens wil ik mijn kamergenoten waar ik het grootste gedeelte van de tijd mee doorbracht bedanken: Solomon, Akmal, Rianne en Marta. We had some interesting talks and discussions, being work related or not, with the window and heater always being our favourite topics. Natuurlijk wil ik mijn paranimfen bedanken voor de (mentale) steun. Anja, jouw dj kwaliteiten en Petra, jouw aanwezigheid aan dezelfde labtafel hebben alles een stuk opgevrolijkt.

Ofcourse I would like to thank my students Kashif Khan, Larissa Rodrigues Soares and Karlijn Remmers. Your work has helped me a lot in the understanding of the matter and I really enjoyed working with you.

Tijdens de uren dat ik niet op het werk was heb ik ook de nodige ontspanning gehad tijdens etentjes, uitgaan, weekendjes weg en yoga. De vriendinnen van de studie: Ellen, Tanya, Nienke, Anneke; Amis d'Or: Lotte, Maartje, Lennart, Johan en Marjon; T.M.S.D.C.D.C. Scotia: Nessie (en al haar bewonderaars), laten we tot City 80.0 gaan!; Margriet, Fianna en Fabiënne. Tevens ook Ben en Annemarie bedankt voor de (spirituele) yoga.

Mijn ouders verdienen natuurlijk alle lof voor hun liefdevolle zorg, relativerende kijk, vertrouwen en begrip. Lieve pap en mam, jullie zijn er altijd als ik jullie nodig heb.

Lieve Rutger, gelukkig weet jij wat het is om een AIO-baan te doen en konden we samen veel grapjes maken om het een en ander te relativeren. Ik heb ook veel geleerd van jou over hoe de academische wereld en het bedrijfsleven in elkaar zitten. Opdracht van Richard Ashley is nu voltooid. Na 10 jaar kijk ik met vreugde naar de nieuwe stappen in onze toekomst samen.

Curriculum Vitae

Anna Marie Christine van Dinther was born in Amsterdam, the Netherlands, on the 10th of August 1984. She finished her secondary education (VWO) in 2002 at the Regionale Scholengemeenschap Broklede in Breukelen. In the same year she started the study Food Technology at Wageningen University and finished her BSc degree in 2005 with a thesis on fractionation of suspensions. After her BSc, she joined the European Master Degree in Food Studies programme, which included taking courses at several universities throughout Europe and working on a project for two years in an international team. Her Master thesis and internship were combined at the Food and Ingredient Functionalility Platform at Nestlé in Beauvais (France). There she worked on flavour delivery by capsules in ice cream.

In 2008 she started to work as Ph.D. student at the Food Process Engineering Group of Wageningen University within the framework of the Institute of Sustainable Process Technology. The result of the work is described in this thesis.

Curriculum Vitae

Publications

Brans, G., A. van Dinther, B. Odum, C.G.P.H. Schroën, R.M. Boom (2007). "Transmission and Fractionation of Micro-sized Particle Suspensions." Journal of Membrane Science **290** (1-2): 230-240.

van Dinther, A.M.C., C.G.P.H. Schroën, R.M. Boom (2011). "High-flux Membrane Separation using Fluid Skimming dominated Convective Fluid Flow." Journal of Membrane Science **371**(1-2): 20-27.

van Dinther, A.M.C., C.G.P.H. Schroën, F.J. Vergeldt, R.G.M. van der Sman, R.M. Boom (2012). "Suspension Flow in Microfluidic Devices — A Review of Experimental Techniques focussing on Concentration and Velocity Gradients." Advances in Colloid and Interface Science **173:** 23-34.

van Dinther, A.M.C., C.G.P.H. Schroën, A. Imhof, H.M. Vollebregt, R.M. Boom (2012). "Flow-induced Particle Migration for improved Membrane Microfiltration and Fractionation Processes." *Submitted for publication*.

van Dinther, A.M.C., C.G.P.H. Schroën, R.M Boom (2012). "Particle Migration leads to Deposition-free Fractionation." *Submitted for publication.*

van Dinther, A.M.C., C.C.P.H. Schroën, R.M. Boom (2012). "Separation of Concentrated Emulsions using Hydrodynamic Interactions." *Submitted for publication.*

Book chapters

van Dinther, A.M.C., C.G.P.H. Schroën, R.M. Boom (2009). "Design of Microsieves and Microsieve Processes for Suspension Fractionation." New Membranes and Advanced Materials for Wastewater Treatment, American Chemical Society. **1022:** 137-149.

Schroën, K., A.M.C. van Dinther, S. Bogale, M. Vollebregt, G. Brans, R.M. Boom (2010). "Membrane Processes for Dairy Fractionation." Membrane Technology: Membranes for Food Applications, Volume 3, Wiley-VCH Verlag GmbH & Co. 25-43.

Training Activities

Conferences

AMK, Aachen, Germany	2008
CHISA, Prague, Czech Republic	2008
NPS, Veldhoven, the Netherlands (flash-presentation and poster)	2009
Fouling and Cleaning in Food Processing, Cambridge, UK (oral)	2010
NPS, Veldhoven, the Netherlands (oral presentation and poster)	2010
ICOM, Amsterdam, the Netherlands (oral presentation)	2011
ICM, Kottayam, India (oral presentation)	2011

Courses

NMR and MRI Applications in Food Systems, VLAG, Wageningen	2008
Experimental fluid dynamics and data interpretation, TUD, Copenhagen	2009
Nanostructured materials and membranes for Food Processing, Itm-Cnr and University of Calabria, Rende and Cetraro, Italy	2010
PhD Competence Assessment, WGS, Wageningen	2008
VLAG PhD introduction week, Bilthoven	2008
Techniques for Writing and Presenting a Scientific Paper, WGS	2009
Talent Class Kernachtig Formuleren, NWO, Den Haag	2009
Sustainable Process, Product and System Design, OSPT, Groningen	2009
Working in Projects, DSTI, Amersfoort	2009
Afstudeervak organiseren en begeleiden, DO, Wageningen	2010
Career Orientation, WGS, Wageningen	2011

Optionals

Process Engineering PhD study tour to Japan	2008
Food Process Engineering PhD study tour to the USA	2010
Lecture 'Publish or Perish', KLV, Wageningen	2008
Brain and Game food and bioprocess engineering group, Wageningen	2008
(Food Sector) Meetings DSTI/ ISPT	2008-2010
Internal Symposium Food Process Engineering, Wageningen	2009-2011
DSTI workshop cross-cultural awareness, Amersfoort	2011

Training Activities

Cover: measurement of fluorescent particles in 100 micron channel at wall and in the middle of the channel. Front and back cover show 2.7 and 1.4 micron particles respectively.